A New Class of Solid State, Single-ion Conductors (H^+ and Li^+): Silicon-based Plastic Crystals

by

Iolanda Santana Klein

A Dissertation Presented in Partial Fulfillment
of the Requirements for the Degree
Doctor of Philosophy

Approved August 2016 by the
Graduate Supervisory Committee:

Charles Austen Angell, Chair
Daniel A. Buttry
Ranko Richert

ARIZONA STATE UNIVERSITY

December 2016

ABSTRACT

Plastic crystals as a class are of much interest in applications as solid state electrolytes for electrochemical energy conversion devices. A subclass exhibit very high protonic conductivity and its members have been investigated as possible fuel cell electrolytes, as first demonstrated by Haile's group in 2001 with $CsHSO_4$. To date these have been inorganic compounds with tetrahedral oxyanions carrying one or more protons, charge-balanced by large alkali cations. Above the rotator phase transition, the HXO_4^- anions re-orient at a rate dependent on temperature while the centers of mass remain ordered. The transition is accompanied by a conductivity "jump" (as much as four orders of magnitude, to ~ 10 $mScm^{-1}$ in the now-classic case of $CsHSO_4$) due to mobile protons. These superprotonic plastic crystals bring a "true solid state" alternative to polymer electrolytes, operating at mild temperatures (150-200ºC) without the requirement of humidification. This work describes a new class of solid acids based on silicon, which are of general interest. Its members have extraordinary conductivities, as high as 21.5 mS/cm at room temperature, orders of magnitude above any previous reported case. Three fuel cells are demonstrated, delivering current densities as high as 225 mA/cm^2 at short-circuit at 130ºC in one example and 640 mA/cm^2 at 87ºC in another. The new compounds are insoluble in water, and their remarkably high conductivities over a wide temperature range allow for lower temperature operations, thus reducing the risk of hydrogen sulfide formation and dehydration reactions. Additionally, plastic crystals have highly advantageous properties that permit their application as solid state electrolytes in lithium batteries. So far only doped materials have been presented. This work presents for the first

time non-doped plastic crystals in which the lithium ions are integral part of the structure, as a solid state electrolyte. The new electrolytes have conductivities of 3 to 10 mS/cm at room temperature, and in one example maintain a highly conductive state at temperatures as low as -30^{o}C. The malleability of the materials and single ion conducting properties make these materials highly interesting candidates as a novel class of solid state lithium conductors.

DEDICATION

To my father, my first Science teacher.

To my mother, my Tibetan singing bowl.

To my sisters, my role models.

"Philosophy [nature] is written in that great book whichever is before our eyes - I mean the universe - but we cannot understand it if we do not first learn the language and grasp the symbols in which it is written. The book is written in mathematical language, and the symbols are triangles, circles and other geometrical figures, without whose help it is impossible to comprehend a single word of it; without which one wanders in vain through a dark labyrinth."

Galileo Galilei

ACKNOWLEDGMENTS

First and most importantly, I would like to thank my advisor Regent's Professor Charles Austen Angell for collecting me as his student. He taught me how to be a scientist and a curious researcher. He didn't let me give up when times were dire, and taught me what receiving a Ph.D. means. Thank you for your friendship, teachings and guidance. Thank you for supporting me during my career, and shaping my future as a scientist. I would also like to thank Dr. Jenny Green for all her help and support during my time at ASU. Thank you for your friendship!

Secondly I would like to thank my family for their unconditional love and support. For picking me up through the hard times and celebrating with me during the good times. Catarina (Cá) e Patricia (Dãrguinha), you are my moral compass and my role models, the best sisters anyone could ever ask for. Maminha e papinha: you are my rock and my entire world. Thank you for being so supportive even when the saudade was so intense. Without you all, I wouldn't have made it.

I would also like to thank Waunita Parrill for all of her help, support and friendship during my time at ASU. From helping with placing orders, travels arrangements, refunds, to tea meetings in her office – my time in the lab wouldn't be the same without you!

I would like to thank my labmates for the support, laughs and help through the days. Be it a science inquiry or a coffee break, you made my days more special and more productive. Thank you for teaching me what you know and letting me teach you as well. I wouldn't have made it without you all: Drs. Kazuhide Ueno, Seung-Yul Lee, Zuofeng

Zhao, Telpriore “Greg” Tucker, Younes Ansari, Leigang Xue, Shuai Wei and Mohammad Hasani.

I would like to acknowledge the LeRoy Eyring Center for Solid State Science and the Magnetic Resonance Research Center at Arizona State University for the use of their facilities. Thank you Drs. Brian Cherry and Emmanual Soignard for training me in NMR and Raman Spectroscopies respectively, and for helping me with my research.

Finally, I would like to thank everyone from the Fall 2010 Chemistry and Biochemistry Ph.D. students. It was an honor to be by your side during our time at ASU. You are the best friends I could have ever asked for. Thank you for your support, for your friendship, for the laughs (and drinks!). Thank you for being my family away from home, and for making Arizona my new home. Special mentions go to Drs. Aurelie Marcotte (sweetsiepoo), Meg Schmierer (TEAM GRADUATE!), Lina Franco (Miss Colombia), Bobby Schmitz (Bobbo), Bennett Addison (Benito), Brian Woodrum (Woody), Adam Monroe (Old Man Monroe), Elana Stennett, Ian Pahk (Dwight), Tylan Watkins; and the soon to be Drs. Kirt Robinson (Kirlando Calrissian), Kristin Johnson and Brian St. Clair (Bwian). A very special mention goes to my fiancé and collaborator, Dr. Stephen Davidowski (Stevesie). Thank you for your love and support, and for collecting all of the solid state NMR in this work. You are the best collaborator anyone could ever ask for.

Financial support for this work was provided by the ARO and the DOE.

TABLE OF CONTENTS

LIST OF TABLES

Table Page

LIST OF FIGURES

Figure Page

CHAPTER 1

INTRODUCTION

1.1 All Solid State Electrochemical Devices

As humankind evolves and society become more dependent on technology, so increases our need to generate and store electrical energy efficiently. From smartphones to laptops, from electric vehicles to the energy grid – energy conversion and storage devices are ubiquitous in today's world. At the heart of energy storage are electrochemical devices – apparatuses that convert chemical energy into electrical energy. Also called galvanic or voltaic cells, these devices take advantage of redox reactions happening within the cell to generate electricity in form of electrons that flow outside of the cell and into a circuit performing electrical work.

Electrochemical cells consist of two electrically conducting elements (the electrodes) physically separated by an electrolyte, Figure 1.1. The electrolyte is an ionic conductor that is responsible for the mass transfer and charge balance in the cell. While electrons flow through an external circuit, the electrolyte provides the cathode with positive charges (cations) to ensure electrical neutrality. Independent of the final state and of the chemistry involved in a given electrochemical cell, an electrolyte is always present and is the common component of all electrochemical devices.

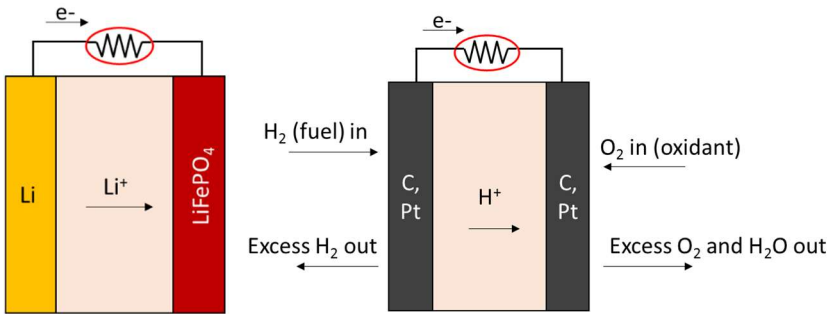

Figure 1.1 – *Left hand panel*: scheme of a lithium ion battery during discharge (i.e., powering an external circuit). Lithium gets oxidized at the anode, generating Li^+ ions according to the half-reaction: $\boldsymbol{Li^0 \rightarrow Li^+ + e^-}$. The Li^+ cations travel through the electrolyte while the electrons move through the external circuit from the anode to the cathode and are available to perform electrical work. At the same time, Li^+ are intercalated at the cathode, and the reduction of Fe^{+3} to Fe^{+2} occurs[1]. *Right hand panel*: scheme of a fuel cell. Hydrogen gas (fuel) is constantly provided at the anode where oxidation occurs. While electrons move from the anode to the cathode in the external circuit, protons migrate to the cathode, and the oxygen reduction reaction happens generating water as the waste product. Both reactions happen in the presence of a catalyst (Pt, in this example).

Devices used for electrochemical energy conversion include fuel cells and batteries, which are the final applications of the electrolytes described in this work. Although the principle of operation is the same (redox reactions happening inside the cell) they differ from each other in the sense that in the fuel cells the fuel (e.g. H_2 gas) is constantly provided. The fuel cell can operate indefinitely as long as enough fuel is provided. In batteries, all of the chemical species necessary for the redox reactions are confined within the cell (with the exception of redox flow batteries, not studied in this work).

The following sections 1.1.1 and 1.1.2 are devoted to a short introduction on Fuel Cells and Li-ion Batteries respectively, with special focus on the electrolyte role and development. Moreover, this work focuses on the development of solid state electrolytes,

so much of the discussion and literature review is directed towards this interesting and challenging field of study. All of the compounds developed in this work are based on silicon, so in section 1.2 a concise introduction to silicon chemistry is given. Lastly, section 1.3 is dedicated to a brief summary of the characterization techniques used in this work.

1.1.1. Electrolytes for Fuel Cells – emphasis on Solid Acid Fuel Cells (SAFC)

Fuel cells are electrochemical energy conversion devices with very attractive advantages and many challenges, and these vary with the kind of fuel cell. In general, one of the biggest advantages is the clean operation, where a safe waste is generated (in general water, but in some cases CO_2 is also produced, Table 1.1). Perhaps the biggest disadvantage is the cost of operation. The catalysts necessary for oxidizing hydrogen gas into protons and reducing oxygen gas into O^{2-} are precious metals or their alloys like Pt, Au, Rh. In practical applications, many unit cells must be joined to make a fuel cell stack to generate the desired voltage, and the price of the catalyst becomes prohibitive. Much of the fuel cell research is devoted to new catalysts and their chemistries, which is outside the scope of the present work.

Fuel cells are classified according to the type of electrolyte used: direct methanol, phosphoric acid, alkaline, polymer electrolyte membrane (PEMFC) or proton exchange membrane, molten carbonate, solid oxide, and more recently, solid acid fuel cells (SAFC). A summary of key characteristics of each fuel cell type is given in Table 1.1.1. Liquid or solid electrolytes can be used, and each have their own set of advantages and drawbacks. Liquid electrolytes have high conductivities but have the disadvantage of the possibility of flooding the electrodes and reducing gas flow. That reduces the performance of the

electrodes, and as a consequence, of the unit cell. Additionally, great care has to be taken to avoid leakage and subsequent ionic shorts. Solid electrolytes eliminate the electrode flooding and leakage problems, but they are generally less conductive than their liquid counterparts. Moreover, solid electrolytes have a more complicated contact interface with the electrodes. This work introduces a new class of solid acids, so special attention will be given here to introducing this class of fuel cells.

Table 1.1 – Overview of fuel cell types. Adapted from reference[2].

Fuel cell	Electrolyte (charge carrier)	Catalyst	Operating T/°C	Waste
Polymer Electrolyte	Polymer (H^+)	Pt	40-80	H_2O
Alkaline	Potassium hydroxide (OH^-)	Pt	65-220	H_2O
Phosphoric Acid	Phosphoric acid, H_3PO_4 (H^+)	Pt	205	H_2O
Molten Carbonate	Molten carbonates (CO_3^{2-})	Electrode material	650	H_2O and CO_2
Solid Oxide	Perovskites (O^{2-})	Electrode material	600-1000	H_2O and CO_2
Solid Acid	$M_yH_z(XO_4)_w$* solid acids (H^+)	Pt	Above T_{pc} transition, usually above 100	H_2O

*M = Cs, Rb, Tl or NH_4; X = S, Se, P; y, z, w = integers.[3,4,5,6]

The class of fuel cells that has been invested in the most is the PEMFC, due to their potential application in electric vehicles. The safe waste product (water), non-corrosive components and mild temperature range of operation renders them relatively safe (excluding the inherent danger of using pure hydrogen gas as a fuel). Low temperatures also translate into lower start time. Disadvantages come from the requirement of water management – the standard PEM Nafion®, developed by Dupont, requires constant

humidification to maintain the high proton conductivity. That generates more engineering problems and adds to the complexity of the system. The lower temperature of operation, compared to other FC systems, makes the catalyst more susceptible to poisoning by CO, sulfur-containing compounds and halogens[2].

An interesting alternative to PEMFCs was introduced relatively recently by Sossina Haile's group in 2001[7]. They were the first to demonstrate the viability of Solid Acid Fuel Cells (SAFC) where the electrolyte of choice are solid acids, compounds of the type $M_yH_z(XO_4)_w$ (M = Cs, NH_4, Rb, Tl; A = S, Se, P; y, z, w = integers)[3,4,5,6] and additionally at least one case of a mixed anion $Cs_2(HSO_4)(H_2PO_4)$[8]. These compounds have a superprotonic phase transition, above the temperature of which their ionic conductivities "jump" several orders of magnitude. Usually those transitions are crystalline phase changes that occur between 50 and 150°C, the exception being $Tl_3H(SO_4)_2$ at -34°C[4]. In the case of the widely studied cesium hydrogensulfate ($CsHSO_4$), the increase is of 3 orders of magnitude (up to the high value of 10^{-2} S/cm) when the material goes from a monoclinic to a tetragonal phase[3].

Solid acids offer attractive advantages over PEMs, including anhydrous proton transport (so no complex humidification system is required); the compounds are usually stable at high temperatures (250°C in the case of $CsHSO_4$), diminishing the catalyst poisoning problem; and the higher temperature of operation in contrast to PEM opens the possibility of reducing the use of precious metals as catalysts[6], reducing the overall cost of the fuel cells. Disadvantages include the increased ductility of the materials above the superprotonic transition and water solubility of these acid salts[7].

The SAFCs performance vary with the electrolyte used and conditions of operation – thickness of both the electrolyte and electrodes, catalyst loading and the humidification of the fuel all play important roles[9]. In the case of CsH_2PO_4 operating under humidified conditions, the performance is competitive with phosphoric acid fuel cells, drawing a maximum current density of 1.85 A/cm^2 at short-circuit and a power peak density of 415 mW/cm^2 [10,11]. Although humidification is not strictly necessary, that increases the operation time of the fuel cells[10].

Although solid acids are a very promising alternative to the Nafion-based humidified PEM fuel cells, many challenges are still present. The extreme malleability of the electrolytes above the superprotonic transition, although advantageous for contact purposes, pose a challenge for practical systems. Therefore, composites of electrolytes with harder materials (SiO_2 for example) have been attempted, but the rigidity is accompanied by a decrease in conductivity[9].

1.1.2. Electrolytes for Li-ion Batteries

Two or more electrochemical cells connected in series to power an external device form a battery. Many different chemistries yield functioning power generating cells, like NiCd, Na, Mg, Al, to cite a few, but the chemistry of choice for powering electric vehicles and portable devices is still lithium. First made commercially viable by Sony in 1991[12] using a carbon intercalation anode and $LiCoO_2$ cathode, the lithium-ion battery gets its name from the Li^+ intercalation/deintercalation chemistry between the sheets of graphite and within the structure of the cathode.

Lithium is both the most electronegative and lightest metal, with a reduction potential of -3.0 V vs NHE (normal hydrogen electrode)[13]. That translates into high voltage devices and very light batteries, which is an important requirement when powering electric vehicles and portable consumer electronics. When used as an anode, it has the very high specific capacity of 3.86 A.h/g but it does not come without its own set of disadvantages. During charge, the polarity of the battery is reversed and lithium ions move from the cathode to the anode. The lithium deposition in the form of lithium metal at the surface of the anode happens in the form of dendrites, which are needle-shaped crystals. With continuous operation, this dendritic growth can be severe enough to reach the cathode, shorting the battery and causing explosions - the solvents used in lithium batteries are generally non-aqueous, organic solvents that are highly flammable (aqueous solvents are not used due to the high voltages of the lithium batteries, ~4V). The problem was solved by using the intercalation carbon anode (0.3V vs Li^+/Li) by the aforementioned Sony effort. There is no Li^0 deposition – Li^+ ions are inserted/removed from the anode, so the dendritic growth is completely avoided. A great part of the research and development effort on lithium batteries is dedicated to developing new anodes and cathodes which is also outside the scope of this work.

The combination of a specific anode and cathode pair in the lithium-ion battery determines the voltage, and consequently the power that can be drawn (note that power is the product of voltage and current). The capacity of the battery, given in units of A.h/g, is also dictated by the electrodes. Since the electrolyte is in direct contact with the electrodes at all times, it is necessary to be always developing new chemistries that are stable with

respect to the new electrode materials and sufficiently sustain good, reversible electrochemistry at the desired potentials.

Today, the "standard" lithium-ion battery consists of an intercalation cathode (e.g. $LiCoO_2$, $LiMnO_2$ or $LiFePO_4$) and a carbonaceous anode. The electrolyte of choice is a solution of 1.0M $LiPF_6$ in a mixture of organic solvents, first introduced by Tarascon and co-workers with ethylene carbonate (EC) or propylene carbonate (PC) and dimethylcarbonate (DMC)[14]. The mixture of solvents is necessary because a balance must be reached between ionicity and fluidity. A solvent of high dielectric constant (in this case EC or PC) is necessary to dissolve the polar lithium salt, and maintain the high conductivity of the solution. As a consequence, the solution has prohibitive viscosity. The solution is to make a mixture with a low viscosity solvent (DMC) – fluidity is necessary for the ions to move freely in the electrolyte. Even though this particular system is stable versus oxidation up until 5V[14], using a liquid electrolyte makes the system prone to leaks, and the flammability of the solvents increases the potential for explosions.

For an electrolyte to be considered suitable for applications in lithium batteries, it should satisfy a series of requirements[13]: it should be a good ionic conductor and an electronic insulator; it should be stable with respect to both cathode and anode (i.e., have a wide electrochemical window); be inert towards cell materials and finally be environmentally safe and robust with respect with temperature variations. Ideally, a single-ion conducting electrolyte would be the preferred choice. A single-ion conductor, as the name suggests, is a material where only one ion "moves" and is therefore solely responsible for the charge passed through it. That avoids concentration polarization within the cell that

sets up an opposing voltage and thus diminishes the cell performance. The measurement of the amount of current that is due to one particular ion in an electrolyte is called the transport or transference number. In a lithium ion electrolyte, a transference number of 1 (t_+=1.0) means that all of the current generated is due to only the lithium ions. Lithium ion transference numbers, in solution, will depend on the salt and the solvents used. According to the extensive review by K. Xu[13], in diluted non-aqueous solutions, t_+ varies from 0.20 to 0.40. That means that the anions are contributing more to the total current than the Li^+ ions. The explanation lies usually with the smaller ionic radius of the Li^+, that makes them very easily solvated, and that solvation "sphere" causes a decrease in its ionic mobility[13].

One approach to avoid both the safety issues associated with liquid electrolytes and low ion transference numbers is to employ solid state electrolytes. Although in general the ionic conductivity of solids is not as high as that of their liquid counterparts, examples of solids that surpass the conductivity of liquids are known: the crystalline lithium superionic conductor $Li_{10}GeP_2S_2$ has a conductivity of 12 mS/cm at 27ºC and it matches or surpasses the conductivities of organic liquid electrolytes like 1M $LiPF_6$ in 1:1 EC:PC[15]. The lithium transference number of 1 in this case translates not only into a high ionic conductivity but also in a very stable electrolyte – the compound is stable up to 5 V vs Li^+/Li. This compound has a three-dimensional structure where a one-dimensional pathway lithium conduction exists along the c-axis[15]. The disadvantage of this electrolyte is the high cost of the material and high toxicity of the reagents, making the scalability for practical use very complicated.

Other solid state electrolytes commonly studied for battery applications include ceramics, glasses, polymers and gels. The most impressive ceramic material is β-alumina, an exceptional Na^+ ion conductivity of 18 mS/cm at room temperature can be achieved depending on the conditions of crystal growth[16]. The drawbacks are that the high conductivity is achieved in the brittle, single-crystal form, which is also prohibitively expensive. Glasses rarely exceed 1 mS/cm conductivities, which is considered the minimum threshold for practical batteries. Polymers can be divided into two subclasses: solid polymer and gel-polymer electrolytes. In solid polymers, the neat polymer itself serves as "solvent" for the lithium salt and as the support matrix. Single Li^+ ion conducting polymers exist, but their conductivities are restricted to 10^{-5} and 10^{-6} S/cm[17]. Gel polymer electrolytes are similar to liquid electrolytes - in this case, the polymer is gelled from an electrolyte solution. Although widely used in commercial cells, they have non-zero anion transfer numbers, and are still prone to overcharging and explosions[13].

Another approach to the electrolyte problem is to use plastic crystals (PCs) as solvent matrices for lithium salts. Plastic crystals are structurally ordered materials, where the centers of mass of the molecules are fixed in the crystal lattice, but they are rotationally disordered, where the molecule (or an ion) is free to rotate around an axis. These materials have a phase transition, above which the rotation movements are activated (T_{pc}, plastic crystalline temperature). They also possess a glass transition temperature (T_g), below which the movement is arrested in the solid state. The great advantage of plastic crystals over glassy materials is that PCs maintain their structure and mechanical rigidity well over the glass transition temperature, up until the melting point is reached.

1.2 Objectives and strategy

In this work, we chose to explore a new strategy to solve the problem of moving ions in a solid state electrolyte for applications in electrochemical energy conversion cells. We have sought to develop a new type of plastic crystal ion conductor, one in which the alkali cation has a transference number of unity, i.e. it is the only mobile species. The strategy was to design an anion that is a soft base, as in Pearson's definition[18], hard acids tend to bond more strongly to hard bases and the same is true for soft pairs. A molecule that is constituted of a hard/soft pair, the hard acid would be thought to be more free to move, uncoupled from the anion. Although the strategy of pairing hard acid/soft base is not new[19] when developing electrolytes, our study is, to the best of our knowledge, the first time that a non-doped ionic plastic crystal is reported with high conductivities (of the order of mS/cm).

The advantages of plastic crystals over glasses and other solid state electrolytes were discussed in section 1.1.2 – the malleability of plastic crystalline solids are a highly desirable trait in solid state batteries, due to the better contact with the electrodes, and ability to move under stress and with the change of shape of the electrodes. Moreover, glasses only retain their shape up to their T_gs, but plastic crystals retain their solidity up to their melting points.

To achieve the objective of synthesizing novel plastic crystals with cationic transfer number of 1, we built on the previous research developed in our lab of SiPOH, a modified phosphoric acid that was very successfully employed as a liquid electrolyte for fuel cell applications[20]. SiPOH is the product of the reaction of $SiCl_4$ and phosphoric acid,

constituted of 6-coordinated silicon centers (as probed by NMR) and phosphoric acid in its structure[21]. The liquid suspension called SiPOH dissolves completely in water, and can be gelled into a polymeric form of exceptional performance as a solid electrolyte, where the silicon geometry becomes tetrahedral[21]. The success of SiPOH warranted further study with a softer anion, and the choice was made to study sulfates and hydrogensulfates from sulfuric acid. Although sulfates are borderline hard bases (although softer than phosphates), the silicon center would "pull" the electron density of the sulfate anions, and make them softer towards the hard alkali cations.

In this work, several novel compounds were synthesized as described in detail in Chapters 2 and 3. First, acid precursors were prepared by reacting $SiCl_4$ and a series of phenylsilanes (strategy discussed in the following section, 1.2.1) with nominally anhydrous sulfuric acid, and in one case, with a mixture of sulfuric and phosphoric acids. The resulting hydrogensulfates were so reactive and highly conductive that they merited their own separate study (Chapter 2). To make the lithium plastic crystals studied in this work, the acid precursors were reacted with lithium amide or lithium chloride. The acidic protons leave the reaction mixture in the form of gaseous products (NH_3 or HCl), and the resulting products are soft, white solids (Chapter 3). The structural characterization of the compounds was done by liquid and solid-state NMR (section 1.3.5) and Raman spectroscopy (section 1.3.6). The electrochemical characterization was performed by Electrochemical Impedance Spectroscopy (section 1.3.4), cyclic voltammetry and fuel cell performance tests were also carried out.

1.2.1. Silicon reactivity and mechanism

To make the series of new compounds, the initial approach was to react different equivalents of nominally anhydrous sulfuric acid with silicon tetrachloride under inert atmosphere:

$$SiCl_4 + xH_2SO_4 \rightarrow SiCl_{4-x}(HSO_4)_x + xHCl \text{ (i)}$$

Subsequent structural characterization by ^{29}Si NMR showed that the compounds were all indeed tetrahydrogensulfated silanes with no chlorine ligands (see Chapter 2 for a more thorough description). In view of this difficulty, a new approach was adopted to obtain a series of different compounds. The extensive work by Eaborn in aromatic substitution reacions[22,23] showed that demetallations of an aryl-MR_3 bond (where M = Si, Ge, Sn Pb) is broken in the direction of $C^- MR_3^+$. In the case of silicon, the electrophilic attack by an E^+A^- species would form a E-Phenyl compound and $ASiMR_3$. Figure 1.2 shows the suggested mechanism when E^+A^- is a sulfuric acid molecule.

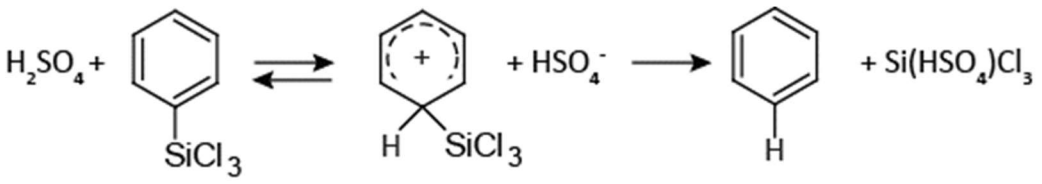

Figure 1.2 - Suggested reaction mechanism of the formation of the precursor used in this study. The cleavage of the phenyl ring happens in two steps: first, protonation of the phenyl ring by sulfuric acid forming a Wheland intermediate, which is the rate determining step of the reaction. Then a nucleophilic attack by the hydrogensulfate anion results in benzene elimination and formation of the trichlorosilylhydrogensulfate. (Adapted from reference[22]).

The aryl-SiR_3 bond was shown to be cleaved much more readily than the aryl-H bonds, at a factor of $4x10^4$ times in aqueous sulfuric acid at 25°C[22]. The attachment of the proton in the 2nd step of the mechanism shown in Figure 1.2 is the rate determining step (as determined experimentally by solvent isotope studies). The C-Si bond is then broken in a fast step after the initial proton-aryl bonding. That is due to the stabilization of the Wheland intermediate by electron release of the CH-$SiMR_3$ system[22].

Literature studies in the synthesis of silicon triflates for applications as catalysts for organic reactions have shown the relative rates of cleavage of the Ph-Si bond with other ligands. Upon attack with triflic acid, it was shown that the phenyl groups get displaced 200x faster than chlorines when they are present, and the breakage of methyl-Si bonds was not observed even after a few days[24]. Another study showed that the relative ease of cleavage of R-Si bonds follow the sequence (from more readily to less readily cleaved) α-naphthyl > Ph > Cl > H >> methyl, ethyl, buthyl[25]. In this work, we show in Chapter 2 that methoxy groups are displaced as easily as phenyl groups, extending the sequence shown above.

With the knowledge of the relative ease of cleavage of different ligands bonded to a Si center, the synthesis strategy adopted in this work was to react a series of phenylsilanes containing different ligands (methyl, chlorine, methoxy, ethoxy) with anhydrous sulfuric acid, and in one case, a mixture of sulfuric and phosphoric acids as described in Chapter 2. Several new compounds (or mixtures of compounds) were obtained and their structures and electrochemistry were characterized with the techniques described in Section 1.3.

1.3 Techniques used in this work

There is extensive high quality literature in the background of the characterization techniques used in this work. Therefore, it is not the objective of this section to dwell in the intricate details of each technique, but to provide a brief summary to guide the reader for a basic understanding of the results to follow. In this section, greater focus will be given to the direct application of the techniques to all solid state systems, as it is the focus of this dissertation.

Here, the same order of presentation of the results in later chapters will be followed: in the following chapters, the conductivity of the new compounds is discussed first, followed by a detailed investigation of their chemical structure by solid state NMR and Raman Spectroscopy. Lastly, fuel cell and battery results are presented, followed by electrochemical characterization by cyclic voltammetry when applicable. Following that order, the first technique to be visited will be Impedance Spectroscopy.

1.3.1. Electrochemical Impedance Spectroscopy

In an electrochemical cell, the sample of interest is placed between two or more electronic conductors (electrodes) and a number of experiments can be performed by changing the current or voltage applied to the system and measuring a response (in voltage or current respectively). If the system of interest is a liquid, the electrodes can be immersed directly inside the sample, along with a supporting electrolyte if applicable. In that type of experiment, the interface between the electrode and the solution is important, and the diffusion of the ionic species in the solution as well.

In the case of a solid electrolyte, the material must be contained between the two electrodes and great care must be taken to provide the best electrical contact possible. In the solid state, interfaces become increasingly important, and there are many of them in a solid cell. Each interface displays a change of a certain physical or chemical property - mechanical, crystallographic, electrical or compositional[26]. With applied electric stimuli, i.e. voltage, each interface will polarize differently (heterogeneous charge distribution arises), resulting in a decrease in the overall bulk conductivity of the material[26].

One of the most widely applied techniques to probe the electrical properties of a material is Impedance spectroscopy. In this experiment, a small sinusoidal voltage is applied to the system, and a resulting oscillating current is measured, Figure 1.3. Impedance (Z) depends on frequency, so in this experiment Z is measured as a function of frequency over a wide range.

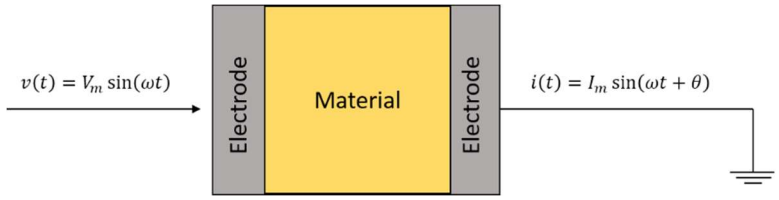

Figure 1.3 – Scheme of a hypothetical Impedance Spectroscopy experiment. The sinusoidal equations that describe the applied voltage and resulting steady-state current are shown. Symbols: v(t) = applied voltage; V_m = amplitude of the voltage; ω = frequency of the oscillation; i(t) = resulting steady-state current; I_m = amplitude of the current; t = time; θ = phase difference between voltage and current.

The impedance Z is defined as:

$$\text{Impedance} = \ Z(\omega) = \frac{v(\omega)}{i(\omega)} \ ; \text{Modulus or Magnitude} = |Z(\omega)| = \frac{|Vm(\omega)|}{|Im(\omega)|}$$

Impedance is an intrinsic property of materials, and is analogue of resistance, although impedance is a more general concept than electrical resistance because it reports the material response to a sinusoidally varying electrical stress, when the current and voltage may become out of phase, leading to energy dissipation from the field. The resistance of the material is the impedance when the phase of the current relative to potential perturbation is zero.

There are many ways to represent Impedance Spectra, but in this work the preferred method used is the Nyquist representation. This method originates from the fact that $Z(\omega)$ is a vectorial quantity, and as such it may be represented as a sum of vectors in a complex plane. A Nyquist plot is a graph of the negative of the imaginary part of impedance, $-Im(Z)$, with respect to its real part, $Re(Z)$. Real electrochemical systems (specially all solid state cells) are incredibly complicated, and have many different elements that will affect how a Nyquist plot appears. As a result, the interpretation of impedance spectra can be a very challenging task. However, it is often shown that a good approximation of a real system can be made by an appropriate equivalent circuit. In summary, an equivalent circuit is an idealized system made of ideal electrical elements (resistors, capacitances, and others) that is assumed to be an appropriate model for the system being studied. Figure 1.4 shows schemes of commonly observed Nyquist plots and their respective equivalent circuits. Equivalent circuits are great aids in the study and interpretation of Impedance spectra.

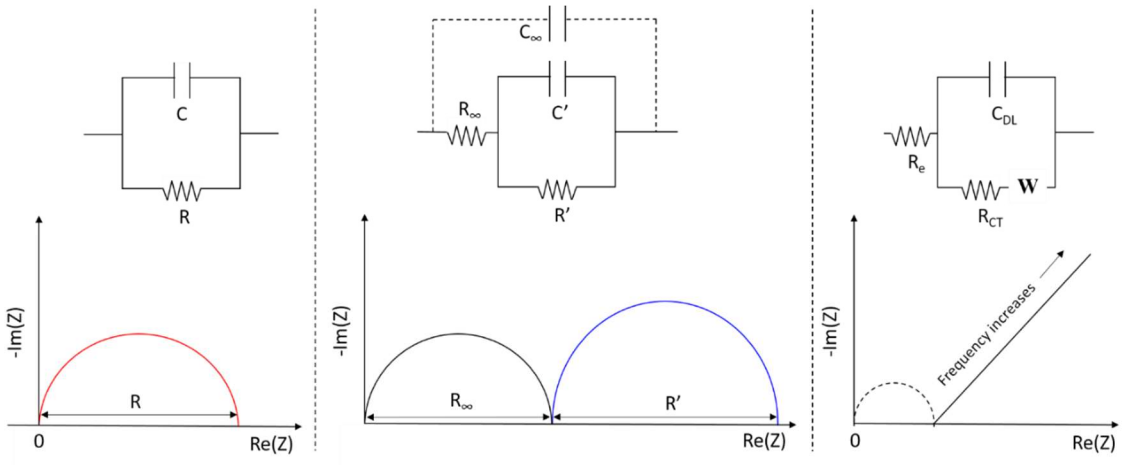

Figure 1.4 – Scheme of equivalent circuits and their respective Nyquist plots. Adapted from references[26,27]. *Left hand panel:* the equivalent circuit is comprised of a capacitance C resulting from the electrode/electrolyte interface, and the electrolyte resistance R in parallel with C. This system is always present in an electrode/electrolyte system, although not always observed. The resulting Nyquist plot is a semi-circle of radius R. *Middle panel:* the equivalent circuit represents a heterogeneous electrode reaction in parallel with the C-R electrode/electrolyte circuit. C' is the double layer capacitance at the electrode and R' is the reaction resistance. *Right hand panel:* Randle's circuit[28] – the electrolyte resistance is in series with a parallel circuit of the double layer capacitance (electrode/electrolyte), and a charge transfer resistance R_{CT} (which is in series with a Warburg Impedance, W). W is an element of diffusion, present when semi-infinite diffusion of a single species is present in the electrochemical system[26,27].

In this work, all of the impedance spectra were collected in the form of Nyquist plots for determination of the novel solid state electrolytes resistances. The resulting plots were always approximately similar to those of Randle's circuits, so the conductivities of the electrolytes were calculated by the usual method according to the equation:

$$\sigma = \frac{l}{A.R}$$

where σ is the ionic conductivity, l is the separation between the electrodes, A is the area of the cross-section of the sample and R is the resistance as determined by Impedance Spectroscopy (i.e. the real part of the complex impedance when the imaginary part is zero). The ratio l/A is the cell constant. When a dip-cell was used, the cell constant was determined by calibration with a 0.01 M KCl solution[29].

1.3.2. Nuclear Magnetic Resonance (NMR) Spectroscopy

NMR Spectroscopy is based on the interaction of an external magnetic field with nuclei of non-zero total spin. This technique is sensitive to the nucleus probed, so every element in the sample can be studied separately (provided it has a non-zero spin). In this work, ^{1}H, ^{29}Si, ^{13}C solid state NMR of the samples where the main techniques used to solve their structures.

In summary, a static magnetic field of magnitude B_0 (taken to be along the z-axis) is applied to the sample of interest. The field interacts with the sample's nuclei, and these rearrange so their net magnetization is aligned with the field. If additionally, a radiofrequency (rf) wave is applied in the form of pulses, its oscillating magnetic field will interact with the net magnetization of the nuclei and cause them to "flip" – the magnetization is then dislocated by a phase angle (the angle between the rf pulse and the z-axis of the static field B_0). After the rf pulse, the nuclei relax back to the ground state, and the net magnetization is once again aligned with B_0, and the nuclei emit radiation that is detected and depends on the frequency. The information obtained is element-sensitive, and provides information on the chemical and electronic environment in the immediate vicinity of the nucleus being probed.

In the solid state, the samples are usually powders. Since the solid has arrested degrees of freedom, the molecules are not free to rearrange themselves like in the liquid state. All the possible orientations of the molecules give rise to different frequencies in an NMR spectrum (chemical shift anisotropy), resulting in a powder pattern – very broad peaks that are of little use to resolve chemical structures. In liquids, chemical shift anisotropy is not observed due to rapid tumbling movement of the molecules, that effectively average all the possible orientations (and therefore the chemical shift dependency on orientation) faster than the NMR time scale.

Magic-angle spinning (MAS) NMR removes the chemical shift anisotropy by spinning the sample tipped at the magic angle (54.74°) at high rates, effectively averaging the different chemical shifts due to particle orientation[30]. Additionally, spinning about the magic angle also eliminates the chemical anisotropy due to dipolar coupling.

In the case of dilute, low abundance spins like ^{29}Si in this work (4.1% abundance), a technique that greatly aids in the quality of the spectra collected is the cross-polarization (CP). In a CP experiment, the magnetization of abundant spins, usually ^{1}H, is transferred to the rare spin, via dipolar coupling[30]. An added advantage of the CP experiment, is that since the transfer of magnetization happens via dipolar coupling, both nuclei have to be in a rigid environment. Moreover, information about the separation of the nuclei can be calculated from CP[30].

1.3.3. Raman Spectroscopy

Approximately, one can separate the energy of a molecule or ion in 3 parts – the rotation of the entire molecule, the vibration of the constituent atoms and the excitation of the electrons (based on the relative frequencies: electrons>>vibrations>>rotation)[31]. In this approximation, the translation of the molecule (or ion) is not taken into account. In the presence of an electromagnetic field (light), a transfer of energy will occur from the field to the molecule when Bohr's condition is satisfied:

$$\Delta E = h\nu$$

Where ΔE = difference in energy between two quantized states, h = Planck's constant and ν = frequency of the incident light. Figure 1.5 shows the hypothetical energy levels of a molecule.

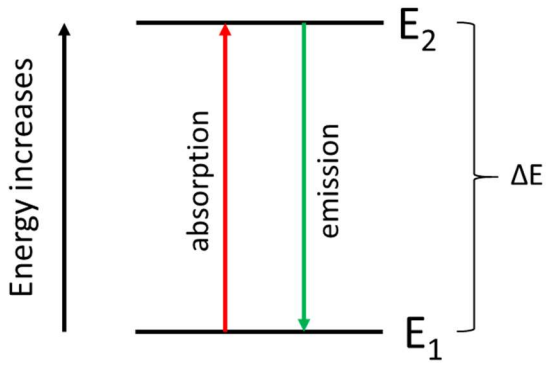

Figure 1.5 – Energy levels of a molecule. The molecule absorbs light of frequency ν when it is excited from level 1 to level 2; the molecule will emit light of frequency ν when relaxing from level 2 to level 1.

In terms of relative energies, the rotational levels are the lowest, followed by vibrational and electronic. Vibrational spectra, through Infrared (IR) and Raman spectroscopies, are observed in the range of 100 to 10000 cm^{-1} (Far IR to Near IR). Not all transitions are allowed, and the selection rules are different for each spectroscopy, as discussed below.

Infrared and Raman spectroscopies yield similar information about symmetry, bonding order and the functional groups of molecules or ions, but they have different physical origins. Infrared spectra originate in transitions between 2 vibrational levels of the molecule in the electronic ground state. For a vibration to be observed, there has to be a change in dipole involved (selection rule for IR). In contrast, Raman spectra originate as a result of the electronic polarization caused by UV or visible light. The selection rule in this case is a change in polarizability as a result of the vibration.

The origin of Raman spectra can be explained satisfactorily by classical theory. The following derivation is demonstrated in Nakamoto's[31] seminal book "Raman and Infrared Spectra of Inorganic and Coordination Compounds", and reproduced here. *Consider a diatomic molecule that is irradiated by light of frequency v, and electric field E. The electric field fluctuates according to: (where E_0 is the amplitude and t is time)*

$$E = E_0 \cos(2\pi\nu t) \quad (1)$$

Due to the radiation, a dipole moment P is induced in the molecule:

$$P = \alpha E \quad (2)$$

Where proportionality constant between the dipole moment and the electric field, α, is the polarizability of the molecule. If as a result of the radiation the molecule vibrates with frequency ν', the nuclear displacement is given by:

$$q = q_0 \cos(2\pi\nu' t) \quad (3)$$

where q_0 is the vibrational amplitude. For small q_0, the polarizability is a linear function of the nuclear displacement q:

$$\alpha = \alpha_0 + \left(\frac{\partial\alpha}{\partial q}\right) q \quad (4)$$

where α_0 is the polarizability at the equilibrium position, and the rate of change of the polarizability with respect to nuclear displacement, $\left(\frac{\partial\alpha}{\partial q}\right)$, is taken at the equilibrium position. Combining equations 1, 2, 3, 4 gives:

$$P = \alpha_0 E_0 \cos(2\pi\nu t) + \frac{1}{2}\left(\frac{\partial\alpha}{\partial q}\right) q_0 E_0 [\cos(2\pi(\nu + \nu')t) + \cos(2\pi(\nu - \nu')t)]$$

The first term describes light of the same frequency as the incident light: the Rayleigh scattering. If the term $\frac{1}{2}\left(\frac{\partial\alpha}{\partial q}\right) q_0 E_0$ is zero, then the entire rest of the equation is zero – therefore it is the selection rule of Raman scattering. That means that if the vibration ν' does not provoke a change of polarizability with respect to the nuclear displacement of the molecule, then ν' is not Raman active. Lastly, the terms in square brackets describe vibrations that are displaced from the incident light's frequency by +ν' and -ν', and are the anti-Stokes and Stokes lines. As a result, Raman spectra vibrations are *shifts* from the incident light frequency. The incident light frequency is set as zero, and the Raman shifts

are distributed as negative (Stokes) and positive (anti-Stokes) peaks in the resulting spectra. Rayleigh scattering is much stronger than the Raman scatterings, therefore a strong light source is employed (lasers).

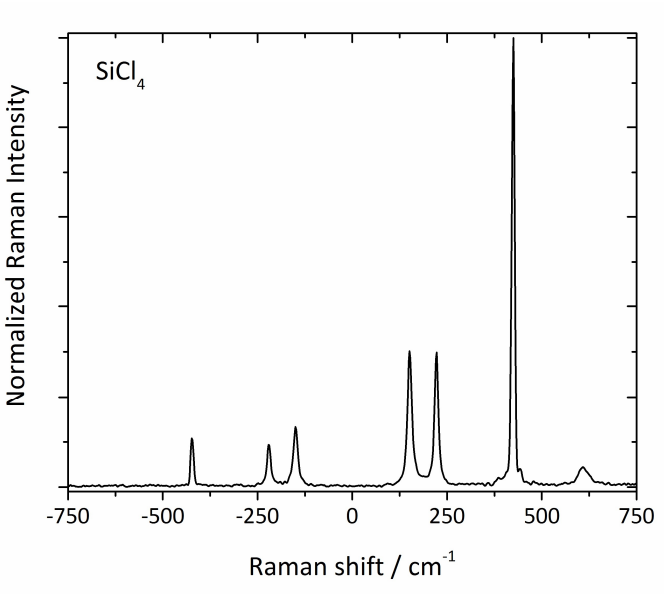

Figure 1.6 – Raman spectrum of silicon tetrachloride. The peaks on the negative side are the Stokes lines, and the peaks on the positive side are the anti-Stokes lines. Molecules at ν are excited to ν' by scattering light of frequency ν- ν' (Stokes). Molecules at ν' revert to ν by scattering light of frequency ν+ ν' (anti-Stokes). The relative intensities come from the relative distribution of molecules in ground and the excited state – the anti-Stokes lines are more intense because there are more molecules in the ground state than in the excited state (Maxwell-Boltzmann distribution law). This spectrum was collected in the Leroy-Eyring Center for Solid State Science at Arizona State University by the author.

To predict if a certain vibration is Raman active, one can recur to group theory. That is because the symmetry of the molecule determines if a change in polarizability will occur. Since the Raman shifts are dependent on the symmetry of the molecule, one can resolve its geometry and functional groups present, as well as bond orders. In the following

chapters, Raman spectroscopy is used alongside solid-state NMR to perform the structural characterization of the new compounds produced in this work.

1.4 References

(1) Padhi, A.; Nanjundaswamya, K.; Goodenough, J. *J. Electrochem. Soc.* **1997**, *144* (4), 1188.

(2) EG&G Technical Services. *Fuel Cell Handbook*, 7th ed.; US Department of Energy: Morgantown, 2004.

(3) Baranov, A. I.; Shuvalov, L. A.; Shchagina, N. M. *JETP Lett.* **1982**, *36* (11), 459.

(4) Matsuo, Y.; Saito, K.; Kawashima, H.; Ikehata, S. *Solid State Commun.* **2004**, *130* (6), 411.

(5) Moskvich, Y. N.; Rozanov, O. V.; Sukhovsky, A. A.; Aleksandrova, I. P. *Ferroelectrics* **1985**, *63* (1), 83.

(6) Haile, S. M.; Chisholm, C. R. I.; Sasaki, K.; Boysen, D. A; Uda, T. *Faraday Discuss.* **2007**, *134*, 17.

(7) Haile, S. M.; Boysen, D. A; Chisholm, C. R.; Merle, R. B. *Nature* **2001**, *410* (6831), 910.

(8) Chisholm, C. R. I.; Haile, S. M. *Solid State Ionics* **2000**, *136*, 229.

(9) Mohammad, N.; Mohamad, A. B.; Kadhum, A. A. H.; Loh, K. S. *J. Power Sources* **2016**, *322*, 77.

(10) Boysen, D. A.; Uda, T.; Chisholm, C. R. I.; Haile, S. M. *Science* **2004**, *303* (2004), 68.

(11) Uda, T.; Haile, S. M. *Electrochem. Solid-State Lett.* **2005**, *8* (5), A245.

(12) Nagaura, T.; Tozawa, K. *Prog. Batter. Sol. Cells* **1990**, *9*, 209.

(13) Xu, K. *Chem. Rev.* **2004**, *104* (10), 4303.

(14) Tarascon, J. M.; Guyomard, D. *Solid State Ionics* **1994**, *69* (3-4), 293.

(15) Kamaya, N.; Homma, K.; Yamakawa, Y.; Hirayama, M.; Kanno, R.; Yonemura,

M.; Kamiyama, T.; Kato, Y.; Hama, S.; Kawamoto, K.; Mitsui, A. *Nat. Mater.* **2011**, *10* (9), 682.

(16) Briant, J.; Farrington, G. *J. Solid State Chem.* **1980**, *33*, 385.

(17) Xu, K. *Chem. Rev.* **2014**, *114*, 11503.

(18) Pearson, G. *J. Am. Chem. Soc.* **1963**, *85* (22), 3533.

(19) Minami, T. *Solid State Ionics for Batteries*; Tatsumisago, M., Wakihara, M., Iwakura, C., Kohjiya, S., Tanaka, I., Eds.; Springer-Verlag: Hicom, 2005.

(20) Ansari, Y.; Tucker, T. G.; Angell, C. A. *J. Power Sources* **2013**, *237*, 47.

(21) Ansari, Y.; Tucker, T. G.; Huang, W.; Klein, I. S.; Lee, S.-Y.; Yarger, J. L.; Angell, C. A. *J. Power Sources* **2016**, *303*, 142.

(22) Eaborn, C. *J. Organomet. Chem.* **1975**, *100*, 43.

(23) Eaborn, C. *J. Chem. Soc.* **1956**, *1* (4858), 4858.

(24) Matyjaszewski, K.; Chen, Y. L. *J. Organomet. Chem.* **1988**, *340*, 7.

(25) Bassindale, A. R.; Stout, T. *J. Organomet. Chem.* **1984**, *271*, C1.

(26) *Impedance Spectroscopy*; MacDonald, J. R., Ed.; John Wiley & Sons: New York, 1987.

(27) *Solid State Electrochemistry*; Bruce, P. G., Ed.; Cambridge University Press: Cambridge, 1995.

(28) Randles, J. E. B. *Discuss. Faraday Soc.* **1947**, *1*, 11.

(29) Lide, D. R. *Handb. Chem. Phys.* **2003**, *53*, 2616.

(30) *Solid-State NMR Spectroscopy Principles and Applications*; Duer, M. J., Ed.; Blackwell Science Ltd: Malden, MA, 2002.

(31) Nakamoto, K. *Infrared and Raman spectra of inorganic and coordination compounds*, 3rd ed.; Wiley: New York, 1978.

CHAPTER 2

SILICON HYDROGENSULFATES: SOLID ACIDS WITH GIANT CONDUCTIVITIES AND POSSIBLE FUEL CELL APPLICATIONS

2.1 Introduction

The best known and most widely applied solid acids are the zeolitic acid catalysts and their mesoporous aluminosilicate cousins which are involved in industrial processes worth many billions of dollars of industrial output every year. We are not concerned with these macromolecular systems in this work but with solid acids that are simple molecular substances in which the unit molecules each carry one or more protons. In the forms of interest, the molecules are free to rotate on their lattice points, passing their protons along random paths in directions determined by any electric field that is applied to them. They lie in between aqueous and molecular liquid acids (like lead battery acid and H_3PO_4) and the solid super acids of the carborane[1] acid type that are mostly well organized crystals that possess either hydrated protonic cations[2] or, more recently, bare protons of exceptional proton activity[3]. The new materials we will introduce herein are closely related to the alkali hydrogen sulfates of Haile and co-authors for fuel cell applications[4,5], but now function above a solid state transition that usually occurs well above 100ºC. Those we will describe below are in most cases well above any transition temperature at ambient temperature, but are also insoluble in water so have the possibility of fuel cell function, and other possible

applications, within the lower (-50 to -100ºC) temperature range. They were initially prepared as precursor stages for the generation of a new class of solid state alkali metal conductors for possible application in the lithium and sodium battery technologies. However, their exceptional characteristics, such as conductivities of ~100 $mScm^{-1}$ at 50ºC (within 20% of that of liquid phosphoric acid), lead us to report them separately for their own special interest. The lithium compounds are reported in Chapter 3.

The new solid acids are silicon derivatives, that were suggested by our recent work on silicophosphates[6,7]. They were initially prepared by reaction of tetrachlorosilane $SiCl_4$ with pure H_2SO_4, to produce $Si(SO_4H)_4$ (a known compound previously prepared during the study of solutions of organosilicon compounds in sulfuric acid, and only characterized by cryoscopy and conductimetry[8]), but have since been prepared under greater control by the reaction of H_2SO_4 with phenyl chlorosilanes, and related phenylated silane derivatives discussed below. The phenyl chlorosilanes, and methyl and alkoxy derivatives, are cheaply available and widely used in a number of synthetic applications due to the ease of cleavage of the aryl-silicon bond[9], allowing for their conversion into useful compounds for a multitude of organic reactions[10]. The phenyl group is much more easily displaced than the chloro ligand[11] which in turn is more easily replaced than alkoxy and methyl ligands, in that order. This has permitted us to produce, at least approximately, all members of the series of chlorosilylsulphuric acids, from $Si(SO_4H)_4$ through $SiCl_3HSO_4$ by simple displacement reactions of the type

$$Ph_xSiCl_{4-x} + xH_2SO_4 \rightarrow Cl_{4-x}Si(HSO_4)_x + xC_6H_6 \quad \text{(i)}$$

where the product benzene is soluble in any unreacted $PhSiCl_3$ starting material and is easily separated from the solid product of the reaction by decantation followed by careful washing with dichloromethane, 1,2-dichloroethane or dioxane and filtering under vacuum (some details, and complications concerning reaction time dependence and dimerization kinetics etc., are given below and in the Methods). The idealized products are designated H4 through H1, for the number of SO_4H groups attached to the Si. By related procedures (see Methods) we have also obtained methyl, methoxy and ethoxy derivatives, designated Me_3H1, $MetOx_3H1$ and $EtOx_3H1$, that also prove to be excellent protonic conductors. Finally, due to the recognized concern of the known instability of sulfur compounds towards hydrogen[12], a mixed sulfate-phosphate compound was also prepared. The compound was named SiP_2S_2 and its idealized formula is $Si(HSO_4)_2(H_3PO_4)_2$. Due to the fundamental difference between this last compound and the others, it will have its own separate discussion.

2.3 Methods

2.3.1 Synthesis of silicon tetrahydrogensulfate (H4) from $SiCl_4$, and an adduct trap for HCl gas.

$Si(HSO_4)_4$, H4: The reaction was performed in a closed system, comprised of a 3-neck Schlenk reaction flask. One of the joints contained a cold finger maintained at a temperature of approximately -20°C and another joint was attached to a tube containing an HCl trap. The HCl trap was a liquid mixture of two adducts: diethylmethylamine (DEMA)/aluminum chloride and 2-methylpyrine/aluminum chloride 70:30 in weight. HCl trap characterization was performed by ^1H NMR. Sulfuric acid (99.999%, Sigma-Aldrich)

and silicon tetrachloride (99%, Sigma-Aldrich) were added to the Schlenk flask under argon atmosphere, in a mole ratio of 4:1. The mixture was kept at 50ºC for 24 hours with constant stirring. The constant evolution of bubbles from the mixture indicated the liberation of HCl gas. The final product was a white solid (H4) and a transparent liquid ($SiCl_4$, confirmed by ^{29}Si-NMR and ICP-OES).

2.3.2 Chlorosilyl hydrogensulfates: H1 and H2

($SiCl_3Ph + H_2SO_4$), H1: trichlorophenylsilane (97%, Sigma-Aldrich) was added to sulfuric acid (99.999%, Sigma-Aldrich) under argon atmosphere, with slight excess of the silane. The mixture was kept under constant stirring in an open vial for different times depending on the preparation: 8 minutes, 32 minutes or 3h30 minutes (approximate times). The final product was a white solid (H1) suspended in a colorless, transparent liquid, which was determined to be a mixture of benzene and excess starting silane, via ^{1}H NMR. The samples were quenched with $LiNH_2$ to stop the reaction and examine the products present via ^{29}Si MAS-NMR. The quenching was done by carefully adding excess $LiNH_2$ to the reaction mixture under N_2 flow and subsequently homogenizing with mortar and pestle.

$SiCl_2(HSO_4)_2$, H2: dichlorodiphenylsilane (97%, Sigma-Aldrich) was added to sulfuric acid (99.999%, Sigma-Aldrich) in a 1:2 mol ratio under argon atmosphere, with slight excess of silane. The mixture was kept under constant stirring in an open vial for different times depending on the preparation: 8 min, 30 min, 60 min and 1h50 min (approximate times). The final product was a white solid (H2) suspended in a colorless,

transparent liquid, which was determined to be a mixture of benzene and excess starting silane via ^{1}H NMR.

2.3.3 Alkoxysilyl hydrogensulfates: MetOx$_3$H1 and EtOx$_3$H1

Si(CH$_3$O)$_3$(HSO$_4$), MetOxH1: trimethoxyphenylsilane (97%, Sigma-Aldrich) was added to sulfuric acid (99.999%, Sigma-Aldrich) in a 1:1 mol ratio under argon atmosphere (with slight excess of silane). The mixture was kept under constant stirring for 30 min. The final product is a white, opaque solid (MetOxH1) and a colorless, transparent liquid, which was determined to be a mixture of benzene, methanol and starting silane via ^{1}H NMR.

Si(CH$_3$CH$_2$O)$_3$(HSO$_4$), EtOxH1: triethoxyphenylsilane (97%, Sigma-Aldrich) was added to sulfuric acid (99.999%, Sigma-Aldrich) in a 1:1 mol ratio under argon atmosphere (with slight excess of silane). The mixture was kept under constant stirring for 30 min. The final product is a white, opaque solid (EtOxH1) and a colorless, transparent liquid, which was determined to be a mixture of benzene, ethanol and starting silane via ^{1}H NMR.

2.3.4 Alkylsylyl hydrogensulfate: Me$_3$H1

Si(CH$_3$)$_3$(HSO$_4$): trimethylphenylsilane (99%, Sigma-Aldrich) was added to sulfuric acid (99.999%, Sigma-Aldrich) in a 1:1 mol ration under argon atmosphere (with slight excess of silane). The mixture was kept under constant stirring for 30 min. The final product is a yellow liquid. NMR: $^{1}H\delta$= 0.37, 11.29 ppm; $^{13}C\delta$=-0.67 ppm; $^{29}Si\delta$=37.34 ppm.

2.3.5 Mixed anion compound, SiP_2S_2

$Si(H_3PO_4)_2(H_2SO_4)_2$: triphenylchlorosilane (97%, Alpha) was melted at 100ºC under argon atmosphere, then a mixture of sulfuric and phosphoric acids was added to it, dropwise (1:2:2 molar ratios, respectively). Following a violent evolution of gas (benzene and hydrochloric acid), a yellow very viscous liquid is formed. Upon standing the liquid slowly crystallizes in the timescale of weeks.

2.3.6 Materials Characterization

Solid-state NMR The solid-state NMR data were collected using a Bruker 400 MHz AVANCE III spectrometer equipped with a 4mm double resonance broad-band magic angle spinning probe at 25 °C. ^{1}H and ^{29}Si NMR data for the solid acid H4, were collected by placing the corrosive material into a 50 µL Kel-F rotor insert obtained from Bruker, to limit the potential for acid exposure to the probe. ^{1}H MAS NMR spectra of this material were collected using a 4.25 µs π/2 pulse, a recycle delay of 10 seconds and 64 scans. The Direct polarization (DP) ^{29}Si spectrum for the solid acid H4 was collected with a 2.3 µs π/6 pulse corresponding to a B_1 field of 35 kHz, a recycle delay of 180 seconds, and 1024 scans. $^{1}H \rightarrow ^{29}Si$ cross polarization (CP) MAS spectrum for H4 was collected with a recycle delay of 1 second, 32k scans, a contact time of 5 ms, a MAS rate of 5 kHz, and a ^{1}H π/2 pulse of 4.0 µs. The CP condition was optimized by setting the ^{29}Si power for the contact pulse at 35 kHz and optimizing the ^{1}H power for the +1 spinning side band of the Hartmann Hahn match condition (40 kHz). During the contact pulse, the ^{1}H rf power was ramped from 50 % to 100 %. CP-MAS and DP-MAS data were collected with approximately 60 kHz two pulse phase modulated (TPPM) ^{1}H decoupling[39] during data

acquisition. ^{29}Si DP-MAS spectra collected on the solid-acid products obtained from reactions quenched with lithium amide, were center packed into 4 mm MAS rotors using Teflon plugs above and below the sample to maximize the amount of sample in the active volume of the spectrometer. Data were obtained using a 1.0 μs π/12 pulse corresponding to a B_1 field of 35 kHz, a recycle delay of 10 seconds, 1-8 k scans, a MAS rate of 5 kHz and no ^{1}H decoupling. Decoupling was not required due to the reaction of lithium amide with a significant portion of the ^{1}H nuclei of the solid acid material, resulting in a substantially reduced ^{1}H dipolar network. ^{13}C DP-MAS NMR data were collected for the MetOxH1 material, by center packing the lithium amide quenched material into a 4 mm MAS rotor using plugs of Teflon. The spectra were collected using a 5.0 μs π/2 pulse, 10 second recycle delay, 256 scans, a MAS rate of 10 kHz, and approximately 60 kHz TPPM ^{1}H decoupling. All solid-state NMR spectra were collected with a MAS rate of 5 kHz, and were externally referenced to TMS in the solid state using adamantane (^{1}Hδ=1.63 ppm, ^{13}Cδ=38.48 ppm) and tetrakis(trimethylsilyl)silane (^{29}Siδ=-9.69 ppm) for ^{1}H, ^{13}C and ^{29}Si spectra respectively[14].

Liquids NMR The liquids NMR spectra were collected using a Varian MR 400 MHz equipped with a 5 mm broadband observe probe. The samples were externally referenced to TMS in the liquid state.

FT-Raman spectroscopy The FT-Raman spectra were collected from 100 to 3500 cm^{-1} using a FT-IR/FT-Raman Bruker IFS66V/S spectrometer using a YAG laser (1064 nm) and a Ge detector. The spectral resolution is 4 cm^{-1}. The samples were inside glass vials under argon atmosphere during the measurements.

Electrochemistry Conductivity data were calculated from Nyquist plots obtained from electrochemical impedance spectroscopy measurements. The spectra were collected in a PARSTAT VMP2 using a 10 mV polarization and frequency range of 200 KHz to 10 Hz. Fuel cell polarization curves were measured using a PARSTAT 2273 with a scan rate of 20 mV/s (H4) and 5 mV/s (MethOxH1), with the samples inside a programmable Vulcan furnace. The membrane electrode assembly (MEA) followed the procedures reported previously by our group[7,15]. The C/Pt gas diffusion electrodes (GDE) were purchased from Advent. Phosphoric acid 85% was lightly brushed on the surface of the electrodes to aid in the gas/electrode/electrolyte interface. In the MetOxH1 experiment, the electrolyte was incorporated in 2 sheets of Celgard 3401 to minimize the effect of fuel crossover. Phosphoric acid 85% was lightly brushed on the Celgard membrane surface to aid in the gas/electrode/electrolyte interface. The SiP_2S_2 viscous liquid was incorporated in a quartz fiber filter paper, and the GDEs were carefully placed on both sides of the membrane. Then the membrane was left to solidify and the measurements were taken on the solid state.

Computer simulations. Gas phase structural optimizations of the compounds H4, H3, H2 and H1 were performed with the software Gaussian[16] package, using Density Functional Theory. The functional B3LYP and the basis set 6-311G(d,p) were used in all of the simulations.

2.4 Results and Discussion

The initial strategy to make the series of compounds in this work was to react different equivalents of nominally anhydrous sulfuric acid with silicon tetrachloride under inert atmosphere:

$$SiCl_4 + xH_2SO_4 \rightarrow SiCl_{4-x}(HSO_4)_x + xHCl \text{ (ii)}$$

The attempt to make all of the combinations, from H4 to H1 (the nomenclature adopted here represents the number of hydrogensulfate groups bonded to the silicon center) was made, but subsequent structural characterization by solid-state NMR showed that the compounds were all indeed H4. A gas-phase computer simulation study was performed using Gaussian with the DFT level of theory and B3LYP functional with 6-311G(d,p) basis set. The geometries of the compounds H4 through H1 were optimized and their energies calculated. Indeed, the lowest energy compound obtained was the tetrahydrogensulfate (H4), see Figure 2.1. That agrees with the experimental observation that the reactions preferentially yield the tetrasulfated structure. Additionally, octahedral geometries were attempted, but none of them yielded stable compounds.

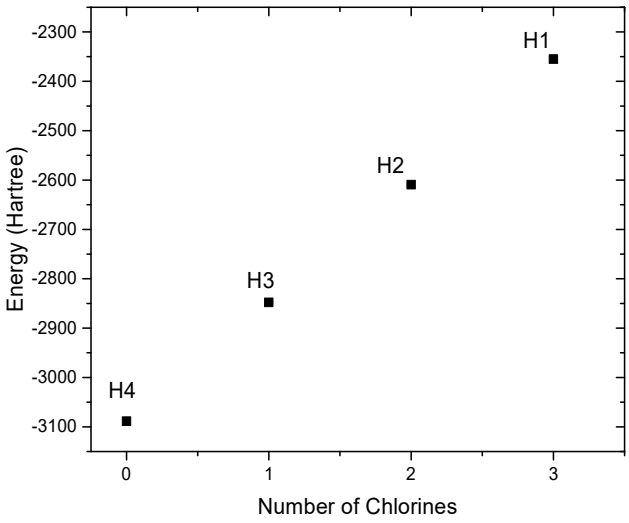

Figure 2.1 – Simulated energies of the chlorohydrogensulfates H4, H3, H2 and H1. Note how the energy of the compounds correlate linearly with the number of chlorines, and increase with the number of chlorines in the structure.

Although different compounds could not be prepared by the $SiCl_4$ synthesis procedure, this was still the preferred method to prepare H4. Another challenge to be overcome in this procedure is the volatility of silicon tetrachloride. Its low boiling point of 60^oC warrants great care to not lose the reagent during the synthesis, which would yield in an excess of sulfuric acid contaminating the product. Simple reflux methods were first employed, but were found unsatisfactory. To ensure that all of the sulfuric acid had reacted, a large excess of silicon tetrachloride was used and a closed system reaction was developed (see Methods). A HCl sink was developed to trap this gas, and thus shifting the equilibrium to the formation of products (and also preventing the system from becoming under dangerously high pressures).

The HCl sink devised was a liquid adduct mixture of (70:30 by weight) $AlCl_3$:DEMA and $AlCl_3$:α-picoline. The idea is to trap the HCl by a Lewis acids base reaction: binding the acidic proton to the lone electron pair of the bases (DEMA and α-picoline) and donation of the chlorine to $AlCl_3$ to form $AlCl_4^-$. An initial test of the capacity of the HCl sink resulted in 14% by weight entrapment. The color of the liquid changes from black to a lighter shade of brown after HCl entrapment. ^1H NMR was performed before and after exposure of the HCl sink, and the results are shown in Figure 2.2.

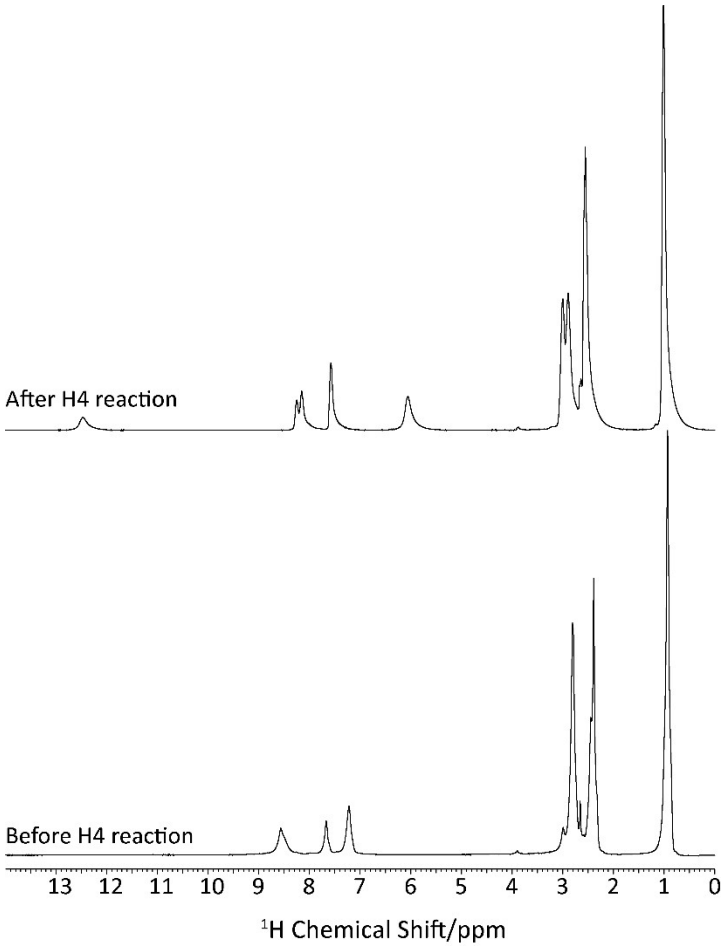

Figure 2.2 - ^{1}H NMR spectra of the HCl trap before (bottom) and after (top) exposure to the atmosphere of the H4 reaction. Note the appearance of 2 peaks after exposure to HCl: at 11 ppm attributed to the protonated α-picoline and at 6 ppm attributed to protonated DEMA.

To produce compounds with chlorine ligands, another strategy was devised, as described in the Introduction and mechanism shown in Chapter 1, section 1.2.1. The acids obtained are translucent or transparent gel-like materials reminiscent of the succinonitrile that has been used as a solid solvent for lithium salts by Armand and coauthors[17]. Me_3H1 is the only liquid acid of the entire series. It is less viscous than dry sulfuric acid, and more

conductive. Strikingly, it is also less conductive than some of the solid acids we have prepared. Indeed, all are excellent protonic conductors. To the best of our knowledge, they have far the highest ambient temperature proton conductivities of any solid state material reported to date.

Some results are shown in Figure 2.3. Conductivities as high as 21.5 mS/cm at room temperature are notable (the case of H1, nominally Cl_3SiSO_4H, but see "structural characterization" section below for refinements). It is remarkable to find a formally solid material that is almost as conductive as liquid phosphoric acid. We draw special attention to the case of Me_3H1 which is found to be a liquid, not a soft solid. Despite its liquid state, the conductivity is significantly lower than those of a number of the other solid acids. This suggests that the conduction mechanism is a quasi-free proton hopping process, that takes advantage of, but is not limited by, the rotational freedom of the globular conjugate base moiety.

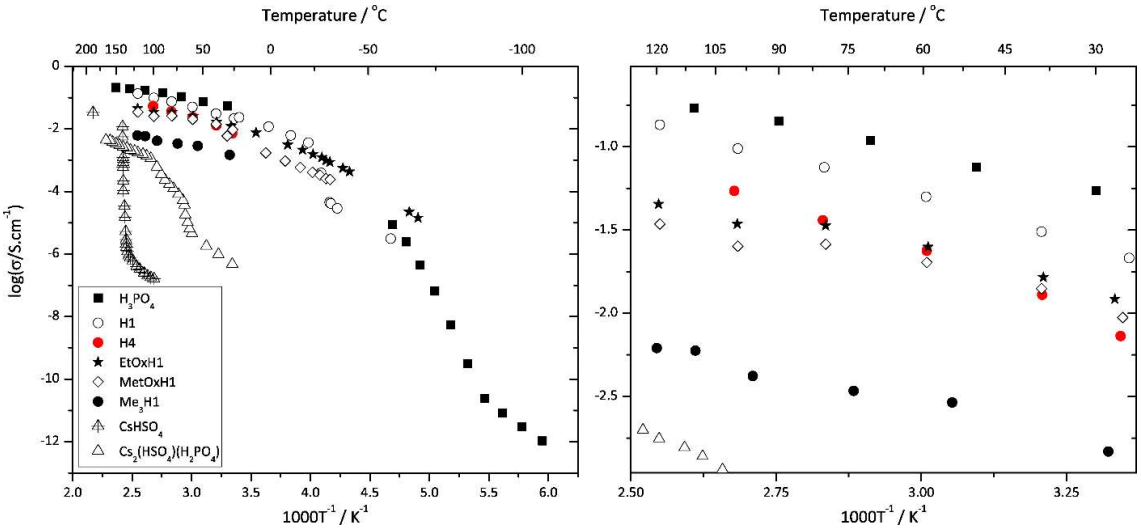

Figure 2.3 - *Left hand panel:* Arrhenius plot of the conductivities of some of the acids synthesized in this work, making comparison with literature data for pure liquid phosphoric acid[18,19], $CsHSO_4$[20], and the previous best case plastic crystal protonic conductor, $Cs_2(HSO_4)(H_2PO_4)$[21]. Note the inferior position of the only liquid acid of our series (Me_3H1) relative to the solid acids H1, $MetOx_3H1$, $EtOX_3H1$. Only in the case designated "H1", is a transition to a less-conducting phase observed (at sub-zero temperatures) during measurement. At sub-zero temperatures, the conductivity of $EtOx_3H1$ exceeds that of liquid phosphoric acid. *Right hand panel:* Details of the region between 30 and 120°C to show the differences in conductivity between the acids prepared in this work.

The chlorinated solid acids prepared in this work are generally highly reactive, fuming in air and reacting with most solvents (exceptions include dichloromethane, and 1,2-dichloroethane which is known to be stable in the presence of strong acids like sulfuric acid[22]) and dioxane, but these do not offer any measurable solubility for the new compounds. Other indications of their reactivity are their destructive corrosion of Teflon-coated spatulas, stainless steel instruments and various plastics. For instance, attempts to use Celgard 3401 as a support results in the immediate and complete destruction of the membrane. The unchlorinated examples of the solid acids are less reactive. Their acidities,

as indicated by the ^{1}H NMR chemical shift of the liquid obtained by proton transfer to diethylmethylamine (acid classification method[23]) are similar to those of methanesulfonic acid and the $HSO4^-$ anion) which is unsurprising. As such it might be expected that they might provide interesting solid electrolytes for fuel cell operation and some trials of this possibility reported at the end of this contribution will provide proof of this principle.

Structures of the solid acid conductors

In order to elucidate the structures that are making these unusual properties possible, we have carried out a series of ^{1}H and ^{29}Si solid-state NMR measurements (experimental details in Methods section). The ^{1}H NMR spectrum of the tetrahydrogensulfate silane (H4) is shown along with a comparable spectrum for adamantane for reference in Figure 2.4. Adamantane is routinely used as a chemical shift standard in solid-state NMR[14] due to its well-characterized plastic crystalline phase at ambient temperatures, which leads to sharp resonances. The C4 relaxation time for adamantine is 18.5 ps at ambient temperature according to multiple sources (quasielastic neutron scattering[24] and NMR spectroscopy[25]). The much narrower line shape of the resonance associated with tetrahydrogensulfate might be partly a consequence of the more globular shape of the tetrahydrogen sulfate (the rotation time for CBr_4 rotator phase is about ~0.5 ps[26]) but might also reflect an additional sharpening due to a faster proton motion which decouples from the molecular rotation, i.e. a superprotonic state consistent with the exceptional conductivity. A further comparison is made with a ^{1}H liquid-state NMR spectrum of anhydrous H_2SO_4, which is of course narrower due to the isotropic tumbling of the molecules in the non-viscous liquid. Finally, we include the narrow resonance from

the only liquid member of the present series of acids, the trimethyl-hydrosulfatosilane, $(CH_3)_3SiSO_4H$, abbreviated Me_3H1 in our figures which is seen to have a similar but less intense resonance, consistent with the single acid proton of this molecule.

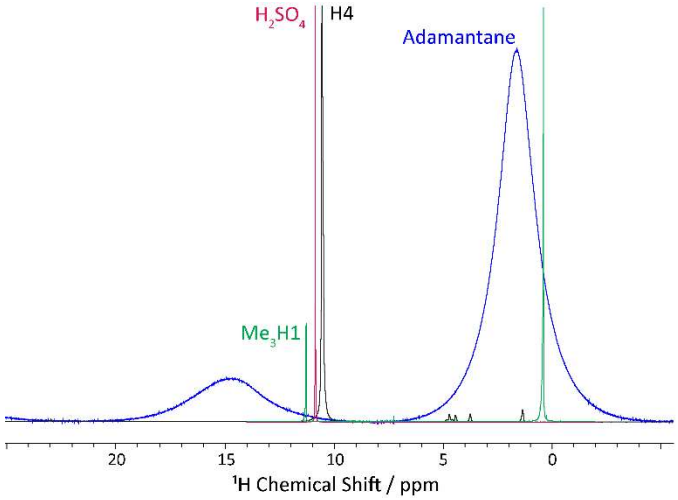

Figure 2.4 - Direct ^1H MAS NMR of the solid acid H4 ($Si(SO_4H)_4$) compared with that for adamantane, and ^1H liquid-state NMR spectra of Me_3H1 ($Si(CH_3)_3SO_4H$) and 99.99% H_2SO_4. MAS rate: 5 kHz. Adamantane is a plastic crystal with reorientation relaxation time of 1.85 x 10^{-11}s. The resonance for H4 protons (all equivalent), is far the sharper, indicative of a much shorter rotation time and/or greater H^+ mobility. The proton spectrum of nominally anhydrous sulfuric acid from Sigma-Aldrich (the same used in the preparations of this work) measured in a regular liquids probe, is included for comparison. Strong arguments against the presence of any residual H_2SO_4 itself in the H4 sample, are provided in text and later figures.

The fact that H4, Me_3H1 and sulfuric acid have similar ^1H chemical shifts is not surprising, since the protons removed in the formation of H4 leaves the oxygen still bonded to the very polarizing Si species. The similarity in chemical shift is also seen in the case of $CsHSO_4$, which exhibits shifts of 11-13 ppm depending on the sample history[27]. The similarity of the ^1H NMR spectra does, however, require some reassurance that the

properties we are observing are not due to residual unreacted H_2SO_4. Firstly, in the synthetic procedure, care was taken to use a large excess of $SiCl_4$ or phenyl silane, and subsequently to wash the solid product thoroughly with 1,2-dichloroethane, followed with a vacuum filtration under inert atmosphere. Additionally, we show in Figure 2.5 that the Raman spectrum of H4 is free of the symmetry-dictated lines characteristic of H_2SO_4, indicating that there is no appreciable unreacted H_2SO_4 in the final material.

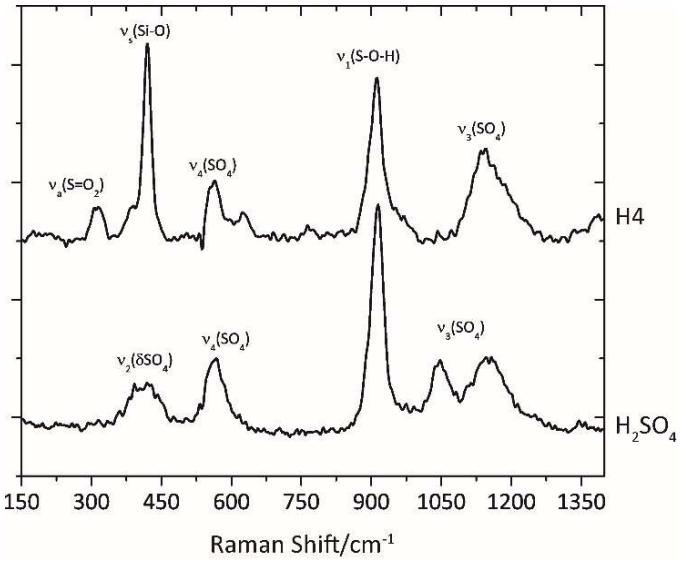

Figure 2.5 - FT-Raman spectra of H4 (top) and sulfuric acid (bottom). Note how the ν_3 peaks, at 1100 cm^{-1}, are split in sulfuric acid; in the H4 spectrum, the ν_3 mode is a single peak. This is analogous to the cases of other hydrogensulfates, like $NaHSO_4$[28] and $CsHSO_4$[29,30]. Legend: s = symmetric, a = asymmetric; ν = stretch, δ = bend.

The most intense peak in the Raman spectrum of H4 is ν_sSiO at 419 cm^{-1}. That is the first difference from the spectrum of pure sulfuric acid, with its most intense peak at 914 cm^{-1} attributed to the ν_1 mode[31,32] (ν_sS-O-H). This mode is also present in H4, at the exact same frequency. That suggests that the strength of the hydrogen bonding in H4 is

comparable to that of sulfuric acid. That is very different from the case of $CsHSO_4$, where the ν_1 mode is located at considerably lower frequencies (860 cm^{-1} at room temperature), albeit dependent on the crystallographic phase[29,30]. That indicates a decrease in the strength of hydrogen bonding when compared to pure sulfuric acid and H4. The second glaring difference between the two spectra is the transformation of sulfuric acid's split ν_3 ($\nu_s S{=}O$) peak at 1048 cm^{-1} after the reaction. This mode appears as a single peak in H4, similarly to other bisulfates, like $NaHSO_4$[28] and $CsHSO_4$[29,30].

More instructive are the ^{29}Si spectra, which we use in different ways. Firstly, there is the simple case of Me_3H1 which is liquid and gives sharp resonance lines despite the low natural abundance of ^{29}Si nuclei. We observe a single ^{29}Si resonance at 37.34 ppm. This value is in good accordance with the literature for a $Si(CH_3)_3SO_3R$ type moiety[33]. Along with unambiguous ^{13}C and ^{1}H (see SI), we can confidently confirm that the target compound Me_3H1 is a simple molecule of formula $Si(CH_3)_3HSO_4$. The material described as MetOxH1, prepared from the 1:1 (molar) reaction of trimethoxyphenyl silane and sulfuric acids, shows two resonances of equal magnitude: -71.4 and -78.4 ppm. These are attributed to a mixture of products, respectively $PhSi(CH_3O)_2(HSO_4)$ and $Si(CH_3O)_3(HSO_4)$[34,35]. A preparation free of unreacted phenyl groups would have a higher conductivity.

Secondly we use ^{1}H to ^{29}Si cross polarization and MAS spectroscopy to confirm that the mobile protons in H4 are indeed in the solid state. In this experiment, magnetization is transferred from ^{1}H to ^{29}Si and the signal from the silicon nuclei is detected. For the magnetization transfer to occur, the nuclei must be dipole coupled. The result is that only

the nuclei that are in close proximity and in an environment that is rigid on the NMR time scale, are detected[36,37]. Figure 2.6 shows both direct and cross polarization (DP and CP) ^{29}Si MAS spectra of H4. The spectra show that the silicon atoms in both experiments are in the same chemical environment. The data are consistent with a central silicon atom bonded to four hydrogensulfate groups. Note there is only a single resonance line, consistent with the single molecular species of the H4 preparation. Note that the resonance is at -118 ppm, well upfield from the value of -108 ppm typical of Si tetra coordinated by oxygen in silica polymorphs[34]. This is consistent with the more highly polarized condition of the coordinating oxygens of the sulfato groups.

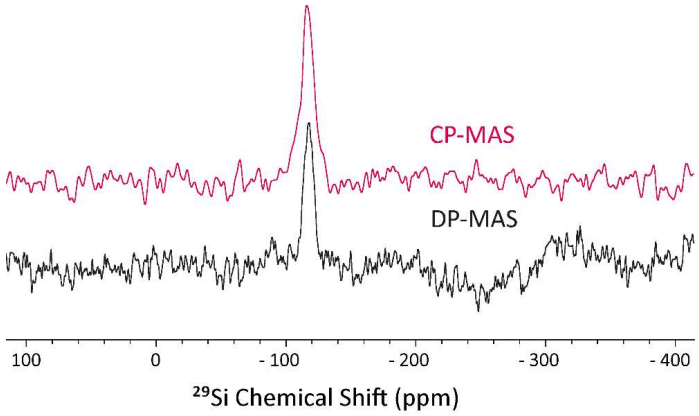

Figure 2.6 – Direct polarization ^{29}Si (DP-MAS, bottom) and cross-polarization ^{1}H-^{29}Si NMR (CP-MAS, top) spectra of H4. The cross polarization experiment demonstrates that the protons are close to the silicon and are rigid, i.e., in the solid state. Spinning rate of 5 kHz.

Thirdly, we use ^{29}Si MAS spectra to explore the more complicated cases of preparations from starting materials containing chlorine. Here, because of the corrosive nature of the chlorinated species we could not risk direct study in the delicate MAS probe so the samples were first neutralized with $LiNH_2$, by solid state reaction in mortar and

pestle. Using the case of target material H1 (nominally $Cl_3Si(HSO_4)$, from starting material Cl_3SiPh) it was found that the structure obtained depended on the time between initiation of the primary reaction and the time at which the reaction was arrested by lithiation. The number of chlorines that were displaced could be determined by comparison with the resonances established by Marsmann[38,34]) from analysis of polysiloxanes obtained from the partial hydrolysis of silicon tetrachloride. These exhibited end (Cl_3SiO-), middle (Cl_2SiO_2-), trifunctional ($ClSiO_3$-) and tetrafunctional (SiO_4-) groups, where the O_n- indicates the number of connections to other silyl groups in the polymer. Our attributions, guided by Marsmann's resonances are shown by vertical dashed lines in Figure 2.7, passing through the spectra of our lithiation-arrested preparations. The reaction times before lithiation are indicated on the individual spectra. The implications of the increasing departure from the intended $Cl_3Si(HSO_4)$ composition in favor of the apparently-preferred symmetric H4 -structure, are stated in the figure caption.

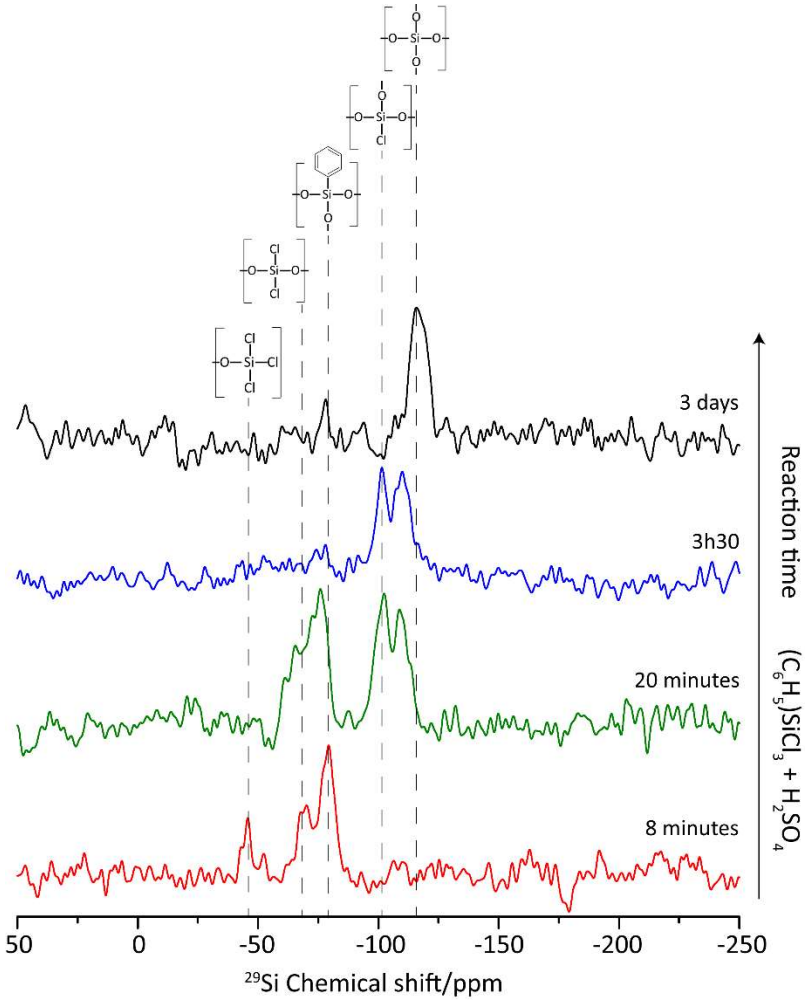

Figure 2.7 - ^{29}Si MAS-NMR of H1 reactions ($Cl_3SiPh + H_2SO_4$) quenched with lithium amide after different reaction times (see Methods), showing the changes that develop in silicon environments as a function of reaction time. Reaction times are marked on the spectra. The figure suggests that for short times the silicon is coordinated mainly by chlorine and oxygen, as expected from equation (i), but that at longer times the chlorine component of already-hydrosulfated molecules is being progressively eliminated by attack of second and third sulfuric acid molecules in preference to the intended formation of additional Cl_3SiSO_4H. The $PhSiO_3$- attribution was made based on references[34,35].

Mixed anion compound: SiP_2S_2

The mixed anion compound warrants its own discussion, due to the striking differences between this and the compounds described earlier in this Chapter. First, this

compound is a very viscous liquid, and its physical state is highly dependent on the preparation method. If the reaction temperature is much higher than 100ºC, the sample readily crystallizes after the evolution of benzene and hydrochloric acid. Therefore, to keep this compound as a liquid, it has to be prepared in small batches (around 200 mg at a time). After crystallization, this compound is soft much like succinonitrile.

The conductivity of both liquid and solid states were assessed, Figure 2.8. Although the conductivity values of the liquid state fluctuate and do not follow the Arrhenius law, the crystallized sample shows a linear correlation. It is remarkable that the conductivities in both states are comparable. That suggests that the protonic relaxation time might be uncoupled from the structural relaxation time.

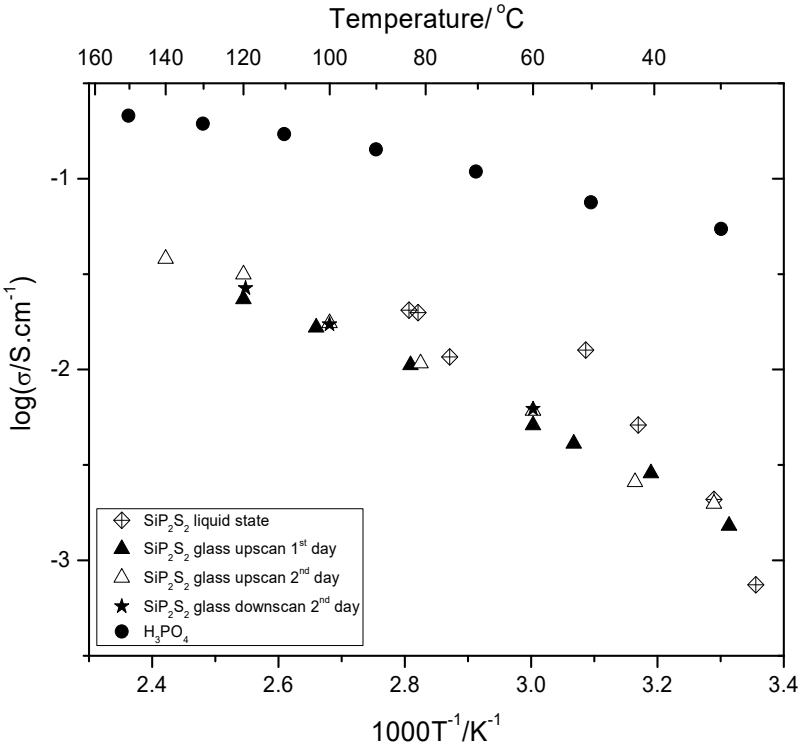

Figure 2.8 – Arrhenius conductivity plot of SiP_2S_2 in the liquid and solid states. Phosphoric acid[17] is shown for comparison.

Structural characterization of SiP_2S_2 was carried out by liquids ^{1}H, ^{31}P and ^{29}Si NMR (Figure 2.9) along with FT-Raman spectroscopy (Figure 2.10). The latter technique was performed in the liquid and crystalline states. The ^{1}H NMR shows acidic protons above 10 ppm and the presence of unreacted phenyl groups around 7 ppm. The ^{31}P NMR shows that there is mainly one phosphorous environment at 2 ppm, which is close in position several hydrogenphosphates: $MgHPO_4.3H_2O$ (1.6 ppm)[39], $NaH_2PO_4.H_2O$ (2.3 ppm)[40] and $K_2HPO_4.3H_2O$ (2.1 ppm)[40]. There are very small additional peaks at -11 ppm, attributed to policondensate phosphates.

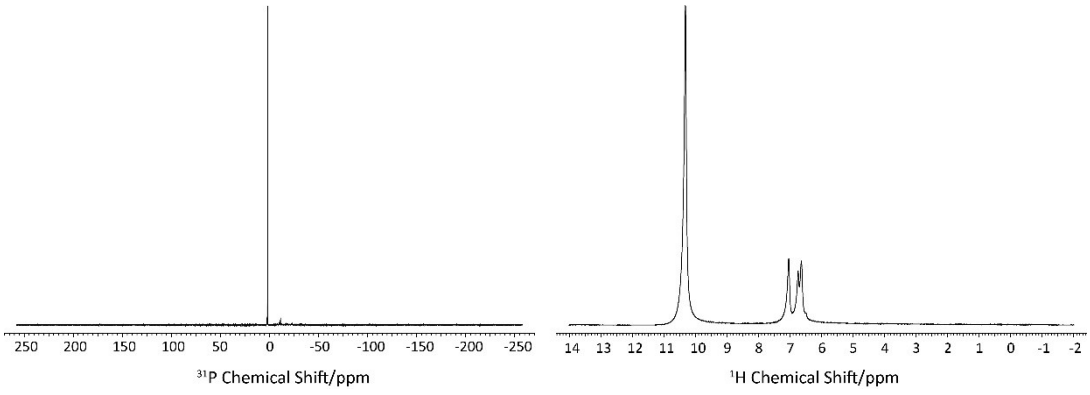

Figure 2.9 – Liquid state ^{31}P (left hand panel) and ^{1}H NMR of SiP_2S_2. The spectra were taken of the neat samples, and externally referenced to Phosphoric acid 85% and TMS, respectively.

The FT-Raman spectra of both liquid and crystallized forms are shown in Figure 2.9. The spectra are dominated by the very intense phenyl normal modes making the identification and interpretation of the very important sulfate and phosphate modes very difficult. The phenyl normal modes are located at 615, 999, 1031, 1165 and 1588 cm^{-1} and are more or less within the 4 cm^{-1} error of the instrument from the literature values of

triphenylchlorosilane[41]. The peak at 320 cm^{-1} is attributed to the skeletal mode of SiCl-bonds[41]. The peaks at 730, 900 and 1128 cm^{-1} can be attributed to νP-O-P[42], ν_sS-O-H[28] and νP-O[42], respectively. The νP-O-P[42] assignment suggest a certain degree of P_2O_7 groups present in the compound. Additionally, we can observe that the spectra are essentially unchanged as a function of crystallization. This result suggests that the solidification of the material is not coming from a polymerization reaction upon standing or a complex gelation process, but rather the crystallization of the liquid form.

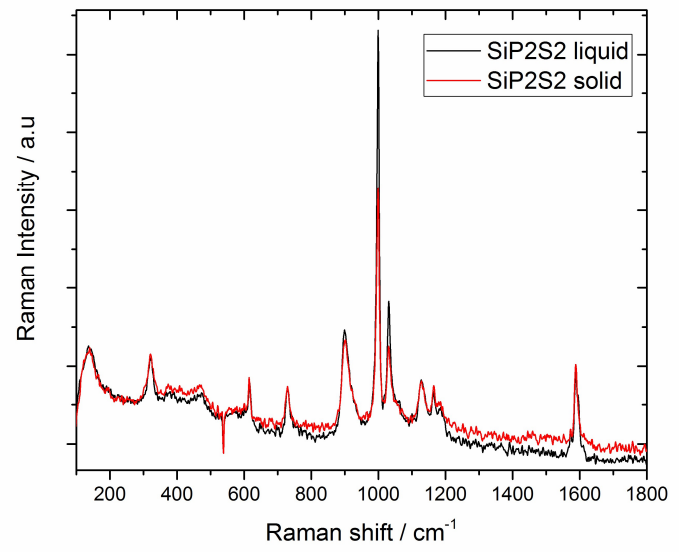

Figure 2.10 – FT-Raman spectra of SiP_2S_2 in viscous liquid form (black line) and crystalline form (red line). The spectra were taken of the same compound, days apart, before and after crystallization took place.

Trial fuel cell applications

While our emphasis in this chapter is on the discovery of a new class of solid acids, the remarkably high conductivities shown in Figure 2.3 suggest that these materials might be strong candidates for electrolytes in all-solid state fuel cells. Since the chlorosilyl hydrogensulfates hydrolyze in water to generate a siloxane and hydrochloric acid, H4,

MetOxH1 and SiP_2S_2 were the candidates of choice for fuel cell performance tests. Tests were carried out in the same Teflon sandwich cell described in a recent paper from this group[7]. Polarization and power curves for these MEAs using the above proton conductors immobilized with the help of a Viton gasket are shown in Figure 2.11. H4 was spread uniformly in a Viton gasket and placed between the GDEs. SiP_2S_2 was impregnated in quartz filter paper while in the viscous liquid state, and the GDEs were carefully placed on both sides forming the MEA. The membrane was then left to stand until the material solidified. In the case of MetOxH1, the electrolyte was placed between 2 sheets of Celgard 3401 and GDEs were placed on either side of the newly formed membrane. It was observed that MetOxH1 does not attack Celgard like H4 and the chlorinated compounds. The use of Celgard in this case was an attempt to fuel crossover. Finally, all of the MEAs were pressed with a vice to ensure good contact.

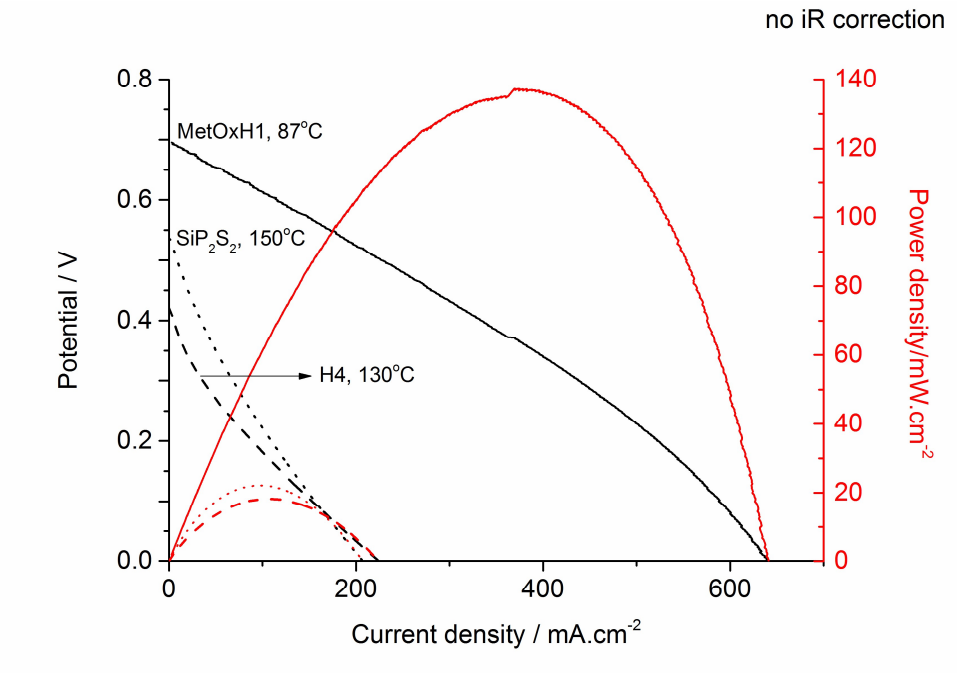

Figure 2.11 - Polarization and power density curves for fuel cells using MetOxH1 (solid lines), H4 (dashed lines) and SiP_2S_2 (dotted lines) as the solid electrolytes. Even though the open circuit potential is considerably lower than the theoretical value in all cases shown, remarkably high maximum current densities of 640, 225 and 207 mA/cm^2 were obtained. Although these are promising results, the fuel cell of H4 is not stable over time, possibly due to the hydrolysis[43] of the electrolyte. These results are not iR corrected.

The open circuit voltages are well below the theoretical value, possibly due to contact issues in the 3-phase boundary (gas/solid electrode/solid electrolyte) and fuel crossover. Similarly, many examples of solid acid fuel cells in the literature have OCVs well below the theoretical value of 1.2 V, as shown in Table 2.1[47]. For example, the solid acid $Tl_3(HSO_4)_2$[44] exhibited a maximum OCV of 0.83V. Although the open circuit voltages might appear comparatively low against the state of the art cesium-based plastic crystals $(CsHSO_4)$[4], $Cs(H_2PO_4)$[45], $Cs(HSO_4)(H_2PO_4)$[21,46], the open circuit current density is almost 6 (H4) and 15 (MetOxH1) times higher than the first solid acid fuel cell described in the

literature[4], despite operating at much milder temperatures. Compared to $Tl_3(HSO_4)_2$[44], MetOxH1 maximum current density is some 5 orders of magnitude higher. The highest OCV shown in Table 2.1 still belongs to the first solid acid fuel cell, $(CsHSO_4)$[4] with 1.11V, but that compound only produced 44 mA/cm^2 of current density at short-circuit and 12 mW/cm^2 power densities.

Table 2.1 – Summary of solid acid fuel cell electrolytes and their fuel cell performances. Reproduced from reference[9].

Electrolyte	Electrocatalyst mixture	Electrode	Assembly method	Operating conditions	Open circuit voltage	Peak power density	Current density
$CsHSO_4$, 1.37 mm thickness	$CsHSO_4$, Pt, C and a volatile organic with mass ratio of 6:10:1:1	Porous graphite	Room temperature pressing method, 490 MPa	150 to 160 °C, water saturated H_2 and O_2 feed	1.11 V	12 mW cm^{-2}	44 mA cm^{-2}
$CsHSO_4$/ alumina	30% Pt/C (Vulcan), 1 mg Pt cm^{-2}	Carbon paper		160 °C, no humidification of H_2 and O_2 feed	0.8 ± 0.05 V	2 mW cm^{-2}	8 mA cm^{-2}
$CsHSO_4$/ porous glass filter paper	20% Pt/C, 0.4 mg Pt cm^{-2}	Carbon cloth impregnated with Nafion®	Hot pressing for 2 minutes at 130 °C and 1000 kgf				No current produced
CsH_2PO_4, 260μm thickness	CsH_2PO_4, Pt, C and naphthalene with mass ratio 6:10:1:1 18 mg Pt cm^{-2}	Carbon paper	Room temperature pressing method, 340 MPa	235 °C, humidified H_2 and O_2 feed, $P_{H2O} = 0.3$ atm.	1.003 V	48.9 mW cm^{-2}	301 mA cm^{-2}
CsH_2PO_4, 100 μm thickness	7.6 mg Pt cm^{-2}	Porous stainless steel		Humidified H_2 and O_2 feed		134 mW cm^{-2}	528 mA cm^{-2}
CsH_2PO_4, 25 μm to 36 μm thickness	CsH_2PO_4, naphthalene, Pt and 50% Pt/C with mass ratio 3:0.5:3:1 7.7 mg Pt cm^{-2}	Porous stainless steel	Slurry deposition and pressing method	Humidified H_2/O_2 feed, $P_{H2O} = 0.3$ atm.	0.96 V on average and maximum of 1.01 V	287 to 415 mW cm^{-2}	
CsH_2PO_4/ SiP_2O_7 , 1.3 mm thickness	Pt/C carbon paper Pt loadings: 1 mg cm^{-2}	Pt/C carbon paper	Room temperature pressing method	0–30% humidity	0.96 V	68 mW cm^{-2}	
$CsH_5(PO_4)_2$/ SiO_2		Pd anode and Pt cathode	Room temperature pressing method, 300 MPa	No humidification of H_2 and O_2 feed	0.85 V	8 mW cm^{-2}	80 mA cm^{-2}
$KH(PO_3H)$, 0.5 mm thickness	$KH(PO3H)$, Pt/C and PTFE in 3:1:1 weight ratio (catalyst loading: 1 mg/cm^2)	Carbon paper	Room temperature pressing method	3% humidification of H_2 and O_2 feed	0.65 V	0.15 mW cm^{-2}	

It is important to note that the solid acid fuel cell tested in this work did not require humidification or high pressure assembly. We are confident that further experiments with attention to fuel crossover problems will lead to OCVs that are closer to the theoretical value, in which case the maximum power output would become rather high when compared to other solid acids. It has not escaped our attention that our fuel cell apparatus is somewhat primitive compared to many of those in the literature and might not be ideal when testing

solid acids. Future work will include improved designs of fuel cells and MEAs to mitigate the fuel crossover problems.

2.5 Conclusions

A new class of solid-state solid acids were prepared with remarkably high conductivies. The structural characterization shows that no excess sulfuric acid is present, and the conductivity is due to the high proton mobility in the new solid compounds. Although some compounds are indeed mixtures formed in the syntheses, their conductivities are still practical for application in fuel cells. The fuel cell measurements showed the feasibility of the application of select compounds as solid state electrolytes. Future work will include proton diffusion studies via NMR, X-ray diffraction measurements and differential scanning calorimetry measurements to assess glass transition temperatures. Finally, further fuel cell performance studies will be carried out where the focus will be directed towards mitigating fuel cross-over effects and thus obtaining OCVs closer to the theoretical value.

2.6 References

(1) Juhasz, M.; Hoffmann, S.; Stoyanov, E.; Kim, K. C.; Reed, C. a. *Angew. Chemie - Int. Ed.* **2004**, *43*, 5352.

(2) Stoyanov, E. S.; Stoyanova, I. V.; Tham, F. S.; Reed, C. A. *J. Am. Chem. Soc.* **2008**, *130* (36), 12128.

(3) Nava, M.; Stoyanova, I. V; Cummings, S.; Stoyanov, E. S.; Reed, C. A. *Angew. Chem. Int. Ed. Engl.* **2014**, *53* (4), 1131.

(4) Haile, S. M.; Boysen, D. a; Chisholm, C. R.; Merle, R. B. *Nature* **2001**, *410* (6831), 910.

(5) Haile, S. M.; Chisholm, C. R. I.; Sasaki, K.; Boysen, D. a; Uda, T. *Faraday*

Discuss. **2007**, *134*, 17.

(6) Ansari, Y.; Ueno, K.; Zhao, Z.; Angell, C. A. *J. Phys. Chem. C* **2013**, *117*, 1548.

(7) Ansari, Y.; Tucker, T. G.; Huang, W.; Klein, I. S.; Lee, S.-Y.; Yarger, J. L.; Angell, C. A. *J. Power Sources* **2016**, *303*, 142.

(8) Flowers, R. H.; Gillespie, R. J.; Robinson, E. A. *Can. J. Chem.* **1963**, *41* (10), 2464.

(9) Eaborn, C. *J. Organomet. Chem.* **1975**, *100*, 43.

(10) Keay, B. A. In *Science of Synthesis, 4: Category 1, Organometallics*; Fleming, I., Ed.; Georg Thieme Verlag: Stuttgart - New York, 2002; p 685.

(11) Matyjaszewski, K.; Chen, Y. L. *J. Organomet. Chem.* **1988**, *340*, 7.

(12) Merle, R. B.; Chisholm, C. R. I.; Boysen, D. a.; Haile, S. M. *Energy and Fuels* **2003**, *17* (1), 210.

(13) Bennett, A. E.; Rienstra, C. M.; Auger, M.; Lakshmi, K. V; Griffin, R. G. *J. Chem. Phys.* **1995**, *103* (16), 6951.

(14) Hayashi, S.; Hayamizu, K. *Bull. Chem. Soc. Jpn.* 1991, pp 685–687.

(15) Ansari, Y.; Tucker, T. G.; Angell, C. A. *J. Power Sources* **2013**, *237*, 47.

(16) Frisch, M. J. et al. *Gaussian 09, Revision A.02*. 2009.

(17) Alarco, P.-J.; Abu-Lebdeh, Y.; Abouimrane, A.; Armand, M. *Nat. Mater.* **2004**, *3* (7), 476.

(18) Greenwood, N. N.; Thompson, a. *J. Chem. Soc.* **1959**, *VI*, 3485.

(19) Wang, Y.; Lane, N. a.; Sun, C. N.; Fan, F.; Zawodzinski, T. a.; Sokolov, A. P. *J. Phys. Chem. B* **2013**, *117*, 8003.

(20) Baranov, A. I.; Shuvalov, L. A.; Shchagina, N. M. *JETP Lett.* **1982**, *36* (11), 459.

(21) Chisholm, C. R. I.; Haile, S. M. *Solid State Ionics* **2000**, *136*, 229.

(22) Hayes, M. J.; Pepper, D. C. *Trans. Faraday Soc.* **1961**, *57*, 432.

(23) Davidowski, S. K.; Thompson, F.; Huang, W.; Hasani, M.; Amin, S. A.; Angell, C.

A.; Yarger, J. L. *J. Phys. Chem. B* **2016**, *120* (18), 4279.

(24) Bee, M.; Amoureux, J. P.; Lechner, R. E. *Mol. Phys.* **2006**, *40* (3), 617.

(25) Amoureux, J. P.; Bée, M.; Virlet, J. *Mol. Phys.* **1980**, *41* (2), 313.

(26) Lynden-Bell, R. M.; McDonald, I. R. *Mol. Phys.* **1981**, *43* (6), 1429.

(27) Hayashi, S.; Mizuno, M. *Solid State Commun.* **2004**, *132* (7), 443.

(28) Zangmeister, C. D.; Pemberton, J. E. *J. Am. Chem. Soc.* **2000**, *122* (15), 12289.

(29) Baran, J.; Marchewka, M. K. *J. Mol. Struct.* **2002**, *614*, 133.

(30) Yamawaki, H.; Fujihisa, H.; Sakashita, M.; Honda, K. *Phys. Rev. B* **2007**, *75* (9), 094111.

(31) Nakamoto, K. *Infrared and Raman spectra of inorganic and coordination compounds*, 3rd ed.; Wiley: New York, 1978.

(32) Walrafen, G.; Yang, W. *J. Solut. ...* **2000**, *29* (10), 905.

(33) Posternak, A. G.; Garlyauskayte, R. Y.; Polovinko, V. V; Yagupolskii, L. M.; Yagupolskii, Y. L. *Org. Biomol. Chem.* **2009**, *7* (8), 1642.

(34) Kintzinger, J.-P.; Marsmann, H. *Oxygen-17 and and silicon-29. (NMR, basic principles and progress; v.17)*, 1st ed.; Diehl, P., Fluck, E., Kosfeld, R., Eds.; Springer-Verlag: Berlin Heidelberg New York, 1981.

(35) Tsumura, M.; Ando, K.; Kotani, J.; Hiraishi, M.; Iwahara, T. *Macromolecules* **1998**, *31* (9), 2716.

(36) Hartmann, S. R.; Hahn, E. L. *Phys. Rev.* **1962**, *128* (5), 2042.

(37) Kolodziejski, W.; Klinowski, J. *Chem. Rev.* **2002**, *102* (3), 613.

(38) Horn, H.-G.; Marsmann, H. C. *Die Makromol. Chemie* **1972**, *162* (1), 255.

(39) Mudrakovskii, I. L.; Shmachkova, V. P.; Kotsarenko, N. S.; Mastikhin, V. M. *J. Phys. Chem. Solids* **1986**, *47* (4), 335.

(40) Turner, G. L.; Smith, K. A.; Kirkpatrick, R. J.; Oldfieldt, E. *J. Magn. Reson.* **1986**, *70* (3), 408.

(41) Smith, A. L. *Spectrochim. Acta Part A Mol. Spectrosc.* **1967**, *23* (4), 1075.

(42) Romain, F.; Novak, A. **1991**, *263*, 69.
(43) Buncel, E. *Chem. Rev.* **1970**, *70* (3), 323.

(44) Matsuo, Y.; Saito, K.; Kawashima, H.; Ikehata, S. *Solid State Commun.* **2004**, *130* (6), 411.

(45) Boysen, D. A.; Uda, T.; Chisholm, C. R. I.; Haile, S. M. *Science* **2004**, *303* (2004), 68.

(46) Yamane, Y.; Yamada, K.; Inoue, K. *Solid State Ionics* **2008**, *179* (13-14), 483.

(47) Mohammad, N.; Mohamad, A. B.; Kadhum, A. A. H.; Loh, K. S. *J. Power Sources* **2016**, *322*, 77.

CHAPTER 3

A NEW CLASS OF FAST ALKALI ION CONDUCTORS: INORGANIC PLASTIC CRYSTALS

3.1 Introduction

The importance of high power portable electrical energy needs no emphasis in a society as devoted to cell phones and laptop computers as ours. The current devices are almost all powered by lithium battery systems in which the ion charge flow that compensates the electron flow from anode to cathode, moves through a liquid electrolyte, commonly immobilized in a gel matrix. In an article assessing conductivity loss due to ion pairing in low dielectric solvents, it was recently lamented, that "*there seems to be little alternative to the compromise that is being made in the adoption of the low ionicity... mixed solvent systems that are currently in use*"[1]. Here we contradict this conclusion by introducing a new class of ionic conducting medium in which the alkali cations are the only mobile species but, unlike their superionic glass relatives, they conduct as well as the liquid electrolytes while being free of their disadvantages. The new materials are salts of alkali cations in which the alkali cations take advantage of rotation of large anions to move freely through the waxy solid medium (glass-like transition at -85ºC), with particular advantages at sub-zero temperatures. Containing anions with elements Si, S, and oxygen, they are non-volatile and non-flammable, inoxidizable, and cheap. Like other plastic crystals, the

materials exhibit (near -90ºC) a glass-like transition where the rotational relaxation time exceeds the measuring time scale.

The problem of moving alkali cations from anode to cathode compartments of electrochemical devices has previously been solved in a number of different ways, each having its own set of advantages and disadvantages. The solution preferred for most devices at this time is transport of Li^+ ions through a molecular solvent blend. The blend is used because no single solvent can dissolve the preferred salt $LiPF_6$ and at the same time yield a sufficiently high ion mobility. The problem is solved by mixing a high polarity but viscous component with an equal amount of a low dielectric constant, low viscosity, co-solvent to increase ion mobility. The "standard electrolyte" used in common lithium ion batteries is $LiPF_6$ dissolved in 1:1 ethylene carbonate-dimethyl carbonate[2]. The solution is often supported within a gel structure. A sacrifice is made in safety (flammability), and also in ionicity[1] and transport number, but the gain in conductivity is the dominant consideration. This solution also seems to be the most satisfactory for use with high voltage cathodes because the carbonates decompose to form very stable interphases - a subject beyond direct discussion in this paper.

A modification of the liquid electrolyte approach that eliminates the molecular solvent, with increase in safety, is the use of ionic liquid solvents for the lithium salt[3,4] but this strategy also has the problem that the lithium ion becomes the least mobile species in the mixture[5,6]. This is due to its greater charge intensity that leads it to dominate the electrostatic (or charge polarization) competition for nearest neighbor anions so that it "digs itself a trap". This long-recognized problem[7] is minimized by choosing the least polarizable

anions possible, hence the predominance of fluorinated anion species in electrolytes of this type. While cells with such electrolytes can function with high cyclability, the lithium ion current, hence also power, is seriously restricted.

An alternative strategy for avoiding molecular solvents, one that also solves some problems stemming from the liquid character of the previous approach, (but does not solve the low conductivity or Li^+-trapping problems) has been promoted by MacFarlane et al[8]. It involves the use of organic cation salts in plastic crystalline states as solvents in which smaller amounts of lithium salts, usually with the same anions, can be dissolved. It is a modification of an earlier binary salt plastic crystal approach[9], which had failed to provide high conductivities. Plastic crystals have also been used as *molecular* solvents with moderate success[10].

Other approaches to this "electrolyte problem" have included crystalline fast ion conductors like sodium β" alumina[11], LISICON and, more recently, complex partly crystalline Lithiophosphate[12] which is more conductive than the "standard" electrolyte, and the crystalline thiophosphogermanate[13] which has the same conductivity as the standard. They can work rather well, partly because the alkali cation is now not only the most mobile ion but usually the *only* mobile ion. However, except for isolated examples like the extraordinary pure single crystal β" alumina (σ_{25^oC} = 0.18 S/cm), the recent but toxic thiophosphogermanate crystal[13] and the remarkable glass ceramic, their conductivities are well below 10^{-2} S/cm at ambient temperature. Furthermore, β" alumina can only be used in its polycrystalline state which is much less conducting than the pure single crystal.

Fast ion glassy and glass-ceramic electrolytes[14,15] appear rather promising, insofar as they can be obtained in the high conducting state by in-situ processing[16], while retaining the single ion conductor advantage, but to date they remain limited by their conductivities that rarely exceed 10^{-3} S/cm.

It is against this backdrop that we have sought to develop a new type of plastic crystal ion conductor, one in which the only mobile species is the alkali cation. The key idea is to ensure that the second nearest neighbor of the alkali cation is a high charge (oxidation number) Lewis acid species, as it is in the alkali metal fast ion conducting glasses. There is a special advantage of plastic crystals over glasses. Glasses only retain their shape up to the glass transition temperature, T_g, where the shear modulus decays to zero on the 100 sec time scale. Plastic crystals also exhibit the glass transition (if they do not first reorganize to closer-packed non-rotator states[17]) but, in contrast to glasses, they retain their solidity (finite shear modulus) up to far higher temperatures. This opens the door to far higher solid state conductivities than have been attained with superionic glasses, as will be seen.

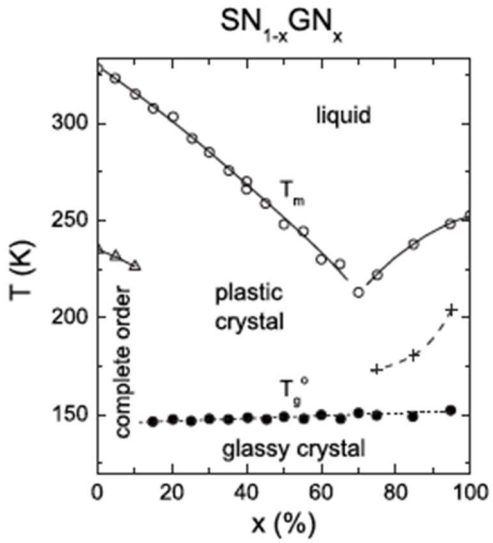

Figure 3.1 - The system succinonitrile-glutaronitrile, showing the depression, and then complete suppression, of the ordering transition of succinonitrile by incorporation of glutaronitrile into the rotator phase lattice. Reproduced with permission from reference[79].

The problem of metastability can often be solved by mixtures, in the same way as glassforming systems can often be generated by judicious mixing of systems that may not be glassforming themselves (witness the classical calcium nitrate-potassium nitrate (CKN) system). Our model system of this type, for the plastic crystal case, is the succinonitrile-glutaronitrile (SN-GN) system of recent study[17]. (Succinonitrile, $CH_2(CN)_2$, itself has been explored as a molecular plastic crystal host for ionic transport[10]). The phase diagram for the SN- GN system is shown in Figure 3.1 where it is seen that the addition of 15% of GN to SN completely suppresses the ordering transition, opening a domain of rotator phase dynamics down to the almost composition-invariant glass transition temperature, for study. Whether or not these are actually in ground thermodynamic states is not an issue in their investigation.

Plastic crystals are usually characterized by the presence of asymmetric particles of globular or short tube-like character, of which the succinonitrile molecule is a good example. Our interest in the possibility of ionic systems of this type has been stimulated by the discovery of siphoric acid, a silicophosphate molecular substance of interest in connection with enhancement of phosphoric acid type fuel cell performance[18]. While phosphate glasses have not in general been good glassy state alkali metal conductors, the possibility of sulfate oxygens, with their lower charge densities, being more amenable to Li^+ mobility, has seemed more attractive.

3.2 Methods

3.2.1 Preparation of the materials

$LiSiCl_3(SO_4)$, Li1: excess trichlorophenylsilane (97%, Sigma-Aldrich) was added to sulfuric acid (99.999%, Sigma-Aldrich) in a 1:1 mol ratio under nitrogen atmosphere. The mixture was kept under constant stirring in an open vial for different times depending on the preparation: 8 minutes, 32 minutes or 3h30 minutes (approximate times). The final product is a white solid (H1) and a colorless, transparent liquid (presumably benzene and excess starting silane, confirmed by ^{1}H-NMR). Lithium amide 95% (Sigma-Aldrich) is added to the resulting solid acid generating ammonia and the final soft solid, Li1.

$Li_3SiCl(SO_4)_3$, Li3: excess chlorotriphenylsilane was solubilized in 1,2-dichloroethane and added to sulfuric acid (99.999%, Sigma-Aldrich) in a 1:3 mol ratio under nitrogen atmosphere. The mixture was kept under constant stirring in an open vial for approximately 20h. The final product is a transparent yellow solid (H3) in 1,2-DCE. The solvent was

evaporated under gentle N_2 flow and washed several times with dichloromethane. Finally, lithium amide 95% (Sigma-Aldrich) was added to the solid acid generating ammonia and the final soft solid, Li3.

$LiSi(CH_3)_3(SO_4)$, LiMethyl: trimethylphenylsilane (99%, Sigma-Aldrich) was added to sulfuric acid (99.999%, Sigma-Aldrich) in a 1:1 mol ratio under argon atmosphere (with slight excess of silane). The mixture was kept under constant stirring for 30 min. The final product is a yellow liquid. NMR: $^{1}H\delta$= 0.37, 11.29 ppm; $^{13}C\delta$=-0.67 ppm; $^{29}Si\delta$=37.34 ppm. Lithium chloride was added to the liquid in a 1:1 molar ration and left stirring for 48 hours under inert atmosphere. Then the product was homogenized in an agate mortar and pestle, resulting in a soft waxy solid. The waxy solid was incorporated in Celgard 3401 by applying pressure with the mortar and pestle.

3.2.2 Materials characterization

Electrochemistry. Conductivity data were obtained by the standard complex impedance method. The electrochemical impedance spectra (EIS) were collected in a PARSTAT VMP2 using 10-100 mV sine amplitudes and a frequency range of 200 KHz to 10 Hz. The samples were carefully packed inside a homemade twin Pt electrode glass dip cell, under inert atmosphere. The cyclic voltammogram of Li1Li3 was obtained with a PARSTAT VMP2 at 1 mV/s. Under argon atmosphere, the sample was impregnated in Celgard and placed inside a stainless steel coin cell with Li foil anode and $LiFePO_4$ cathode purchased from MTI Corporation. The cyclic voltammogram of LiMethyl was obtained in a PARSTAT 2273 at 20 mV/s. The sample was impregnated in Celgard and placed inside a stainless steel coin cell with 2 Li foil electrodes, under argon atmosphere. The lithium ion

transference numbers were obtained by the potentiostatic polarization method described in the literature[19,20] using a PARSTAT VMP2. The electrolytes were packed in coin cells with 2 lithium foil electrodes. First, an EIS was recorded with a 10 mV sine amplitude and immediately after that a DC polarization of 10 mV was applied to the cell. The current response was recorded for 1h until the steady state was reached. Finally, another EIS with a sine amplitude of 10 mV is recorded. Then the transference number was calculated with the equation $t_+ = \frac{I_{ss}(\Delta V - I_0 R_0)}{I_0(\Delta V - I_{ss} R_{ss})}$, where I_{ss} is the steady state current, ΔV is the DC bias, I_0 is the initial current, R_0 is the initial electrolyte resistance and R_{ss} is the steady state electrolyte resistance.

Nuclear Magnetic Resonance Spectroscopy. The solid-state NMR data were obtained using a Bruker 400 MHz AVANCE III spectrometer equipped with a 4 mm double resonance broad-band magic angle spinning probe. ^{1}H NMR data for the solid acid H1 and the lithiated version of it Li1, were collected by placing the corrosive materials into 50 µL Kel-F rotor inserts obtained from Bruker. Although using a rotor insert reduces the amount of sample in the active volume of the probe, it minimizes the risk of the probe being exposed to corrosive materials. ^{1}H MAS NMR spectra of these materials were collected using a 4.0 µs π/2 pulse, a recycle delay of 15 seconds and 4 scans. All solid-state NMR spectra were collected with a MAS rate of 5 kHz, and the probe temperature maintained at 25 °C. The ^{1}H chemical shifts were externally referenced to TMS in the solid state using adamantane (^{1}Hδ=1.63 ppm)[21].

Differential Scanning Calorimetry. Measurements were made using a DSC-7, Perkin Elmer. The calibration was done immediately before the measurements by the two-point method with indium (melting point at 156.6ºC) and cyclohexane (solid-solid transition at 86.6ºC) as the references for high and low temperature regions, respectively. The samples were sealed in aluminum pans under nitrogen atmosphere and scanned at a rate of 20K/min under helium atmosphere.

3.3 Results and Discussion

Samples in this study were prepared by two-step reactions. First, a solid acid precursor is prepared as described in Chapter 2. The second step consists of neutralizing the precursor with lithium amide or lithium chloride, which yields soft, waxy white solids products. These indeed prove to have remarkably high conductivities as shown in the Arrhenius plot, Figure 3.2. The synthetic methods, and the thorough structural characterization of the acid precursor compounds (and indeed some of the lithium salts) were reported in Chapter 2. The reaction mechanism involves the protonation (and subsequent elimination as benzene) of the phenyl groups in the silyl reagents. This reaction mechanism[22], was used in the past to substitute phenyl groups by triflates as an attempt to make silylating agents for organometallic chemistry[23,24]. The selectivity of the reaction of an acid towards the phenyl groups, as opposed to the chlorines[24], allow for the synthesis of silyl hydrogensulfates with different numbers of chlorides in the same molecule. The mechanism, difficulties and detailed structures are found in Chapter 2.

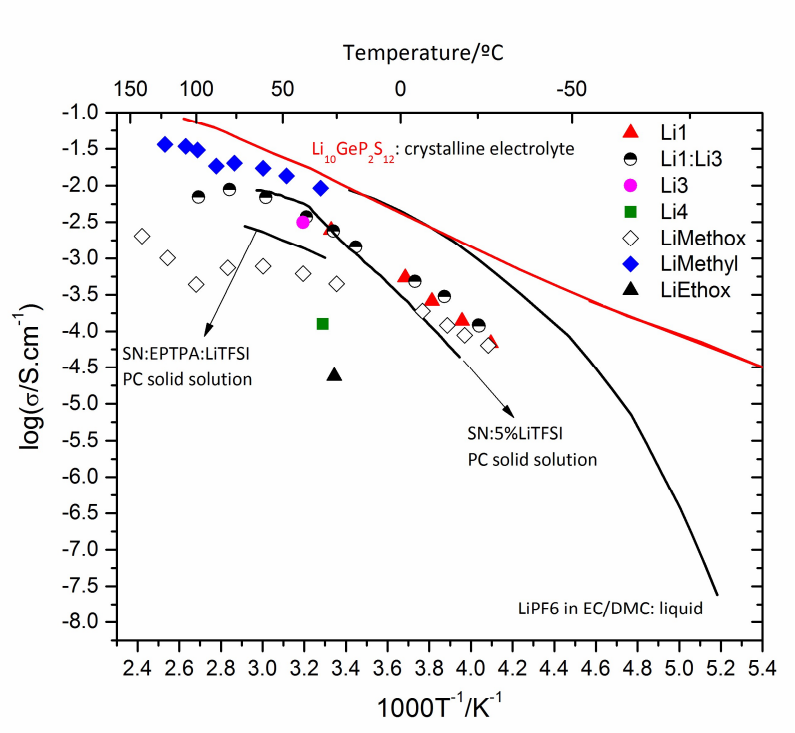

Figure 3.2 - Arrhenius plots of conductivities of the new solid state conductors (colored squares) and select literature compounds (solid lines): the crystalline $Li_{10}GeP_2S_{12}$[13]; the standard electrolyte $LiPF_6$ in organic carbonates[25]; and two solutions[10,26] in plastic crystals. Even though the new compounds presented in this work have comparable conductivities with the plastic crystal solutions already presented in the literature, it is important to remember that in the latter systems the lithium ion transference number is smaller than unity; in the new systems, all of the ionic current should be due to Li^+. The best candidate for battery applications would appear to be that designated LiMe1 [$Li(CH_3)_3SiSO_4$]. In the case of the LiMethyl compound, the conductivity is even higher than the PC solutions presented.

Although the soft, waxy lithium salts obtained in this work are very highly conducting, they are prone to crystallization events that turn them into hard powders of low conductivity. The crystallization can happen suddenly on heating the sample to higher temperature (e.g. 90ºC), as seen in the DSC study of Li1 in Figure 3.3, or just by letting the sample rest for 24h or more at ambient temperature. Before crystallization the materials

behave like those of Figure 1, exhibiting a glass transition on cooling, and on reheating, at around -80ºC, see Figure 3.3 and insert. On crystallization, the conductivity of the materials drops several orders of magnitude which renders them unsuitable for energy applications. To avoid the crystallization, a suitable second component needs to be found, as exemplified in Figure 3.1. The solid solution was obtained simply by mixing the freshly made salts with the help of a mortar and pestle, or by ball milling for an hour or two.

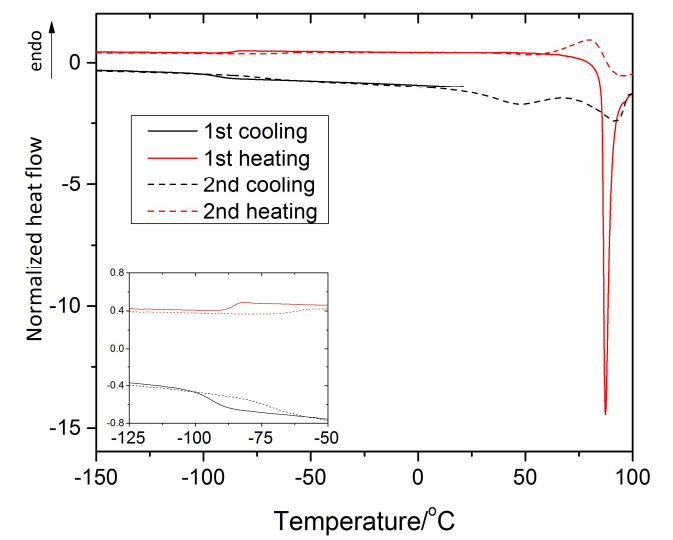

Figure 3.3 – Differential scanning calorimetry study of Li1. In the insert, bottom left, the T_g is shown around -80ºC. Note the ordering process that (during cooling) begins abruptly at 80ºC ends in a (cooling) glass transition at -80ºC as the rotational degrees of freedom are arrested in a glass transition. Note that not only the crystallization (ordering) event is irreversible, but that also the glass transition is suppressed after the first heating/cooling cycle.

A major early concern, that the high conductivities we were recording were due to protons that had not been completely eliminated in our preparation, is put to rest by the ^{1}H MAS NMR spectra of Figure 3.4. The quantitative NMR experiment shows that, by using

the phenyl group elimination for preparation of the precursor solid acid, the possibility of excess H_2SO_4 has been eliminated and, further, that the vast majority of the acidic protons can be neutralized by the reaction with lithium amide.

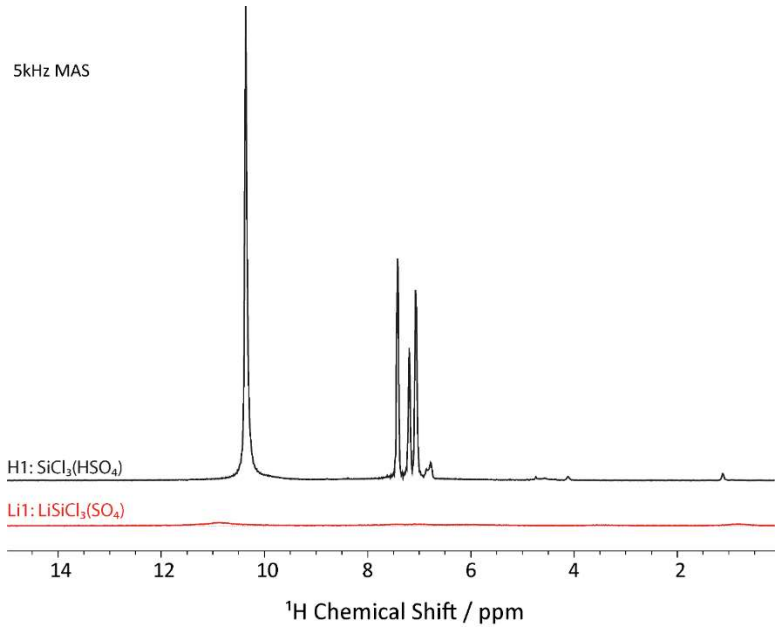

Figure 3.4 - MAS ^{1}H NMR of the precursor (on top) and Li1 (bottom) showing that the lithiation process adopted in this work successfully suppresses all of the protons in the Li1 compound (Figure adapted from reference[27]).

Electrochemical measurements

That the new compounds are promising candidates for all solid state lithium-ion batteries has been confirmed by cyclic voltammetry using the high voltage $LiCoO_2$ and $LiFePO_4$ cathodes. Coin cells were built using Li foil anodes and the LiMethyl and Li1:Li3 electrolytes incorporated in Celgard (Methods section). The cyclic voltammograms show

the reversible Fe^{+3}/Fe^{+2} pair in the case of Li1:Li3 (Figure 3.5a) and Co^{+3}/Co^{+2} pair in the case of LiMethyl (Figure 3.5b) for many cycles.

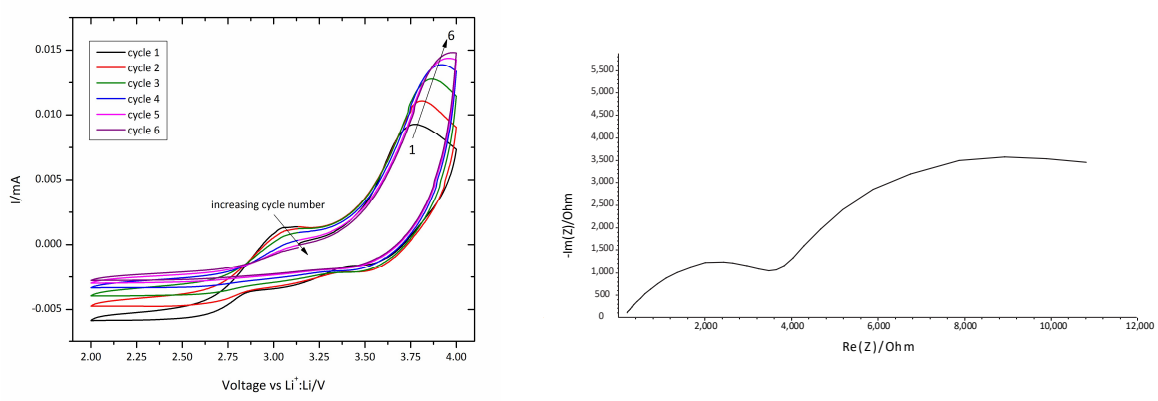

Figure 3.5 – a) Cyclic voltammetry of a Li/Li1Li3/$LiFePO_4$ half cell and b) EIS spectrum of the same cell (right). The cyclic voltammogram shows the lithium intercalation-deintercalation in the cathode at 3.5 V vs Li. With increasing cycle number, the current of the Fe^{+2}/Fe^{+3} oxidation increases and the oxidation of the impurity at 3V decrease until it is completely depleted by the 6th cycle. The EIS shown on the right of the same cell is typical of an intercalation cathode/Li half cell[28].

Confirmation that the lithium ions are responsible for the high conductivities reported in Figure 3.2 was obtained by lithium transference number measurements. The transference numbers were obtained by the usual impedance/DC polarization method for solid state electrolytes described in the literature[19,20] (see Methods section). The LiMethox compound yielded a transference number ~1.00. The transference number for the LiMethyl electrolyte could not be determined at this point, due to currents that were prohibitively high for our potentiostat.

A lithium stripping/deposition plot for the latter cell was obtained using a different potentiostat that allowed for currents of the order of 1 A, and is shown in Figure 3.6. While

there appears to be a certain overpotential for the lithium stripping and deposition (0.9 and -0.9 V vs Li, respectively), the behavior is comparable to that reported for a solid electrolyte cell working at very much smaller currents by reference[29]. The currents obtained in the present work are very high, especially when considering that this system is an all solid state cell. It is also important to note that no H^+/H_2 pair was detected from the lithium stripping/deposition experiment, which again demonstrates that the lithiation was successful.

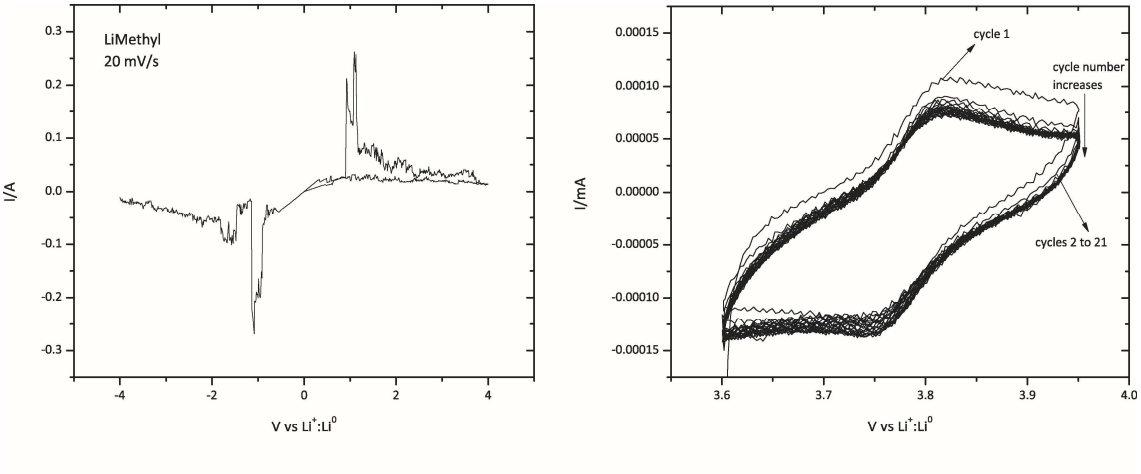

Figure 3.6 – All solid state electrochemistry experiments of the LiMethyl electrolyte, incorporated in Celgard 3401. Left hand panel: lithium stripping/deposition at 20 mV/s of the LiMethyl electrolyte, obtained in a symmetrical Li/Li coin cell. Note the very high currents. Right hand panel: Li/LiMethyl/$LiCoO_2$ half-cell showing lithium insertion through the Co^{+3}/Co^{+2} pair, reversibly around 3.8 V.

3.4 Conclusions

At this point our research, that has been aimed at producing a new type of solid state alkali ion conducting material, appears to have been successful. Much remains to be done to the making of lithium batteries and other electrochemical devices based on the

above-described materials as electrolytes. Since the electrolytes contain, or can be prepared to contain, only elements in their maximum oxidation states (oxygen excepted), they should be quite inert to oxidizing conditions at cathodes, hence should offer good possibilities for solving the high voltage cathode side reaction problem. The electrolytes of choice for further study should be LiMethyl and LiMethox, to avoid side reactions of the Li anode with chlorines in Li1Li3 case. It is also possible that this type of electrolyte might be of immediate interest as a solution to the lithium-air cathode problems, and this is one of the domains in which our future work will be concentrated.

3.5 References

(1) Lee, S. Y.; Ueno, K.; Angell, C. A. *J. Phys. Chem. C* **2012**, *116* (45), 23915.

(2) Tarascon, J. M.; Guyomard, D. *Solid State Ionics* **1994**, *69* (3-4), 293.

(3) Seki, S.; Kobayashi, Y.; Miyashiro, H.; Ohno, Y.; Usami, A.; Mita, Y.; Kihira, N.; Watanabe, M.; Terada, N. *J. Phys. Chem. B* **2006**, *110* (21), 10228.

(4) Sakaebe, H.; Matsumoto, H. *Electrochem. commun.* **2003**, *5* (7), 594.

(5) Hayamizu, K.; Aihara, Y.; Nakagawa, H.; Nukuda, T.; Price, W. S. *J. Phys. Chem. B* **2004**, *108* (50), 19527.

(6) Ye, H.; Huang, J.; Xu, J. J.; Khalfan, A.; Greenbaum, S. G. *J. Electrochem. Soc.* **2007**, *154* (11), A1048.

(7) Cooper, E. I.; Angell, C. A. *Solid State Ionics* **1983**, *9-10* (PART 1), 617.

(8) Macfarlane, D. R.; Macfarlane, D. R.; Huang, J.; Huang, J.; Forsyth, M.; Forsyth, M. *Nature* **1999**, *402* (DECEMBER), 1998.

(9) Cooper, E. I.; Angell, C. A. *Solid State Ionics* **1986**, *18-19* (PART 1), 570.

(10) Alarco, P.-J.; Abu-Lebdeh, Y.; Abouimrane, A.; Armand, M. *Nat. Mater.* **2004**, *3* (7), 476.

(11) Briant, J.; Farrington, G. *J. Solid State Chem.* **1980**, *33*, 385.

(12) Seino, Y.; Ota, T.; Takada, K.; Hayashi, A.; Tatsumisago, M. *Energy Environ. Sci.* **2014**, *7* (2), 627.

(13) Kamaya, N.; Homma, K.; Yamakawa, Y.; Hirayama, M.; Kanno, R.; Yonemura, M.; Kamiyama, T.; Kato, Y.; Hama, S.; Kawamoto, K.; Mitsui, A. *Nat. Mater.* **2011**, *10* (9), 682.

(14) Hayashi, A.; Kama, S.; Mizuno, F.; Tadanaga, K.; Minami, T.; Tatsumisago, M. *Solid State Ionics* **2004**, *175* (1-4), 683.

(15) Hayashi, A.; Minami, K.; Ujiie, S.; Tatsumisago, M. *J. Non. Cryst. Solids* **2010**, *356* (44-49), 2670.

(16) Hayashi, A.; Noi, K.; Sakuda, A.; Tatsumisago, M. *Nat. Commun.* **2012**, *3* (May), 856.

(17) Bauer, T.; Köhler, M.; Lunkenheimer, P.; Loidl, A.; Angell, C. A. *J. Chem. Phys.* **2010**, *133* (14).

(18) Ansari, Y.; Tucker, T. G.; Angell, C. A. *J. Power Sources* **2013**, *237*, 47.

(19) Evans, J.; Vincent, C. A.; Bruce, P. G. *Polymer (Guildf).* **1987**, *28* (13), 2324.

(20) Zugmann, S.; Fleischmann, M.; Amereller, M.; Gschwind, R. M.; Wiemhöfer, H. D.; Gores, H. J. *Electrochim. Acta* **2011**, *56* (11), 3926.

(21) Hayashi, S.; Hayamizu, K. *Bull. Chem. Soc. Jpn.* 1991, pp 685–687.

(22) Eaborn, C. *J. Organomet. Chem.* **1975**, *100*, 43.

(23) Bassindale, A. R.; Stout, T. *J. Organomet. Chem.* **1984**, *271*, C1.

(24) Matyjaszewski, K.; Chen, Y. L. *J. Organomet. Chem.* **1988**, *340*, 7.

(25) Stallworth, P. .; Fontanella, J. .; Wintersgill, M. .; Scheidler, C. D.; Immel, J. J.; Greenbaum, S. .; Gozdz, A. . *J. Power Sources* **1999**, *81-82*, 739.

(26) Kim, S.-H.; Choi, K.-H.; Cho, S.-J.; Park, J.-S.; Cho, K. Y.; Lee, C. K.; Lee, S. B.; Shim, J. K.; Lee, S.-Y. *J. Mater. Chem. A* **2014**, *2* (28), 10854.

(27) Angell, C. A.; Klein, I. S.; Tucker, T. G. Inorganic plastic crystal electrolytes. WO2014153146 A1, 2014.

(28) Fan, J.; Fedkiw, P. S. *J. Power Sources* **1998**, *72*, 165.

(29) Shekibi, Y.; Rüther, T.; Huang, J.; Hollenkamp, A. F. *Phys. Chem. Chem. Phys.* **2012**, 14, 4597.

CHAPTER 4

EXCESS THERMODYNAMIC PROPERTIES OF GLASSFORMING LIQUIDS: THE RATIONAL SCALING OF HEAT CAPACITIES, AND THE THERMODYNAMIC FRAGILITY DILEMMA RESOLVED.

4.1 Introduction

The concept of fragility in liquids[1,2] has been given a great deal of attention by workers in the viscous liquid and glasses field. While the basic phenomenon has been widely used to classify liquids (and also the related plastic crystal phases that freeze-in orientational degrees of freedom during extended cooling[3-5], the full understanding of fragility itself is proving slow to arrive.

A development that should have been of help but has instead become a source of confusion, was the proposal of a thermodynamic equivalent of the kinetic quantity, viz. the "thermodynamic fragility"[6]. Thermodynamic fragility was defined initially using a dimensionless quantity $S_{ex}(T_g)/S_{ex}(T)$ that was shown to yield a pattern similar to that for the liquid viscosity (log plot) vs scaled reciprocal temperature T_g/T. Studies showed that this quantity, or a more easily determined variant of it (in which $S_{ex}(T_g)$ was replaced by $\Delta H_m/T_g$)[7]), correlated quite well with the dynamic quantity log(viscosity). The thermodynamic fragility has the advantage that it could be understood in terms of the molecular parameters of simple excitation models for glassformer thermodynamics[8,9].

Unfortunately, several groups have taken the position that thermodynamic fragility should be represented by the excess heat capacity, in unscaled or unsuitably scaled, form. Works like the impressive data collection of Huang and McKenna[10] that illustrate the lack of correlation of this excess quantity with the kinetic fragility, have become highly cited, and assist in creating a state of disenchantment in the field with thermodynamic fragility as a concept. A primary purpose of this contribution is to point out as strongly as possible that excess heat capacity should ***not*** be expected to correlate with kinetic fragility unless it is first subjected to a rational scaling, which has so far not been properly documented.

We commence with a general, and much needed, review of the different sorts of fluctuations that get "frozen in" in the glass transition process, (and indeed define that process) and their connection to response functions that are better known as derivatives of extensive thermodynamic properties, like volume and enthalpy. After all, the glass transition is not only the temperature at which the structure becomes fixed during cooling, but also the temperature at which the slow component of the fluctuations in extensive thermodynamic properties become frozen. Remember that each of the response functions is a sum of components that are collision-based (vibrational time-scale) fluctuations and configuration-based (structural relaxation time scale) and only the latter component time scale is diverging as T_g is approached.

The configuration-based derivative quantities behave very differently from each other with increase of temperature above T_g, and this is not often discussed, probably because it is neither well studied nor well understood. We recently showed, for one "model" system, orthoterphenyl (OTP), how the compressibility (particularly the excess over the

vibrational component) increases as T rises above T_g, while the excess heat capacity, scaled as we elaborate in this chapter, does the opposite[11]. The expansion coefficient, being proportional to the product of entropy and volume fluctuations is, not surprisingly, nearly temperature independent.

The common derivative functions, and also their relation to fluctuations according to Landau and Lifschitz[12], are:

Isothermal compressibility, $\kappa_T = -1/V(\partial V/\partial P)_T = -\langle(\Delta V)^2\rangle /Vk_BT$ (1)

Constant volume heat capacity, $C_v = (\partial E/\partial T)_V = k_BT^2/\langle(\Delta T)^2\rangle$ (2)

Constant pressure heat capacity, $C_p = (\partial H/\partial T)_p = \langle(\Delta S)^2\rangle /k_B$ (3)

Isobaric expansion coefficient, $\alpha_p = 1/V(\partial V/\partial T)_P = \langle(\Delta S.\Delta V)\rangle/Vk_BT$ (4)

In each case, there will be fast and slow components of the response function, determined by fast fluctuations (like sound waves - fast damping shear modes and slow-damping longitudinal waves - and librations) and slow fluctuations that change the local structure, and potential energy, and entropy. We now examine their behavior in the order compressibility, heat capacity (which is our main concern), and expansivity, before applying the results of our considerations to the question of thermodynamic fragility.

4.2 Results and Discussion

Compressibilities of glassforming liquids.

We have collected as many data on the compressibility of glassforming liquids as are readily available, and present them, together with some data on non-glassformers, in

Figure 4.1. Since the compressibility of solid phases is generally rather small by comparison with that of liquids, the strongly increasing behavior with increasing temperature must be due to the slow density fluctuations characteristic of the liquid state in every case. This is quite striking to anyone familiar with the oppositely directed behavior of many glassforming liquid heat capacities, indeed almost all liquid heat capacities after the vibrational contribution has been subtracted and, in particular, after the appropriate scaling to which we draw attention in this paper, has been applied.

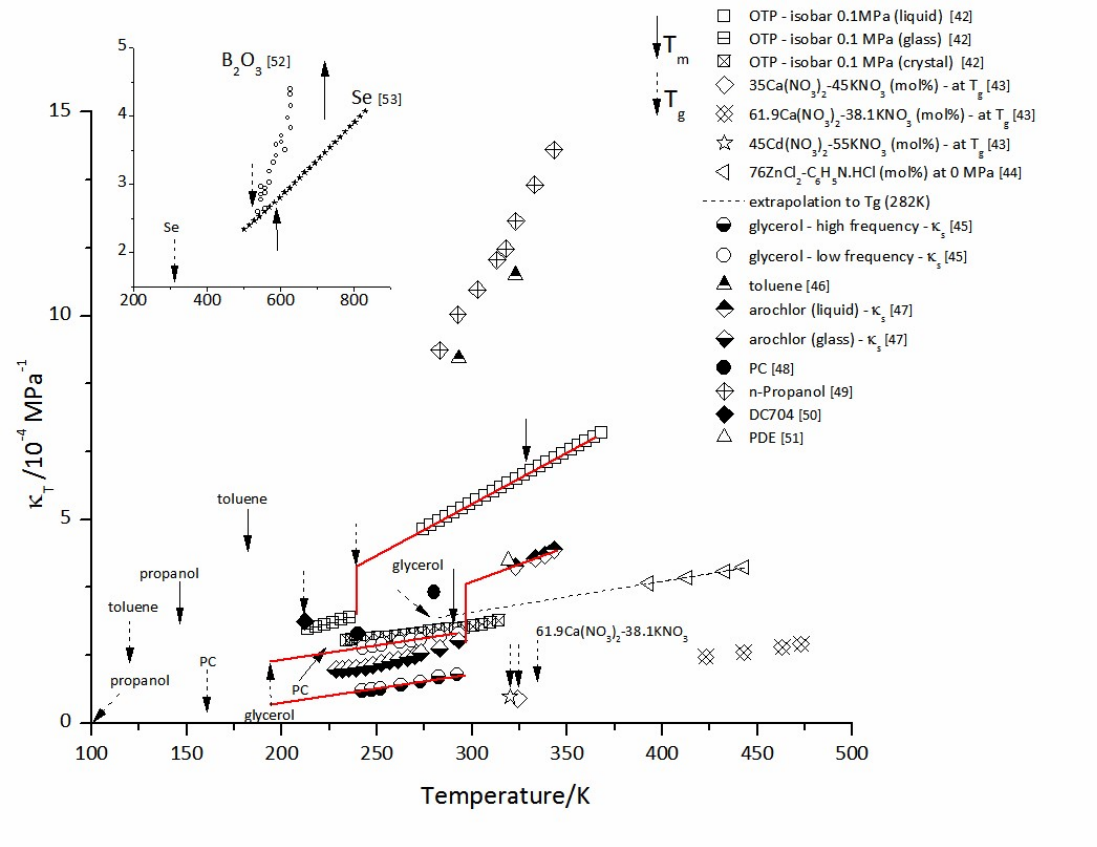

Figure 4.1 - Compressibilities of glassforming liquids. Solid arrows denote T_m and dashed arrows denote T_g. All examples show a jump at T_g and then a linear increase above T_g, with slope greater than that of glass or crystal. Extrapolations of available data to T_g would suggest rather small $\Delta\kappa_T$ values for the low T_g liquids like toluene and propanol. For glycerol, and arochlor, data are adiabatic values from sound velocity data, and high and low frequency points indicate the $\Delta\kappa_S$ values (in these cases, the label "glass" means non-relaxing on the ultrasonic time scale). On the scale of this plot, an isothermal value κ_T for glycerol is indistinguishable from the κ_S datum at the same T. References for the data are given in the legend after each symbol identification. Data for two other liquids that fall in the already crowded portion of Figure 4.1 have been omitted for clarity.

The increased compressibilities, and the temperature dependences of compressibility for liquids with low glass temperatures, are quite striking. It should be related to the observations made in negative pressure studies of liquids that show how, at

ambient pressure, these less cohesive liquids are closer to their spinodal limits of mechanical stability (which lie at negative pressures hence are not much studied). The stability limit in question is the stability against cavitation under isotropic tension (which is the formally correct meaning of "negative pressure". The cavitation event returns the system to its stable state of an ambient pressure liquid in equilibrium with its vapor. Simple theory (e.g. van der Waals) tells us that as the mechanical stability limit is approached, the compressibility must diverge, which is all we need to understand the pattern of Figure 4.1.

There are experimental data to support the above reasoning. The experimental limits to stretching of simple liquids like heptane and ethanol at 25ºC, which agree with the theoretical expectations, are reported by Caupin et al.[13] to lie in the range -20 to -30 MPa (-200 to -300 atm), while that for OTP is much larger, namely at about -120 MPa[14-17]. Since ambient pressure (for which all Figure 4.1 data are presented), is much further from the spinodal limit in the case of OTP than in the case of ethanol or heptane, the fluctuations in volume of the former should be much smaller than those of the latter. This would rationalize the relation between the κ_T values and also their temperature dependence, seen in Figure 4.1.

Heat capacities of glassforming liquids, and a problem

The heat capacity "jump" observed at the glass transition, which is a consequence of the increase in mean square entropy fluctuation in the time window of the experiment in which "broken ergodicity" is being restored, is a highly variable quantity amongst different glassforming materials. For some glassformers, the liquid heat capacity at T_g can be as much as three times the glassy state value, e.g. $H_2SO_4.3H_2O$[18,19]. The ratio $C_{p(l)}/C_{p(g)}$ at T_g

is particularly marked for hydrogen-bonded liquids and for molecular liquids with very low glass temperatures[20]. On the other hand, it can be a tiny fraction of the glassy state heat capacity in other cases, like truly dry SiO_2 (or its weak field analog BeF_2), and especially glassy water itself[21]. In the case of very low temperature molecular glassformers, the heat capacity is increasing rapidly as the glass transition is approached from above, whereas with SiO_2 and BeF_2 the opposite is true.

These trends are very diagnostic in theoretical considerations of viscous liquids and the glassy states, but before they can be properly considered another and different problem has to be confronted. The problem is that a diagram like Figure 4.1 cannot be constructed with simple molar heat capacity data because the value of the molar heat capacity depends very much on how many atoms or structural groups make up the molecule. The reason for this is not difficult to see, but correcting for it is not straightforward and has been the subject of much discussion and argument concerning what constitute the "rearrangeable entities" or "beads" in a given glassformer. These are needed so the molar heat capacity can be scaled to heat capacity "per mole of beads"[22-25]. It is obvious enough for an elemental glassformer like Se, but what is it in a case like the fragile liquid 1,3-diphenyl-1,1,3,3-tetramethyldisiloxane (PMS) for which complete thermal characterization is available[26]. Perhaps more acutely, how should we scale the heat capacity for the model "strongly correlating" molecular liquid, tetramethyl-tetraphenyl-trisiloxane, a commercial silicone oil (DC704) used by Gunderman et al. to predict the density scaling exponent, and show that the Prigogine-Defay ratio is close to unity, for "simple" liquids[27]. This difficulty motivates a major component of this article because a satisfactory resolution

is necessary before an appropriate comparison can be made with the density fluctuation-based behavior reported in Figure 4.1.

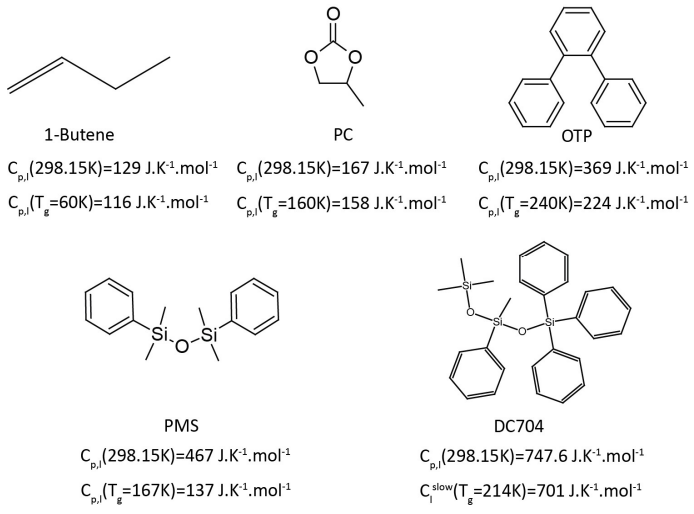

Scheme 1. Molecular structures for 1-butene, propylene carbonate (PC), orthoterphenyl (OTP), 1,3-diphenyl-1,1,3,3,-tetramethyldisiloxane (PMS), and DC704. The molar heat capacities of liquid at T_g and at 298.15K are under each structure.

Looking at the thermodynamic definitions above, one notes that except for the heat capacity, the response functions contain a scaling by an extensive property, namely the volume of the material whose change of volume with temperature (or pressure) is being measured. The lack of an absolute value for the enthalpy eliminates a similar scaling for $(\partial H/\partial T)_p$ which results in heat capacities, and jumps in heat capacity, that increase with the size of the molecule, at least when the molecule has many flexible units. For making

comparisons of the heat capacity, and the jump in heat capacity at T_g, amongst different substances it has been obvious that some sort of scaling is necessary.

The answer most generally adopted is to present comparisons on a “per bead” basis[22] where the "bead" is seen as the unit that absorbs the heat by its determination of the potential energy landscape. Nobody is really satisfied with this solution because the definition of a "bead" is very uncertain and leaves much room for subjective adjustment. Some of the efforts are compared in refs[24,25,28]. Another way of scaling the excess heat capacity is to normalize by the heat capacity of the glassy state at T_g. This approach, mentioned already above, has been used since the first fragility papers[1], and was the one adopted by Huang and McKenna in their exhaustive discussion of thermodynamic vs kinetic fragilities covering many classes of glassformers[10]. It is a way of making allowance for the fact that in classical physics, the heat capacity of a molecule with n independent (classically excited) particles will be $3nk_B$. Furthermore, if some of the vibrations are not excited at T_g because the bonding interactions are too strong for them to act as independent classical particles, then the degree to which the heat capacity falls below 3R per mole of particles will take their lack of independence, in both glassy and liquid states, into account. The generally unsatisfying correlations that are obtained with this seemingly reasonable approach[10], provide one of the motivations for the present article. We make further reference to these later, but first provide our resolution of the heat capacity scaling problem in the following major section.

A new, or unexploited, approach to heat capacity scaling

In refs.[5,6] we made a rather different suggestion, which brings the definition of heat capacity more into line with those for the other response functions. It is based on the recognition that heat capacity can be defined equally correctly as $(\partial S/\partial \ln T)_p$, indeed this has long been one of the bases on which graphical estimates of the Kauzmann temperature for glass-forming liquids have been made[29,30]. We refer here to the plotting of C_p for the liquid and crystal states of a glassformer (e.g. glycerol[31]) against lnT (or logT) and extrapolating the liquid heat capacity until the area between it and the crystal heat capacity (bounded at high temperature by the melting temperature) is equal to the entropy of fusion, ΔS_f (separate shaded area). Two examples[19,29] are shown in Figure 4.2.

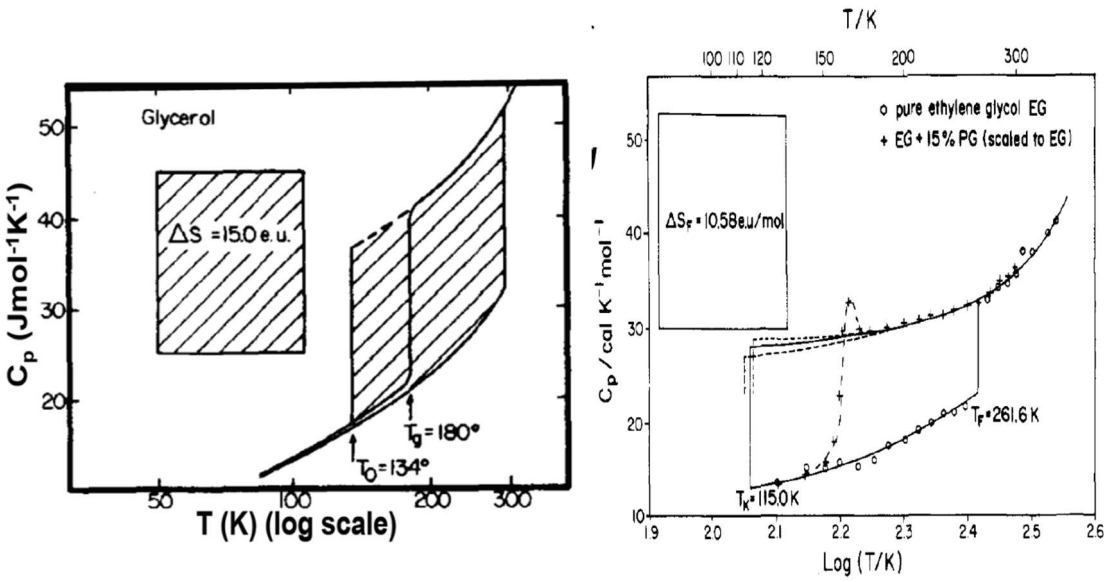

Figure 4.2 - Applications of the relation $C_p = (\partial S/\partial \ln T)_p$ in integrated form $S = \int C_p d\ln T$, to estimate the Kauzmann temperature, To or T_K, for a glassformer glycerol and a non-glassformer (ethylene glycol). From Refs[19,29], by permission.

Now, since entropy, in contrast to enthalpy, does possess an absolute value thanks to the third law of thermodynamics, we can define a scaled heat capacity, by analogy to the expressions for compressibility and expansivity, by normalizing $C_p = (\partial S/\partial \ln T)_p$ by the absolute entropy S. Thus we define the rationally scaled heat capacity C_p^* by

$$C_p^* = (\partial S/\partial \ln T)_p/S = C_p/S \quad (5)$$

This may be used to present data for different liquids in the same way as we have presented data for compressibility in Figure 4.1, without any reference to beads and such so long as we have access to the molar entropy data. We have discussed this insight elsewhere[5], but only briefly, and so here make a full evaluation of its merits and limitations.

First we must recognize a limitation, or at least a complication, in data analysis by this approach. When it comes to mixtures of components, the measurement of compressibility and expansivity remains straightforward. For heat capacity by the above scaling expression, however, one must deal with the entropy of mixing which is not measurable with the same simplicity as the measurement of volume of the solution. For this reason, we will confine our attention to the heat capacities and entropies of pure substances.

In Figure 4.3 we present entropy-scaled heat capacity data in relation to temperature for as many of the substances of Figure 4.1 as possible, and include others for which the compressibilities are not yet available.

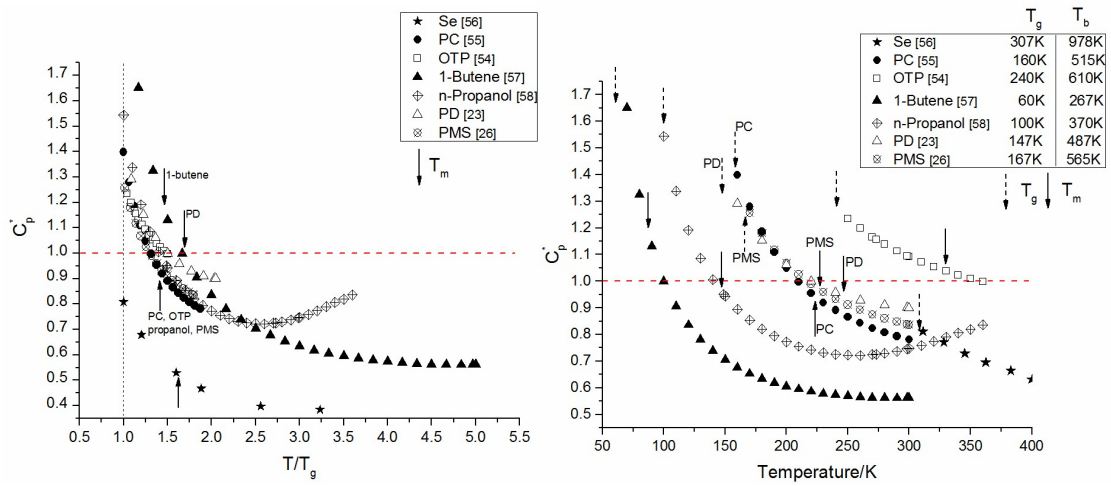

(a) (b)

Figure 4.3 - (a) Temperature dependence of the new (rationally scaled) heat capacity, $C_p^* = C_p$ (molar)/S(molar) for various glassforming liquids. C_p^* is dimensionless. T_g and T_m are marked by arrows to each curve. PD, not previously mentioned, is 1,3-propane diol, data from ref.[23]. References for other data sources are provided in the legend. **(b)** C_p^* vs T/T_g. Note the extent to which different liquids are collapsed to a common behavior by this scaling, and the extreme behavior of the liquid with the lowest T_g (1-butene)

We may note immediately that, (1) molar heat capacities that were spread over a very large range depending on molecular size, are now all found spread around the value unity, and (2) since the total entropy is decreasing as temperature decreases, the effect on the heat capacity has been to increase the number of substances that have total scaled liquid heat capacities C_p^* that are increasing with decreasing temperature. In fact, it is only propanol that has any positively sloping component at all. We thus make more obvious, the qualitative difference between the temperature dependence of compressibility (Figure 4.1) and that of rationally scaled heat capacity (the first decreasing as the glass transition is approached while the second is now increasing).

Cases like selenium[32] that are known to be have a sort of phase transition due to a ring-chain equilibrium, peaking near the T_g, do not seem so exceptional in this rationally scaled C_p representation.

Furthermore, if we recognize that the part of glassformer physics that deals with the metastable ***liquid*** state, is mainly concerned with the configurational properties of the liquid state, and accordingly focus attention on the ***difference*** between liquid state and glassy (or crystalline) state heat capacities, then we are lead to plot $C_{p,ex}/S_{ex}$ (which we should designate ΔC_p* to be consistent with Figure 4.2), against T. The more rapid decrease in S_{ex}, relative to $S_{(total)}$, leads to an even sharper increase in the scaled (excess) heat capacity with decreasing temperature. This is shown in Figure 4.4. It is strongly suggestive of an impending phase transition, though the order of the transition is not indicated and it is apparently driven by entropy fluctuations, not volume fluctuations.

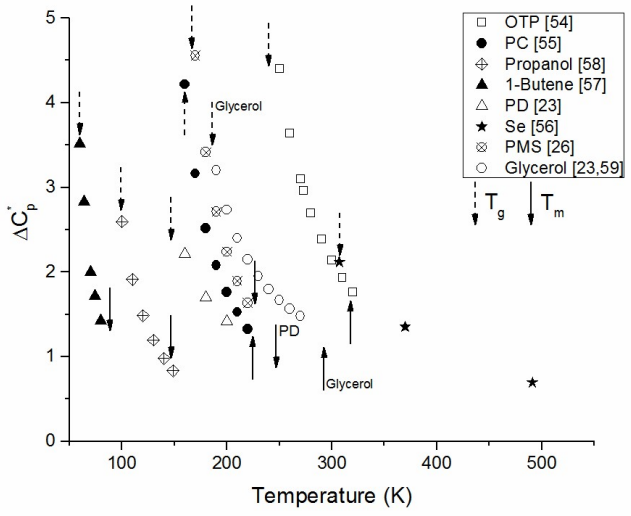

Figure 4.4 - Excess heat capacity scaled by excess entropy as function of temperature, for the molecular liquids of Figure 4.3. The sharply increasing behavior of all these cases, whether strong or fragile in kinetic character, as T_g is approached is quite striking.

Finally, in Figure 4.5, we show the excess heat capacity function in the new scaling, ΔC_p^* (i.e. $C_{p,ex}/S_{ex}$) against temperature, now normalized by T_g. The arrows now all indicate melting points, which the dubious "2/3 rule" (attributed to Kauzmann[33]) would lead one to expect to fall at 1.5 - indeed most of them are close to this value.

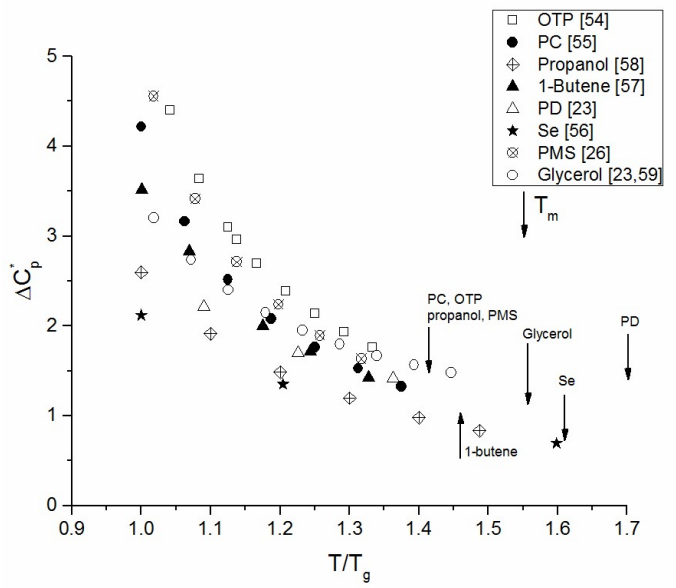

Figure 4.5 - Rationally scaled excess heat capacity as function of T/T_g. The arrows indicate the equilibrium melting points of the liquids which, according to the "2/3 rule" for T_g/T_m, should lie close to 1.5 on this temperature scale. Note the low and/or slow-rising position of non-fragile liquids, n-propanol, PD, and glycerol, compared with high and fast- rising values of fragile liquids OTP, PMS and PC.

If there were to be any relation between a heat capacity function and the kinetic fragility, it should appear in this figure. One would expect to see propanol, with the lowest kinetic fragility, at one extreme, and propylene carbonate, with the highest kinetic fragility, at the other extreme, with glycerol and PD somewhere in the middle. While this is roughly the case, and while all the fragile liquids lie near the top of the figure, the order amongst

the latter is not correct (to the extent that the kinetic fragility has been correctly attributed). There is much crowding at the fragile end. We give further consideration of these relationships in the last section of this Chapter.

We noted earlier that it is the liquids with the lower T_gs that have the most sharply decreasing compressibilities with decreasing temperature (see Figure 4.1). Now we see that it is the same low T_g liquids that have the most sharply increasing heat capacities, with decreasing temperature, and this is made especially striking when the latter are scaled as we are suggesting in this article. It is a challenge to theory to explain this relationship.

The thermal expansivity

The thermal expansivity, defined by Eq. 4, is determined by a cross-correlation of volume fluctuation and entropy fluctuation and it is therefore not too surprising to find its behavior in temperature, being some average of the other two, but occasionally taking negative values in the case of anomalous liquids not considered in this paper. Negative values are forbidden for κ_T and C_p, C_v that depend on a square of the relevant fluctuation.

Since density measurements are so simple to perform and so frequently made, over extended ranges of temperature, expansion coefficients should be widely available.

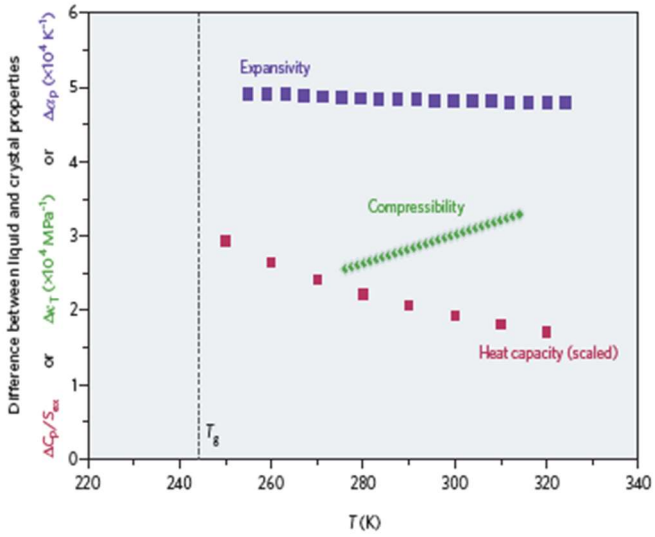

Figure 4.6 - Expansivity of OTP contrasting with the compressibility and S_{ex}-scaled heat capacity. (from ref.[11] with permission of McMillan Publ. Co)

However, except for a few anomalous liquids like water and some of its solutions, and certain chalcogenides with metal-insulator transitions, they are so uninteresting that they are rarely reported (except in the form of coefficients of a linear equation for the density). We earlier drew attention[11] to the contrasting slopes of $C_{p,ex}/S_{ex}$ v T and κ_T vs T for the particular case of orthoterphenyl. (reproduced in Figure 4.6). The detailed arguments of this paper explain the choice of scaling for the heat capacity used for this plot.

Relation to Thermodynamic Fragility

In this section we return to the question of thermodynamic fragility. In particular we ask if the new scaling of C_p leads to any modification of the conclusions of ref.[10] and others based on the jump of C_p, relative to the Cp of the glass at T_g, as the primary

quantification of the quantity in question (as was also done, without much consideration of alternatives, in the original paper on this subject[1]). The alternative proposition was that thermodynamic fragility should be judged by the rate at which the excess entropy, relative to its value at T_g, builds up as temperature rises above T_g. The two are rather different. If the excess heat capacity were to remain constant at the value observed at T_g, then the C_p ratio at T_g would also indicate the rate at which entropy builds up with increasing temperature, namely:

$$S_{ex} = \int_{Tg}^{T} \Delta C_p \, d\ln T \quad (6)$$

However, according to Figs 4 and 5 it does not remain constant and departure from constancy differs for different glassformers. According to the Adam-Gibbs theory of relaxation processes, the relaxation time temperature dependence is controlled by the rate at which the configurational entropy changes with temperature according to

$$\tau = \tau_0 \exp[C/(TS_c)] \quad (7)$$

Where C is a constant containing a basic activation energy, and S_c is the configurational entropy. In testing the Adam-Gibbs theory, S_c is generally assumed to be the quantity that we have represented as S_{ex}[34] which is assessed using Eq. (6). Indeed, it is the only easily assessed quantity that can be used except in computer simulation studies of the problem[35]. S_{ex} is the more cautious as it allows for the possibility that part of the excess heat capacity arises from changes in the vibrational density of states with increasing temperature (and volume)[36,37]. It probably does not matter much anyway since there is reason to believe that S_c is proportional S_{ex}[6].

The build-up of entropy during heating above T_g is correctly represented by Eq. 6 irrespective of the previous discussion of scaling of heat capacity, but since the entropy itself will depend on the size and floppiness of the molecules, it needs to be scaled by the excess entropy at some reference point. In ref.[6] this reference point was chosen to be T_g, (see Figure 4.7 below) which made possible the construction of an "excess entropy generation" plot which has essentially the same character as the corresponding kinetic fragility plot (same ordering of liquids, notwithstanding their very different chemical characters). In ref.[7], on the other hand, it was in effect chosen to be the melting point, by the presence of the readily accessible fusion enthalpy ΔH_m in an empirical expression for the thermodynamic fragility,

$$m = 56\ T_g \Delta C_p(T_g)/\Delta H_m \quad (8)$$

which was shown to correlate well with the kinetic fragility. This is the same expression as that derived by Wolynes and co-workers from Random First Order Transition (RFOT) theory, except for the numerical constant which was found to be 52 in the latter work[38].

Noting that the slope of the correlation plot is 1.45, close to the popular relation between T_m and T_g, (2/3 rule), Wang et al multiplied the RHS of Eq.(8) by unity (T_m/T_m) to obtain a modified version of Eq. (8),

$$m = 56\ (T_g/T_m)\Delta C_p(T_g)T_m/\Delta H_m \quad (9)$$

Which, on substituting $T_g/T_m = 0.66$ and $T_m/\Delta H_m = \Delta S_m$, yields the simple relation:

$$m = 37.5\Delta C_p(T_g)/\Delta S_m \quad (10)$$

This was also noted by Lubchenko and Wolynes[39]. This provides the correlation with the kinetic fragility ***m*** index, shown in Figure 4.8. The relation to the "rational scaling" of $\Delta C_{p,ex}$ of the present Figure 4.5, is not difficult to see. If we had an empirical relation between ΔS_m and $\Delta S(T_g)$ we could convert the Eq. (10) relation to get the thermodynamic fragilities of the liquids of Figure 4.5 from the values of Fig. 5 at T_g. The advantage of Eq. (10) is, of course, that there are many ΔS_m data, compared with few ΔS_{ex} at T_g data.

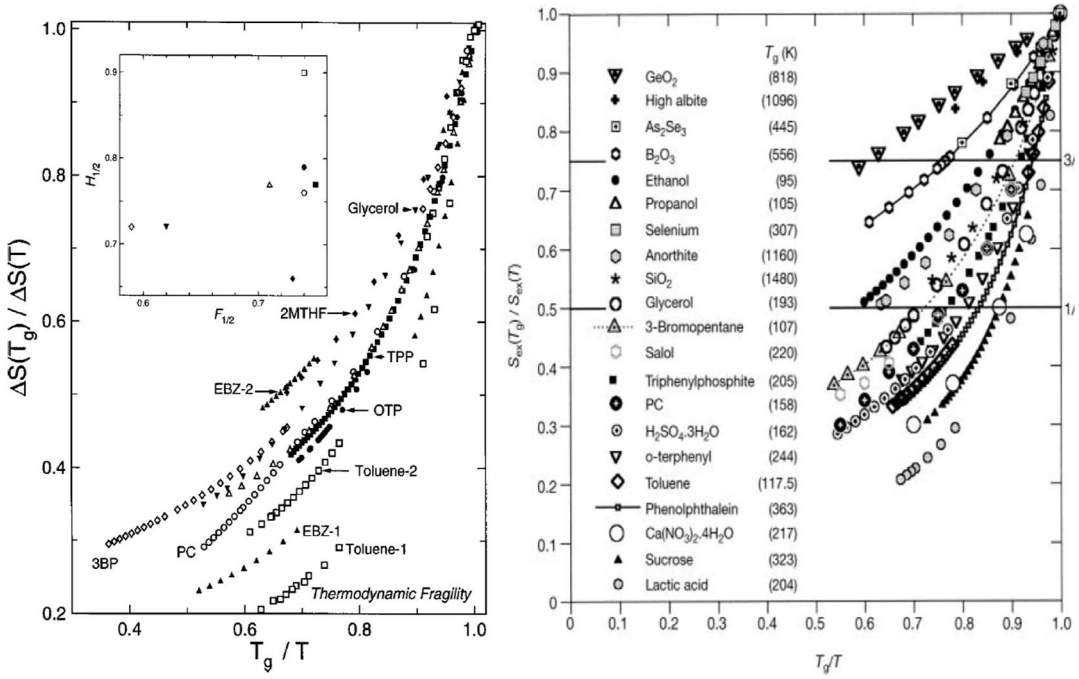

Figure 4.7 – Left hand panel: Earlier studies of the rate at which the excess entropy, scaled by the value at T_g changes with temperature above the glass transition temperature. Right hand panel: A note of caution introduced by the high quality data of ref.[40] on molecular liquids where it is shown that there are alternative assessments of the excess entropy possible, depending on how the data near, but below T_g are treated (see the cases of toluene and ethyl benzene). (LH Panel reproduced from ref.[6] by permission of McMillan Press, Inc. RH panel reproduced from ref.[40] by permission of authors K. L. Ngai and O. Yamamuro, and Amer. Inst. Physics.)

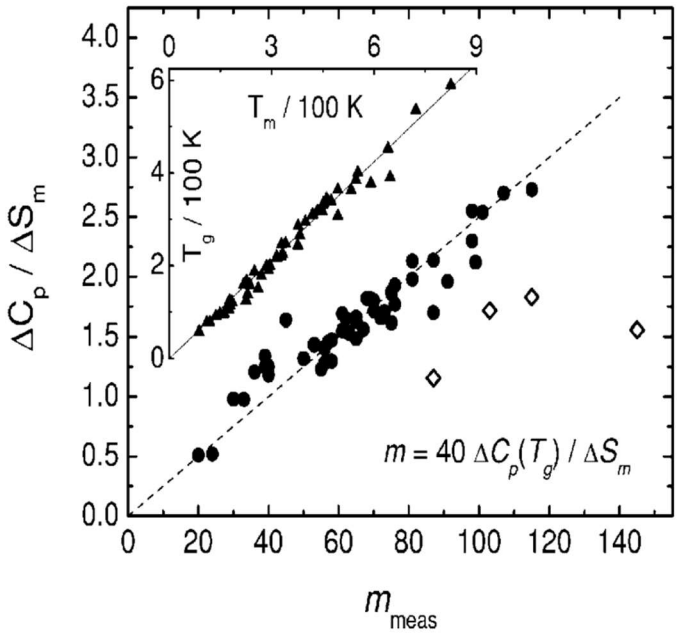

Figure 4.8 - The correlation of the Eq. (10) fragility with the kinetic fragility of many liquids (see Table 1 in ref.[7]). Dashed line is the prediction of Eq. (10) with numerical constant of 40. Note the test of the "2/3 rule" in the insert. (Reproduced from Wang et al., ref.[7] with permission of Amer. Inst. Phys.)

4.3 Conclusion

An important conclusion is that it is the increase of heat capacity at T_g, relative to the excess entropy of the liquid, not relative to the heat capacity of the glass as initially proposed[1], that is the better indicator of the thermodynamic fragility (if it is to be judged by data at a single point, namely T_g). The dangers of this restriction are indicated in the case of kinetic fragility where major differences in the ordering of molecular liquids are found[41] depending on whether the ***m*** fragilities, determined at T_g or the $F_{1/2}$ fragilities[34], determined half way between T_g and the high temperature limit, are used. Possible sources of such aberrant behavior on the part of certain liquids have been discussed elsewhere[9]. For

this reason, the presentation of the whole excess entropy development plots of Figure 4.7, like the whole kinetic fragility plots, are to be preferred over any single point assessments.

The extent to which these considerations will really resolve the issues discussed in ref.[10] and related papers will only be decided by future more extensive studies, but we hope that the present observations will provide some useful guidelines.

4.4 References

(1) Angell, C. A. *Relax. complex Syst. ed. by K. L. Ngai G. B. Wright (NTIS, Springfield, Va.)* **1985**, 1.

(2) Angell, C. A. *J. Non. Cryst. Solids* **1991**, 13.

(3) Brand, R.; Lunkenheimer, P.; Loidl, A. *J. Chem. Phys.* **2002**, *116* (23), 10386.

(4) Bauer, T.; Köhler, M.; Lunkenheimer, P.; Loidl, A.; Angell, C. A. *J. Chem. Phys.* **2010**, *133* (14).

(5) Angell, C. A.; Hemmati, M. In *AIP Conference Proceedings*; 2013; Vol. 1518, pp 9–17.

(6) Martinez, L. M.; Angell, C. A. *Lett. to Nat.* **2001**, *410*, 663.

(7) Wang, L. M.; Angell, C. A.; Richert, R. *J. Chem. Phys.* **2006**, *125* (7).

(8) Angell, C. A.; Richards, B. E.; Velikov, V. *J. Phys. Condens. Matter* **1999**, *11* (10A), A75.

(9) Angell, C. A. In *Fragility of glass-forming liquids*; Greer, A. L., Kelton, K., Sastry, S., Eds.; Hindustan Book Agency: Gurgaon, 2014; p 530.

(10) Huang, D.; McKenna, G. B. *J. Chem. Phys.* **2001**, *114* (13), 5621.

(11) Angell, C. A.; Klein, I. S. *Nature Physics*. 2011, pp 750–751.

(12) Landau, L.; Lifschitz, E. M. *Statistical Physics*; Pergamon and Addison-Wesley: Reading, 1958.

(13) Caupin, F.; Arvengas, A.; Davitt, K.; Azouzi, M. E. M.; Shmulovich, K. I.;

Ramboz, C.; Sessoms, D. a; Stroock, A. D. *J. Phys. Condens. Matter* **2012**, *24* (28), 284110.

(14) Zheng, Q.; Green, J.; Kieffer, J.; Poole, P. In *Liquids under Negative Pressure*; Kluwer Academic Publisher, 2002; pp 1–46.

(15) Davitt, K.; Rolley, E.; Caupin, F.; Arvengas, A.; Balibar, S. *J. Chem. Phys.* **2010**, *133* (17), 174507.

(16) Davitt, K.; Arvengas, A.; Caupin, F. *EPL (Europhysics Lett.* **2010**, *90* (1), 16002.

(17) Kunzler, J. E.; Giauque, W. F. *J. Am. Chem. Soc.* **1952**, *74* (21), 5271.

(18) Angell, C. A.; Rao, K. J. *J. Chem. Phys.* **1972**, *57* (1), 470.

(19) Tatsumi, S.; Aso, S.; Yamamuro, O. *Phys. Rev. Lett.* **2012**, *109* (4), 1.

(20) Amann-Winkel, K.; Gainaru, C.; Handle, P. H.; Seidl, M.; Nelson, H.; Böhmer, R.; Loerting, T. *Proc. Natl. Acad. Sci. U. S. A.* **2013**, *110* (44), 17720.

(21) Wunderlich, B. *J. Phys. Chem.* **1960**, *64*, 1052.

(22) Takeda, K.; Yamamuro, O.; Tsukushi, I.; Matsuo, T.; Suga, H. *J. Mol. Struct.* **1999**, *479* (2-3), 227.

(23) Moynihan, C. T.; Angell, C. A. *J. Non. Cryst. Solids* **2000**, *274* (1), 131.

(24) Stevenson, J. D.; Wolynes, P. G. *J. Phys. Chem. B* **2005**, *109* (31), 15093.

(25) Fujimori, H.; Mizukami, M.; Oguni, M. *J. Non. Cryst. Solids* **1996**, *204* (1), 38.

(26) Gundermann, D.; Pedersen, U. R.; Hecksher, T.; Bailey, N. P.; Jakobsen, B.; Christensen, T.; Olsen, N. B.; Schrøder, T. B.; Fragiadakis, D.; Casalini, R.; Michael Roland, C.; Dyre, J. C.; Niss, K.; Schrøder, T. B.; Fragiadakis, D.; Casalini, R.; Roland, C. M.; Dyre, J. C.; Niss, K. *Nat. Publ. Gr.* **2011**, *7* (10), 816.

(27) Matyushov, D. V.; Angell, C. A. *J. Chem. Phys.* **2007**, *126* (9).

(28) Angell, C. A.; Smith, D. L. *J. Phys. Chem.* **1982**, *86* (19), 3845.

(29) Angell, C. A.; Sare, E. J. *J. Chem. Phys.* **1970**, *52* (3), 1058.

(30) Parks, G. S.; Thomas, S. B.; Gilkey, W. A. *J. Phys. Chem.* **1929**, *34* (9), 2028.

(31) Grønvold, F. *J. Chem. Thermodyn.* **1973**, *5* (4), 525.

(32) Kauzmann, W. *Chem. Rev.* **1948**, *43* (2), 219.

(33) Richert, R.; Angell, C. A. *J. Chem. Phys.* **1998**, *108* (21), 9016.

(34) Sastry, S. *Nature* **2001**, *409* (6817), 164.

(35) Angell, C. A.; Yue, Y.; Wang, L.-M.; Copley, J. R. D.; Borick, S.; Mossa, S. *J. Phys. Condens. Matter* **2003**, *15* (11), S1051.

(36) Xia, X.; Wolynes, P. G. *Proc. Natl. Acad. Sci.* **2000**, *97* (7), 2990.

(37) Lubchenko, V.; Wolynes, P. G. *J. Chem. Phys.* **2003**, *119* (17), 9088.

(38) Ngai, K. L.; Yamamuro, O. *J. Chem. Phys.* **1999**, *111* (23), 10403.

(39) Wang, L. M.; Velikov, V.; Angell, C. A. *J. Chem. Phys.* **2002**, *117* (22), 10184.

(40) Naoki, M.; Koeda, S. *J. Phys. Chem.* **1989**, *93*, 948.

(41) Rao, K. J.; Helphrey, D. B.; Angell, C. A. *Phys. Chem. Glas.* **1973**, *14*, 1.

(42) Pollard, L. J.; Crowe, M. L.; Strauss, W. *J. Chem. Eng. Data* **1971**, *16*, 1.

(43) Litovitz, T. A.; Sette, D. *J. Chem. Phys.* **1953**, *21*, 17.

(44) Lide, D. R. *Handb. Chem. Phys.* **2003**, *53*, 2616.

(45) Litovitz, T. A. *J. Acoust. Soc. Am.* **1958**, *30* (9), 856.

(46) Grzybowski, A.; Paluch, M.; Grzybowska, K. *J. Phys. Chem. B* **2009**, *113* (21), 7419.

(47) Abdulagatov, I. M.; Safarov, J. T.; Aliyev, F. S.; Talibov, M. A.; Shahverdiyev, A. N.; Hassel, E. P. *Fluid Phase Equilib.* **2008**, *268* (1-2), 21.

(48) Casalini, R.; Roland, C. M. *Phys. Rev. Lett.* **2014**, *113* (8), 1.

(49) Corsaro, R. D. *Phys. Chem. Glas.* **1976**, *17* (1), 13.

(50) Abowitz, G. *Scr. Metall.* **1977**, *11* (5), 353.

(51) Chang, S. S.; Bestul, A. B. *J. Chem. Phys.* **1972**, *56* (1), 503.

(52) Fujimori, H.; Oguni, M. *J. Chem. Thermodyn.* **1994**, *26* (4), 367.

(53) Stolen, S.; Grande, T. *Chemical Thermodynamics of Materials: Macroscopic and Microscopic Aspects*; John Wiley & Sons, 2004.

(54) Takeda, K.; Yamamuro, O.; Suga, H. *J. Phys. Chem. Solids* **1991**, *52* (4), 607.

(55) Counsell, J. F.; Lees, E. B.; Martin, J. F. *J. Chem. Soc. A Inorganic, Phys. Theor.* **1968**, 1819.

(56) Gibson, G. E.; Giauque, W. F. *J. Am. Chem. Soc.* **1923**, *45* (1), 93.

CHAPTER 5

SUMMARY

This work describes the synthesis and characterization of novel inorganic plastic crystals and their applications as electrolytes in all solid state electrochemical cells. The compounds developed in this work are a series of silicon and sulfate based solid acids and lithium salts, with different ligands in each composition. Both classes of compounds exhibit remarkable ionic (H^+ and Li^+) conductivity, and functioning cells for both examples are shown. A thorough Introduction of this work in given on Chapter 1, starting with the fundamentals of electrochemical cells and their applications as energy conversion devices. Special attention is given to the role and development of solid state electrolytes in that context. A succinct overview of silicon chemistry is given, and finally a summary of the characterization techniques used in this work are reviewed.

The solid acids were initially developed as precursor compounds for the synthesis of the lithium salts, but their high protonic conductivity, within 20% of liquid phosphoric acid and 3 orders of magnitude higher than the current state of the art in solid acid electrolytes, demanded further research on their own. Chapter 2 is devoted to the development and characterization of the solid acids, cells using these compounds as electrolytes are shown.

Chapter 3 is dedicated to the lithium salts prepared using the solid acids of Chapter 2 as precursors. The resulting compounds are ionic plastic crystals: structurally ordered but orientationally disordered materials, and in this case, they exhibit remarkable ionic conductivity. Electrochemical cells that employ examples of the materials prepared in this Chapter are demonstrated, and it is shown that cycling of cells are possible with these materials.

Finally, Chapter 4 introduces a new approach to the scaling of heat capacities of glassforming liquids. First, thermodynamic response functions of liquids at temperatures above T_g are reviewed – compressibility, thermal expansion and heat capacity. The compressibility and thermal expansion are self-scaled by volume, which allows to the direct comparison of different substances. The opposite is true for heat capacity, and there is much controversy in the literature about a proper scaling method that would allow for comparison of different compounds. Here we attempt to solve the problem by defining heat capacity as an entropy derivative and subsequently scaling it by the absolute excess entropy at T_g. The thermodynamic fragility concept is then discussed in the context of the new scaling approach.

REFERENCES

CHAPTER 1

(1) Padhi, A.; Nanjundaswamya, K.; Goodenough, J. *J. Electrochem. Soc.* **1997**, *144* (4), 1188.

(2) EG&G Technical Services. *Fuel Cell Handbook*, 7th ed.; US Department of Energy: Morgantown, 2004.

(3) Baranov, A. I.; Shuvalov, L. A.; Shchagina, N. M. *JETP Lett.* **1982**, *36* (11), 459.

(4) Matsuo, Y.; Saito, K.; Kawashima, H.; Ikehata, S. *Solid State Commun.* **2004**, *130* (6), 411.

(5) Moskvich, Y. N.; Rozanov, O. V.; Sukhovsky, A. A.; Aleksandrova, I. P. *Ferroelectrics* **1985**, *63* (1), 83.

(6) Haile, S. M.; Chisholm, C. R. I.; Sasaki, K.; Boysen, D. A; Uda, T. *Faraday Discuss.* **2007**, *134*, 17.

(7) Haile, S. M.; Boysen, D. A; Chisholm, C. R.; Merle, R. B. *Nature* **2001**, *410* (6831), 910.

(8) Chisholm, C. R. I.; Haile, S. M. *Solid State Ionics* **2000**, *136*, 229.

(9) Mohammad, N.; Mohamad, A. B.; Kadhum, A. A. H.; Loh, K. S. *J. Power Sources* **2016**, *322*, 77.

(10) Boysen, D. A.; Uda, T.; Chisholm, C. R. I.; Haile, S. M. *Science* **2004**, *303* (2004), 68.

(11) Uda, T.; Haile, S. M. *Electrochem. Solid-State Lett.* **2005**, *8* (5), A245.

(12) Nagaura, T.; Tozawa, K. *Prog. Batter. Sol. Cells* **1990**, *9*, 209.

(13) Xu, K. *Chem. Rev.* **2004**, *104* (10), 4303.

(14) Tarascon, J. M.; Guyomard, D. *Solid State Ionics* **1994**, *69* (3-4), 293.

(15) Kamaya, N.; Homma, K.; Yamakawa, Y.; Hirayama, M.; Kanno, R.; Yonemura, M.; Kamiyama, T.; Kato, Y.; Hama, S.; Kawamoto, K.; Mitsui, A. *Nat. Mater.* **2011**, *10* (9), 682.

(16) Briant, J.; Farrington, G. *J. Solid State Chem.* **1980**, *33*, 385.

(17) Xu, K. *Chem. Rev.* **2014**, *114*, 11503.

(18) Pearson, G. *J. Am. Chem. Soc.* **1963**, *85* (22), 3533.

(19) Minami, T. *Solid State Ionics for Batteries*; Tatsumisago, M., Wakihara, M., Iwakura, C., Kohjiya, S., Tanaka, I., Eds.; Springer-Verlag: Hicom, 2005.

(20) Ansari, Y.; Tucker, T. G.; Angell, C. A. *J. Power Sources* **2013**, *237*, 47.

(21) Ansari, Y.; Tucker, T. G.; Huang, W.; Klein, I. S.; Lee, S.-Y.; Yarger, J. L.; Angell, C. A. *J. Power Sources* **2016**, *303*, 142.

(22) Eaborn, C. *J. Organomet. Chem.* **1975**, *100*, 43.

(23) Eaborn, C. *J. Chem. Soc.* **1956**, *1* (4858), 4858.

(24) Matyjaszewski, K.; Chen, Y. L. *J. Organomet. Chem.* **1988**, *340*, 7.

(25) Bassindale, A. R.; Stout, T. *J. Organomet. Chem.* **1984**, *271*, C1.

(26) *Impedance Spectroscopy*; MacDonald, J. R., Ed.; John Wiley & Sons: New York, 1987.

(27) *Solid State Electrochemistry*; Bruce, P. G., Ed.; Cambridge University Press: Cambridge, 1995.

(28) Randles, J. E. B. *Discuss. Faraday Soc.* **1947**, *1*, 11.

(29) Lide, D. R. *Handb. Chem. Phys.* **2003**, *53*, 2616.

(30) *Solid-State NMR Spectroscopy Principles and Applications*; Duer, M. J., Ed.; Blackwell Science Ltd: Malden, MA, 2002.

(31) Nakamoto, K. *Infrared and Raman spectra of inorganic and coordination compounds*, 3rd ed.; Wiley: New York, 1978.

CHAPTER 2

(1) Juhasz, M.; Hoffmann, S.; Stoyanov, E.; Kim, K. C.; Reed, C. a. *Angew. Chemie - Int. Ed.* **2004**, *43*, 5352.

(2) Stoyanov, E. S.; Stoyanova, I. V.; Tham, F. S.; Reed, C. A. *J. Am. Chem. Soc.* **2008**, *130* (36), 12128.

(3) Nava, M.; Stoyanova, I. V; Cummings, S.; Stoyanov, E. S.; Reed, C. A. *Angew. Chem. Int. Ed. Engl.* **2014**, *53* (4), 1131.

(4) Haile, S. M.; Boysen, D. a; Chisholm, C. R.; Merle, R. B. *Nature* **2001**, *410* (6831), 910.

(5) Haile, S. M.; Chisholm, C. R. I.; Sasaki, K.; Boysen, D. a; Uda, T. *Faraday Discuss.* **2007**, *134*, 17.

(6) Ansari, Y.; Ueno, K.; Zhao, Z.; Angell, C. A. *J. Phys. Chem. C* **2013**, *117*, 1548.

(7) Ansari, Y.; Tucker, T. G.; Huang, W.; Klein, I. S.; Lee, S.-Y.; Yarger, J. L.; Angell, C. A. *J. Power Sources* **2016**, *303*, 142.

(8) Flowers, R. H.; Gillespie, R. J.; Robinson, E. A. *Can. J. Chem.* **1963**, *41* (10), 2464.

(9) Eaborn, C. *J. Organomet. Chem.* **1975**, *100*, 43.

(10) Keay, B. A. In *Science of Synthesis, 4: Category 1, Organometallics*; Fleming, I., Ed.; Georg Thieme Verlag: Stuttgart - New York, 2002; p 685.

(11) Matyjaszewski, K.; Chen, Y. L. *J. Organomet. Chem.* **1988**, *340*, 7.

(12) Merle, R. B.; Chisholm, C. R. I.; Boysen, D. a.; Haile, S. M. *Energy and Fuels* **2003**, *17* (1), 210.

(13) Bennett, A. E.; Rienstra, C. M.; Auger, M.; Lakshmi, K. V; Griffin, R. G. *J. Chem. Phys.* **1995**, *103* (16), 6951.

(14) Hayashi, S.; Hayamizu, K. *Bull. Chem. Soc. Jpn.* 1991, pp 685–687.

(15) Ansari, Y.; Tucker, T. G.; Angell, C. A. *J. Power Sources* **2013**, *237*, 47.

(16) Frisch, M. J. et al. *Gaussian 09, Revision A.02*. 2009.

(17) Alarco, P.-J.; Abu-Lebdeh, Y.; Abouimrane, A.; Armand, M. *Nat. Mater.* **2004**, *3* (7), 476.

(18) Greenwood, N. N.; Thompson, a. *J. Chem. Soc.* **1959**, *VI*, 3485.

(19) Wang, Y.; Lane, N. a.; Sun, C. N.; Fan, F.; Zawodzinski, T. a.; Sokolov, A. P. *J. Phys. Chem. B* **2013**, *117*, 8003.

(20) Baranov, A. I.; Shuvalov, L. A.; Shchagina, N. M. *JETP Lett.* **1982**, *36* (11), 459.

(21) Chisholm, C. R. I.; Haile, S. M. *Solid State Ionics* **2000**, *136*, 229.

(22) Hayes, M. J.; Pepper, D. C. *Trans. Faraday Soc.* **1961**, *57*, 432.

(23) Davidowski, S. K.; Thompson, F.; Huang, W.; Hasani, M.; Amin, S. A.; Angell, C. A.; Yarger, J. L. *J. Phys. Chem. B* **2016**, *120* (18), 4279.

(24) Bee, M.; Amoureux, J. P.; Lechner, R. E. *Mol. Phys.* **2006**, *40* (3), 617.

(25) Amoureux, J. P.; Bée, M.; Virlet, J. *Mol. Phys.* **1980**, *41* (2), 313.

(26) Lynden-Bell, R. M.; McDonald, I. R. *Mol. Phys.* **1981**, *43* (6), 1429.

(27) Hayashi, S.; Mizuno, M. *Solid State Commun.* **2004**, *132* (7), 443.

(28) Zangmeister, C. D.; Pemberton, J. E. *J. Am. Chem. Soc.* **2000**, *122* (15), 12289.

(29) Baran, J.; Marchewka, M. K. *J. Mol. Struct.* **2002**, *614*, 133.

(30) Yamawaki, H.; Fujihisa, H.; Sakashita, M.; Honda, K. *Phys. Rev. B* **2007**, *75* (9), 094111.

(31) Nakamoto, K. *Infrared and Raman spectra of inorganic and coordination compounds*, 3rd ed.; Wiley: New York, 1978.

(32) Walrafen, G.; Yang, W. *J. Solut. …* **2000**, *29* (10), 905.

(33) Posternak, A. G.; Garlyauskayte, R. Y.; Polovinko, V. V; Yagupolskii, L. M.; Yagupolskii, Y. L. *Org. Biomol. Chem.* **2009**, *7* (8), 1642.

(34) Kintzinger, J.-P.; Marsmann, H. *Oxygen-17 and and silicon-29. (NMR, basic principles and progress; v.17)*, 1st ed.; Diehl, P., Fluck, E., Kosfeld, R., Eds.; Springer-Verlag: Berlin Heidelberg New York, 1981.

(35) Tsumura, M.; Ando, K.; Kotani, J.; Hiraishi, M.; Iwahara, T. *Macromolecules* **1998**, *31* (9), 2716.

(36) Hartmann, S. R.; Hahn, E. L. *Phys. Rev.* **1962**, *128* (5), 2042.

(37) Kolodziejski, W.; Klinowski, J. *Chem. Rev.* **2002**, *102* (3), 613.

(38) Horn, H.-G.; Marsmann, H. C. *Die Makromol. Chemie* **1972**, *162* (1), 255.

(39) Mudrakovskii, I. L.; Shmachkova, V. P.; Kotsarenko, N. S.; Mastikhin, V. M. *J. Phys. Chem. Solids* **1986**, *47* (4), 335.

(40) Turner, G. L.; Smith, K. A.; Kirkpatrick, R. J.; Oldfieldt, E. *J. Magn. Reson.* **1986**, *70* (3), 408.

(41) Smith, A. L. *Spectrochim. Acta Part A Mol. Spectrosc.* **1967**, *23* (4), 1075.

(42) Romain, F.; Novak, A. **1991**, *263*, 69.

(43) Buncel, E. *Chem. Rev.* **1970**, *70* (3), 323.

(44) Matsuo, Y.; Saito, K.; Kawashima, H.; Ikehata, S. *Solid State Commun.* **2004**, *130* (6), 411.

(45) Boysen, D. A.; Uda, T.; Chisholm, C. R. I.; Haile, S. M. *Science* **2004**, *303* (2004), 68.

(46) Yamane, Y.; Yamada, K.; Inoue, K. *Solid State Ionics* **2008**, *179* (13-14), 483.

(47) Mohammad, N.; Mohamad, A. B.; Kadhum, A. A. H.; Loh, K. S. *J. Power Sources* **2016**, *322*, 77.

(1) Lee, S. Y.; Ueno, K.; Angell, C. A. *J. Phys. Chem. C* **2012**, *116* (45), 23915.

(2) Tarascon, J. M.; Guyomard, D. *Solid State Ionics* **1994**, *69* (3-4), 293.

(3) Seki, S.; Kobayashi, Y.; Miyashiro, H.; Ohno, Y.; Usami, A.; Mita, Y.; Kihira, N.; Watanabe, M.; Terada, N. *J. Phys. Chem. B* **2006**, *110* (21), 10228.

(4) Sakaebe, H.; Matsumoto, H. *Electrochem. commun.* **2003**, *5* (7), 594.

(5) Hayamizu, K.; Aihara, Y.; Nakagawa, H.; Nukuda, T.; Price, W. S. *J. Phys. Chem. B* **2004**, *108* (50), 19527.

(6) Ye, H.; Huang, J.; Xu, J. J.; Khalfan, A.; Greenbaum, S. G. *J. Electrochem. Soc.* **2007**, *154* (11), A1048.

(7) Cooper, E. I.; Angell, C. A. *Solid State Ionics* **1983**, *9-10* (PART 1), 617.

(8) Macfarlane, D. R.; Macfarlane, D. R.; Huang, J.; Huang, J.; Forsyth, M.; Forsyth, M. *Nature* **1999**, *402* (DECEMBER), 1998.

(9) Cooper, E. I.; Angell, C. A. *Solid State Ionics* **1986**, *18-19* (PART 1), 570.

(10) Alarco, P.-J.; Abu-Lebdeh, Y.; Abouimrane, A.; Armand, M. *Nat. Mater.* **2004**, *3* (7), 476.

(11) Briant, J.; Farrington, G. *J. Solid State Chem.* **1980**, *33*, 385.

(12) Seino, Y.; Ota, T.; Takada, K.; Hayashi, A.; Tatsumisago, M. *Energy Environ. Sci.* **2014**, *7* (2), 627.

(13) Kamaya, N.; Homma, K.; Yamakawa, Y.; Hirayama, M.; Kanno, R.; Yonemura, M.; Kamiyama, T.; Kato, Y.; Hama, S.; Kawamoto, K.; Mitsui, A. *Nat. Mater.* **2011**, *10* (9), 682.

(14) Hayashi, A.; Kama, S.; Mizuno, F.; Tadanaga, K.; Minami, T.; Tatsumisago, M. *Solid State Ionics* **2004**, *175* (1-4), 683.

(15) Hayashi, A.; Minami, K.; Ujiie, S.; Tatsumisago, M. *J. Non. Cryst. Solids* **2010**, *356* (44-49), 2670.

(16) Hayashi, A.; Noi, K.; Sakuda, A.; Tatsumisago, M. *Nat. Commun.* **2012**, *3* (May), 856.

(17) Bauer, T.; Köhler, M.; Lunkenheimer, P.; Loidl, A.; Angell, C. A. *J. Chem. Phys.* **2010**, *133* (14).

(18) Ansari, Y.; Tucker, T. G.; Angell, C. A. *J. Power Sources* **2013**, *237*, 47.

(19) Evans, J.; Vincent, C. A.; Bruce, P. G. *Polymer (Guildf).* **1987**, *28* (13), 2324.

(20) Zugmann, S.; Fleischmann, M.; Amereller, M.; Gschwind, R. M.; Wiemhöfer, H. D.; Gores, H. J. *Electrochim. Acta* **2011**, *56* (11), 3926.

(21) Hayashi, S.; Hayamizu, K. *Bull. Chem. Soc. Jpn.* 1991, pp 685–687.

(22) Eaborn, C. *J. Organomet. Chem.* **1975**, *100*, 43.

(23) Bassindale, A. R.; Stout, T. *J. Organomet. Chem.* **1984**, *271*, C1.

(24) Matyjaszewski, K.; Chen, Y. L. *J. Organomet. Chem.* **1988**, *340*, 7.

(25) Stallworth, P. .; Fontanella, J. .; Wintersgill, M. .; Scheidler, C. D.; Immel, J. J.; Greenbaum, S. .; Gozdz, A. . *J. Power Sources* **1999**, *81-82*, 739.

(26) Kim, S.-H.; Choi, K.-H.; Cho, S.-J.; Park, J.-S.; Cho, K. Y.; Lee, C. K.; Lee, S. B.; Shim, J. K.; Lee, S.-Y. *J. Mater. Chem. A* **2014**, *2* (28), 10854.

(27) Angell, C. A.; Klein, I. S.; Tucker, T. G. Inorganic plastic crystal electrolytes. WO2014153146 A1, 2014.

(28) Fan, J.; Fedkiw, P. S. *J. Power Sources* **1998**, *72*, 165.

(29) Shekibi, Y.; Rüther, T.; Huang, J.; Hollenkamp, A. F. *Phys. Chem. Chem. Phys.* **2012**, 14, 4597.

(1) Angell, C. A. *Relax. complex Syst. ed. by K. L. Ngai G. B. Wright (NTIS, Springfield, Va.)* **1985**, 1.

(2) Angell, C. A. *J. Non. Cryst. Solids* **1991**, 13.

(3) Brand, R.; Lunkenheimer, P.; Loidl, A. *J. Chem. Phys.* **2002**, *116* (23), 10386.

(4) Bauer, T.; Köhler, M.; Lunkenheimer, P.; Loidl, A.; Angell, C. A. *J. Chem. Phys.* **2010**, *133* (14).

(5) Angell, C. A.; Hemmati, M. In *AIP Conference Proceedings*; 2013; Vol. 1518, pp 9–17.

(6) Martinez, L. M.; Angell, C. A. *Lett. to Nat.* **2001**, *410*, 663.

(7) Wang, L. M.; Angell, C. A.; Richert, R. *J. Chem. Phys.* **2006**, *125* (7).

(8) Angell, C. A.; Richards, B. E.; Velikov, V. *J. Phys. Condens. Matter* **1999**, *11* (10A), A75.

(9) Angell, C. A. In *Fragility of glass-forming liquids*; Greer, A. L., Kelton, K., Sastry, S., Eds.; Hindustan Book Agency: Gurgaon, 2014; p 530.

(10) Huang, D.; McKenna, G. B. *J. Chem. Phys.* **2001**, *114* (13), 5621.

(11) Angell, C. A.; Klein, I. S. *Nature Physics*. 2011, pp 750–751.

(12) Landau, L.; Lifschitz, E. M. *Statistical Physics*; Pergamon and Addison-Wesley: Reading, 1958.

(13) Caupin, F.; Arvengas, A.; Davitt, K.; Azouzi, M. E. M.; Shmulovich, K. I.; Ramboz, C.; Sessoms, D. a; Stroock, A. D. *J. Phys. Condens. Matter* **2012**, *24* (28), 284110.

(14) Zheng, Q.; Green, J.; Kieffer, J.; Poole, P. In *Liquids under Negative Pressure*; Kluwer Academic Publisher, 2002; pp 1–46.

(15) Davitt, K.; Rolley, E.; Caupin, F.; Arvengas, A.; Balibar, S. *J. Chem. Phys.* **2010**, *133* (17), 174507.

(16) Davitt, K.; Arvengas, A.; Caupin, F. *EPL (Europhysics Lett.* **2010**, *90* (1), 16002.

(17) Kunzler, J. E.; Giauque, W. F. *J. Am. Chem. Soc.* **1952**, *74* (21), 5271.

(18) Angell, C. A.; Rao, K. J. *J. Chem. Phys.* **1972**, *57* (1), 470.

(19) Tatsumi, S.; Aso, S.; Yamamuro, O. *Phys. Rev. Lett.* **2012**, *109* (4), 1.

(20) Amann-Winkel, K.; Gainaru, C.; Handle, P. H.; Seidl, M.; Nelson, H.; Böhmer, R.; Loerting, T. *Proc. Natl. Acad. Sci. U. S. A.* **2013**, *110* (44), 17720.

(21) Wunderlich, B. *J. Phys. Chem.* **1960**, *64*, 1052.

(22) Takeda, K.; Yamamuro, O.; Tsukushi, I.; Matsuo, T.; Suga, H. *J. Mol. Struct.* **1999**, *479* (2-3), 227.

(23) Moynihan, C. T.; Angell, C. A. *J. Non. Cryst. Solids* **2000**, *274* (1), 131.

(24) Stevenson, J. D.; Wolynes, P. G. *J. Phys. Chem. B* **2005**, *109* (31), 15093.

(25) Fujimori, H.; Mizukami, M.; Oguni, M. *J. Non. Cryst. Solids* **1996**, *204* (1), 38.

(26) Gundermann, D.; Pedersen, U. R.; Hecksher, T.; Bailey, N. P.; Jakobsen, B.; Christensen, T.; Olsen, N. B.; Schrøder, T. B.; Fragiadakis, D.; Casalini, R.; Michael Roland, C.; Dyre, J. C.; Niss, K.; Schrøder, T. B.; Fragiadakis, D.; Casalini, R.; Roland, C. M.; Dyre, J. C.; Niss, K. *Nat. Publ. Gr.* **2011**, *7* (10), 816.

(27) Matyushov, D. V.; Angell, C. A. *J. Chem. Phys.* **2007**, *126* (9).

(28) Angell, C. A.; Smith, D. L. *J. Phys. Chem.* **1982**, *86* (19), 3845.

(29) Angell, C. A.; Sare, E. J. *J. Chem. Phys.* **1970**, *52* (3), 1058.

(30) Parks, G. S.; Thomas, S. B.; Gilkey, W. A. *J. Phys. Chem.* **1929**, *34* (9), 2028.

(31) Grønvold, F. *J. Chem. Thermodyn.* **1973**, *5* (4), 525.

(32) Kauzmann, W. *Chem. Rev.* **1948**, *43* (2), 219.

(33) Richert, R.; Angell, C. A. *J. Chem. Phys.* **1998**, *108* (21), 9016.

(34) Sastry, S. *Nature* **2001**, *409* (6817), 164.

(35) Angell, C. A.; Yue, Y.; Wang, L.-M.; Copley, J. R. D.; Borick, S.; Mossa, S. *J. Phys. Condens. Matter* **2003**, *15* (11), S1051.

(36) Xia, X.; Wolynes, P. G. *Proc. Natl. Acad. Sci.* **2000**, *97* (7), 2990.

(37) Lubchenko, V.; Wolynes, P. G. *J. Chem. Phys.* **2003**, *119* (17), 9088.

(38) Ngai, K. L.; Yamamuro, O. *J. Chem. Phys.* **1999**, *111* (23), 10403.

(39) Wang, L. M.; Velikov, V.; Angell, C. A. *J. Chem. Phys.* **2002**, *117* (22), 10184.

(40) Naoki, M.; Koeda, S. *J. Phys. Chem.* **1989**, *93*, 948.

(41) Rao, K. J.; Helphrey, D. B.; Angell, C. A. *Phys. Chem. Glas.* **1973**, *14*, 1.

(42) Pollard, L. J.; Crowe, M. L.; Strauss, W. *J. Chem. Eng. Data* **1971**, *16*, 1.

(43) Litovitz, T. A.; Sette, D. *J. Chem. Phys.* **1953**, *21*, 17.

(44) Lide, D. R. *Handb. Chem. Phys.* **2003**, *53*, 2616.

(45) Litovitz, T. A. *J. Acoust. Soc. Am.* **1958**, *30* (9), 856.

(46) Grzybowski, A.; Paluch, M.; Grzybowska, K. *J. Phys. Chem. B* **2009**, *113* (21), 7419.

(47) Abdulagatov, I. M.; Safarov, J. T.; Aliyev, F. S.; Talibov, M. A.; Shahverdiyev, A. N.; Hassel, E. P. *Fluid Phase Equilib.* **2008**, *268* (1-2), 21.

(48) Casalini, R.; Roland, C. M. *Phys. Rev. Lett.* **2014**, *113* (8), 1.

(49) Corsaro, R. D. *Phys. Chem. Glas.* **1976**, *17* (1), 13.

(50) Abowitz, G. *Scr. Metall.* **1977**, *11* (5), 353.

(51) Chang, S. S.; Bestul, A. B. *J. Chem. Phys.* **1972**, *56* (1), 503.

(52) Fujimori, H.; Oguni, M. *J. Chem. Thermodyn.* **1994**, *26* (4), 367.

(53) Stolen, S.; Grande, T. *Chemical Thermodynamics of Materials: Macroscopic and Microscopic Aspects*; John Wiley & Sons, 2004.

(54) Takeda, K.; Yamamuro, O.; Suga, H. *J. Phys. Chem. Solids* **1991**, *52* (4), 607.

(55) Counsell, J. F.; Lees, E. B.; Martin, J. F. *J. Chem. Soc. A Inorganic, Phys. Theor.* **1968**, 1819.

(56) Gibson, G. E.; Giauque, W. F. *J. Am. Chem. Soc.* **1923**, *45* (1), 93.

APPENDIX A

PERMISSION FROM CO-AUTHORS

Chapter 4 is a published work in the Journal of Non-Crystalline Solids. The article was received by the publisher on March 12nd 2016, revised on May 26th 2016 and accepted on June 5th 2016. Available online August 25th 2016. DOI: 10.1016/j.jnoncrysol.2016.06.006

All co-authors granted permission for the use of this previously published work in this Dissertation.